8-2019

# The Synthesis and Characterization of 2-Arachidonoyl Glycerol

Shawn Alan Bydalek
sabydalek@yahoo.com

UNIVERSITY OF NORTHERN COLORADO

Greeley, Colorado

The Graduate School

# THE SYNTHESIS AND CHARACTERIZATION OF 2-ARACHIDONOYL GLYCEROL

A Thesis Submitted in Partial Fulfillment
of the Requirement for the Degree of
Master of Science

Shawn Bydalek

College of Natural and Health Sciences
Department of Chemistry and Biochemistry

August 2019

This Thesis by: Shawn Bydalek

Entitled: *The Synthesis and Characterization of 2-Arachidonoyl glycerol*

has been approved as meeting the requirement for the Master of Science in College of Natural and Health Sciences in Department of Chemistry and Biochemistry

Accepted by the Thesis Committee:

_____

Richard M. Hyslop, Ph.D., Research Advisor

_____

David L. Pringle, Ph.D., Committee Member

_____

Michael M. Mosher, Ph.D., Committee Member

Accepted by the Graduate School

_____

Linda L. Black, Ed.D.
Associate Provost and Dean
Graduate School and International Admissions
Research and Sponsored Projects

# ABSTRACT

Bydalek, Shawn. *The Synthesis and Characterization of 2-Arachidonoyl Glycerol.* Unpublished Master of Science thesis, University of Northern Colorado, 2019

Cannabinoids are a structurally diverse class of compounds that act as ligands at the cannabinoid receptors, $CB_1$ and $CB_2$, through which the majority of the physiological effects of these compounds are mediated. Endocannabinoids (endogenous cannabinoids) are a subset of the cannabinoid family and include 2-arachidonoyl glycerol (2-AG) and *N*-arachidonoyl ethanolamide, and like most cannabinoids, these compounds have been shown to have anti-neoplastic effects on various cancer lines. The synthesis of 2-AG from dihydroxyacetone was selected as a research goal to try to improve yield over older published synthetic methods, to keep 2-AG in a protected form to avoid isomerization and other unwanted side reactions, and ultimately to experiment with further chemical modification of 2-AG and observe how this affects its anti-neoplastic activity. The methodology employed used the silyl ether protecting reagent *t*-BDPSiCl and yields up to the esterification step were excellent. Esterification with $SOCl_2$ did not return yields on par with previous steps, but improvements in yield were seen by increasing reaction temperature. Analysis of deprotection was complicated by difficulties with the HPLC methodology, but the protecting group was found to be amenable to a single flask synthesis in DMF using $SOCl_2$, which is a highly appealing quality to this methodology.

ACKNOWLEDGEMENTS

I cannot overexpress my gratitude to my research advisor, mentor, and friend Dr. Richard Hyslop, who has gone above and beyond the call of duty in every capacity he was able. I know he knows what his guidance, counsel, and encouragement have meant to me through all the challenges I have faced, both in and out of the university, and immortalizing my gratitude with these words is a small way to repay his kindness to and faith in me. The world would be a better place with more people like him.

I am especially indebted to my family, whose love and support has enabled me to even entertain the dream of pursuing a career in science. My graduate studies came with challenges I never anticipated, and the years that encompassed my time at UNCO have been some of the most challenging I have ever endured. Without my family to be a rock of support, I do not know if I would have made it. To my mother, father, brothers, and sister, you have my whole heart.

I owe dear thanks to my friends as well, many of whom I met and became close with at UNCO. A graduate program is in many ways a trial by fire and friendships forged in fire tend to be the strongest. I specifically am grateful to have met and gotten to know Danea, Jesus, Cory, Jess, Matt, Travis, and Chris. The times I have spent with each of them have given me great memories, and knowing so many bright, reliable, and hard-working people has been an inspiration to me to do my best. Having true and good friends is an element of life that everyone needs, and I am grateful for mine. Again, they know how I feel, but not writing it down would be a disservice.

My sincere gratitude goes to my other committee members, Drs. Michael Mosher and David Pringle. Beyond being great professors and chemists, both of these men have been gracious with their time, knowledge, and counsel, and I am indebted to them for being a part of my committee. From helping me with interpreting spectra, to giving me instruction on instrumentation, to simply offering small words of advice or encouragement, I cannot thank them enough.

I am also grateful to the professors who I studied with in my time at UNCO, specifically Dr. Murielle Watzky-Brewer, who graciously undertook an independent study in Bioinorganic chemistry with me and who helped and supported me in my time at UNCO. I extend my sincere gratitude to Dr. Steve Mackessy as well, who permitted me to use his research lab for cell culture and assay analysis when it would have been incredibly easy to do otherwise. I was voracious to learn and had a lot of ambition, and I count myself fortunate to have encountered so many willing to aid me.

The Department of Chemistry and Biochemistry stockroom, specifically Tessa Johnson and her replacement, Scott Newkirk, have my unending gratitude for their excellence in professionalism, laboratory upkeep, and support. Having worked in the stock room myself, I know how many hats and responsibilities they had to juggle, and it is impressive that they can do all those tasks and still be so helpful. I cannot count on one hand how many times Tessa and Scott have done all they were able to fulfill my requests and facilitate my ability to conduct my research. I am also grateful to the administrative staff, specifically Jeannyce Nalley and her replacement Rosanna Parks, who helped me in keeping organized and taken care of within the department itself.

My peers in the graduate school also have my sincere gratitude. I must specifically mention two individuals, both formerly PhD candidates in the Biology department. Thomas McCabe went above and beyond the call of duty in instructing me in proper cellular culture procedure and was always willing to lend a hand in helping me accomplish my work. I cannot thank him enough for all he did for me. I am also grateful to Anthony Saviola, who likewise offered guidance and assistance in the Microbiology lab, and whose insights helped me tremendously. I cannot forget my peers in the Chemistry and Biochemistry department as well, beyond those who I was fortunate enough to get to know personally. The camaraderie of the department and the professionalism of the graduate students was always something I was grateful for, and it certainly made the experience all the richer for having so many talented individuals to work with.

Finally, I express my gratitude to the many students who helped me along the way. Specifically, I must thank three students from my alma mater, Hastings College, for their work and assistance in the laboratory during the months of January 2015 and 2016. To Sienna Lee Athy, Liz Tidwell, and Peyton VanWinkle, I cannot say thank you enough for your hard work and alacrity in the research lab, and I cannot wait to see what your bright futures hold. To the students who I was privileged to have taught in lab, whose curiosity and burgeoning interest in the sciences served to remind me of the spark that started me on this path, I also express my sincere gratitude.

I cannot close without expressing my gratitude to the University of Northern Colorado for providing the resources and laboratory space that work such as this might be

undertaken. It is my sincere hope that the university will continue to grow and be a place for cultivating curiosity, knowledge, and excellence in all its students.

TABLE OF CONTENTS

LIST OF TABLES

LIST OF FIGURES

# CHAPTER I

# INTRODUCTION

## History

*Cannabis sativa*, colloquially referred to as marijuana, is a flowering plant which has been utilized medicinally, ceremonially, and recreationally across various cultures and times (Lambert & Fowler, 2005). Inhalation of smoke from the plant or using the plant material in food preparation (baking) and then consuming that food leads to psychoactive effects, generally characterized as a sensation of euphoria and has been linked with various other physiological outcomes, such as stimulation of appetite or attenuation of short-term memory. The underlying mechanism by which these effects were mediated remained a mystery for over half of the twentieth century, owing primarily to difficulties in isolating and purifying the individual components in crude extracts. This changed in 1964 when Raphael Mechoulam and his research team from the Hebrew University in Jerusalem isolated and characterized the first psychoactive constituent (-)-$\Delta^1$-tetrahydrocannabinol or (-)-THC, or simply THC (see Figure 1 for the $\Delta^1$ numbering scheme used by Mechoulam and Figure 2 for the $\Delta^9$ numbering scheme also commonly used by *Cannabis* researchers) from *C. sativa* (Gaoni & Mechoulam, 1964). The elucidation of the structure of THC reinvigorated the research involving marijuana and the chemical constituents of the plant, at least abroad.

The history of marijuana use and regulation in the United States is characterized by turbidity. Passage of the Marihuana Tax Act in 1937 brought marijuana directly under

federal purview, an action that was railed against by many for its apparent intention to sabotage the hemp industry, in addition to its other primary purpose to act as a legal cudgel to prosecute specific populations of recreational users, primarily poor black farmers who were singled out for being "deviant." The subsequent passage of the Controlled Substances Act in the latter part of 1970 classified marijuana as a Schedule I substance, labeling it as a substance with "no currently accepted medical use and high potential for abuse". As a consequence of these social mores, research of marijuana in the U.S. languished (Peters & Nahas, 1992).

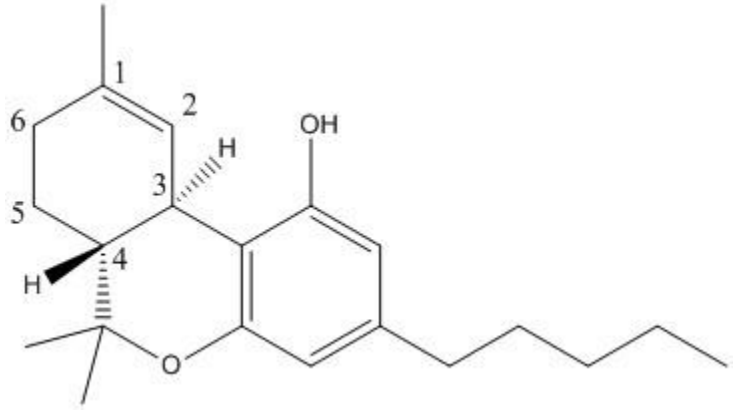


*Figure 1*. $\Delta^1$ Numbering scheme for THC.

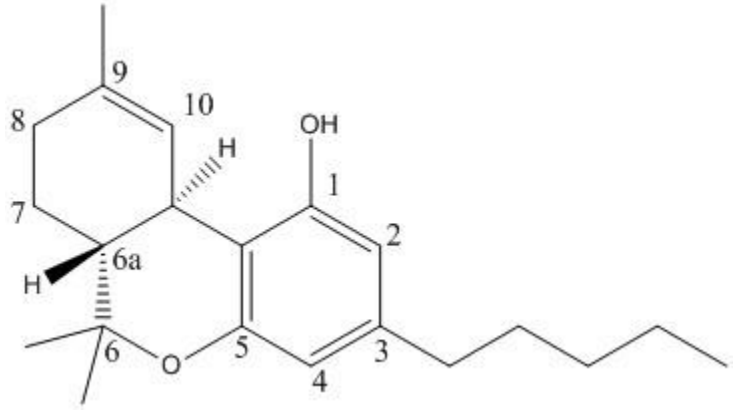


*Figure 2*. $\Delta^9$ Numbering scheme for THC.

Nonetheless, progress continued apace, although not without new challenges. The primary problem confronting *Cannabis* researchers was determining how these compounds were eliciting their physiological effects. Initially it was presumed that, owing to the hydrophobic nature of THC and other major *Cannabis* constituents, physiological activity was affected primarily through non-specific interactions with cellular membranes, similar to general anesthetics such as halothane (Petrocellis & Di Marzo, 2009). In addition, early research conducted with synthesized (+)-THC showed comparable activity with that of naturally occurring (-)-THC, which provided further evidence that bioactivity of THC was probably owed to non-specific interactions of some sort (Dewey, Martin, & May, 1984). However, other research conducted by Mechoulam indicated that the activity of THC was, in fact, enantioselective. Mechoulam's group published results in 1980 demonstrating that (-)-THC exhibited psychoactivity in rhesus monkeys at 50 μg/kg, while (+)-THC showed no activity at 1 mg/kg (Mechoulam et al., 1980). These results strongly suggested that the physiologically active components of marijuana were acting at a specific receptor, or possibly some specific membrane element. Confirmation of this did not come until 1988, when Devane and colleagues used [$^{3}$H]CP-55, 940 (Figure 3), a THC analogue with less hydrophobic nature, to identify a G-protein coupled receptor in rat brain that inhibits adenylate cyclase activity in a dose-dependent, stereoselective manner, indicating that the receptor was of the $G_{i/o}$ sub-type (Devane, Dysarz, Johnson, Melvin, & Howlett, 1988).

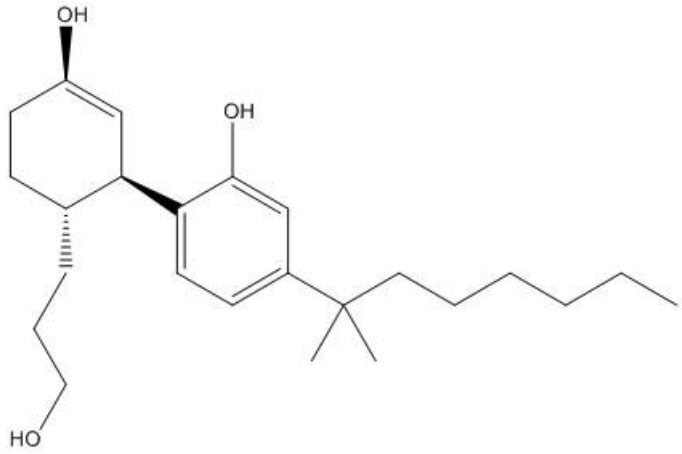


*Figure 3*. CP-55,940, a potent $CB_1$ agonist.

The receptor was subsequently screened out of the library of orphan G-protein coupled receptors and designated cannabinoid receptor 1 ($CB_1$) by Matsuda and colleagues (Matsuda, Lolait, Brownstein, Young, & Bonner, 1990). The location of the receptor and its specificity for THC made it the leading candidate for the mediator of the psychoactive effects of marijuana. Later another cannabinoid receptor, dubbed $CB_2$, was identified through homology cloning and was found to be surprisingly disparate from $CB_1$ in its amino acid sequence, with just 44% overall sequence similarity, although this jumps to 68% when considering transmembrane domains only (Munro, Thomas, & Abu-Shaar, 1993). Whereas $CB_1$ is primarily located in the brain, $CB_2$ was found to be located primarily in immune tissues (spleen, tonsils, lymph nodes, and in various leukocytes) and is presumed to be the key element in the immune suppressing effect of cannabinoids (Flygare & Sander, 2008). The identification of these receptors rationalized the stereospecificity of THC challenge as detailed previously, but it did not repudiate the possibility that non-specific interactions played some element in physiological outcomes for cannabinoid use, and indeed, that interaction is still presumed to play at least some

role in the physiological effects (Makriyannis, 1995). Furthermore, the potential cellular targets of cannabinoids are not exhausted by the identification of these two receptors, and further research has vetted several other potential cellular targets which do not bear further discussion at this point. In the aftermath of identification of these two receptors, there was an obvious question: if there is an exogeneous compound which activates a naturally occurring receptor, what is the endogenous counterpart?

An answer to this question came in 1992 when William Devane and his colleagues published a paper on the isolation and structure of a brain constituent that demonstrated activity at the cannabinoid receptors (Devane et al., 1992). The compound was an arachidonic acid derivative, arachidonylethanolamide (Figure 4), named "anandamide" by its discoverers (from the Sanskrit word "ananda" which means bliss). Three years later, another arachidonic acid derivative, 2-arachidonoyl glycerol (Figure 5), was identified almost simultaneously by Mechoulam (Mechoulam et al., 1995) and Sugiura (Sugiura et al., 1995) as having activity at the cannabinoid receptors. These two compounds constituted the first members of a new sub-class of cannabinoids, the endocannabinoids, and since their discovery numerous other compounds have been added to this sub-class (Figure 6).

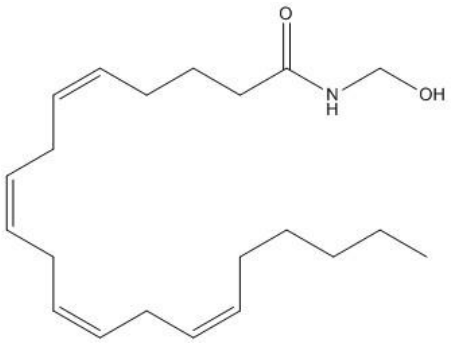


*Figure 4*. Arachidonyl ethanolamide (anandamide).

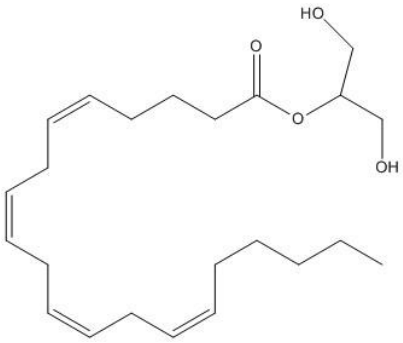


*Figure 5*. 2-Arachidonoyl glycerol (2-AG).

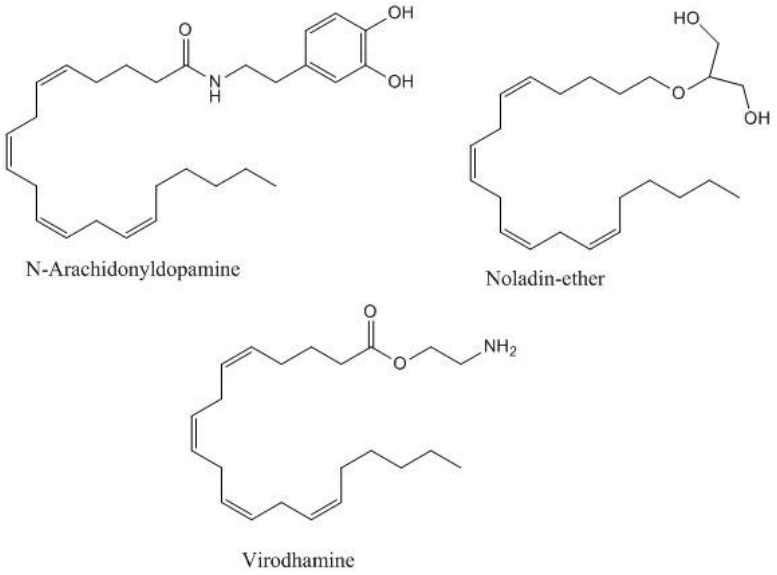


*Figure 6*. Additional endocannabinoids.

Identification of natural ligands for the cannabinoid receptors effectively canonized a new signaling system, and re-primed interest in cannabinoids and their pharmacological effects. One of the earliest noted, and surprisingly overlooked, of these effects was the concentration-dependent growth inhibition of Lewis lung adenocarcinoma xenografts in mice (Munson, Harris, Friedman, Dewey, & Charchman, 1975). Results from research conducted to examine the effects of marijuana use on intact cell and cell component integrity, such as a study where the prevalence of chromosome breakage in marijuana smoking vs. non-smoking groups was observed across a group of 60 total individuals (Stenchever, Kunysz, & Allen, 1974), indicated that marijuana use had deleterious effects on replicative elements of the cell. For instance, in the Stenchever study, there were approximately 2-3 times as many incidences of chromosome breakage in groups that smoked marijuana versus those that did not, irrespective of the amount of self-reported use of marijuana and the use of potentially interfering agents (caffeine, tobacco, etc.). In the case of the Munson experiment, treatment with 100 mg/kg of THC across a period of 30 days increased mean survival time for murine specimens with xenografts by 36% compared to controls. The results of the Munson study were essentially disregarded despite their success, being succeeded by research investigating the palliative uses for cannabinoids (Lucas Jr. & Lazlo, 1980), which to date are the only therapeutic uses for which THC can be prescribed (Bifulco & Di Marzo, 2002). In light of the current medical landscape, this seems like either an egregious oversight or a tragic choice. According to the WHO's fact sheet (http://www.who.int/mediacentre/factsheets /fs297/en/), cancer is the second leading cause of death in the world as of 2015, and the probability that it will eventually become number one is extremely high, given that age is

a major risk factor for cancer development, and the median age of U.S. citizens has continued to rise steadily with time (https://www.census.gov/library/visualizations/2017/comm/median-age.html).

Regardless of the direction of research in the past, the last two decades have been replete with studies confirming the anti-cancer effects of cannabinoids across a wide variety of cancer cell types, including glioma (Salazar et al., 2009), pancreatic (Carracedo et al., 2006), breast (Caffarel et al., 2010), and a diverse array of other cancer types (Velasco, Sanchez, & Guzman, 2012). The seemingly ubiquitous effect of cannabinoids to impede growth, induce cell death, and inhibit invasiveness of cancer across a wide range of sub-types indicates an extremely promising avenue to explore for developing new treatment modalities for a disease which by its very nature demands treatment methods that balance efficacy with quality of life considerations (Cella & Cherin, 1988). This is a monumental task, and its difficulties are compounded by the reality that many standard treatment methods are non-specific and can inadvertently cause further damage, or even novel neoplasias themselves (Patrick, 2013). Considering these challenges, cannabinoids are attractive as potential treatment formulations on their own or as part of a comprehensive treatment package to ameliorate undesirable side effects, improve selectivity in treatment outcomes, and improve overall quality of life for patients.

## Statement of Difficulties and The Research Goal

The process of rigorously evaluating the potential for cannabinoids to act as anti-cancer agents requires that they be gathered or synthesized in sufficient amounts for further experimental use. This presents little challenge for evaluating phytocannabinoids, since marijuana can be grown relatively easily (acquisition of which is only limited by

Federal law), and the pertinent components can be extracted through simple solid phase extraction and then purified. The endocannabinoids present a more formidable challenge, as extraction from organic material is limited by the concentration present in tissue, typically in the nmol/g or even pmol/g range, and in some cases below the limits of detection (Mechoulam, Fride, & Di Marzo, 1998). Limited bioavailability could explain (in part at least) why the cost for 5 mg of 2-arachidonylglycerol is $300.00 from Sigma-Aldrich as of 3/31/18 (https://www.sigmaaldrich.com/catalog/product/sigma/a8973?lang =en& region=US), whereas arachidonic acid ($20:4^{5,8,11,14}$) is concurrently priced at $124.00 for 250 mg (https://www.sigmaaldrich.com/catalog/product/sigma/10931?lang =en&region =US).

The background information and effects of the phytocannabinoids as anti-cancer agents is already well established (Mechoulam & Shabat, 1999), but there are still key unresolved questions and avenues to explore for the endocannabinoids (as will be explored later in Chapter II). Due to this, the synthesis of 2-arachidonoyl glycerol was selected as a research goal. It seemed highly prudent to pursue a method for synthesizing 2-arachidonyl glycerol as opposed to purchasing it directly from a manufacturer, given the price of arachidonic acid discussed previously. Moreover, and of primary interest, is the potential to modify 2-arachidonoyl glycerol in a variety of ways, from fatty acid chain modification or substitution, to glyceride addition, extension, or modification aimed at increasing overall efficacy of the modified compound, either directly or through a greater combined effect. Direct synthesis also affords the ability to generate 2-AG in a protected form, whereupon chemical de-protection or activation can generate 2-AG on demand,

ameliorating certain issues regarding compound availability and stability (see Chapter II for more information).

Development of a synthetic method for production of 2-AG was sought for the aforementioned reasons. The core goal of the research was to develop a methodology at least as effective as previous methods in synthesizing 2-AG, with the hope of improving yield while concomitantly investigating permutations of 2-AG for use in activity assays.

# CHAPTER II

# LITERATURE REVIEW

## Overview

The literature review will establish important background information concerning the endocannabinoid signaling system (ECS). By looking more closely at this receptor system, it will be established how individual activation of each receptor in this system is directly linked to the anti-cancer activity of cannabinoid challenge, the relevant research data on binding of cannabinoids to these receptors, discussion of relevant structure activity relationship data for cannabinoids of interest for these receptors, and other pertinent information concerning endocannabinoids interacting with this receptor system. Next, relevant physiological and chemical data for 2-AG will be established, followed by a review of previous synthetic methodology for 2-AG culminating in the introduction of the synthetic methodology that will be used for this research.

## The Endocannabinoid Signaling System

The ECS formally consists of the two cannabinoid receptors, $CB_1$ and $CB_2$, their endogenous ligands (the endocannabinoids), and the enzymes that catalyze the formation and subsequent degradation of the endocannabinoids themselves (Wang & Ueda, 2009). The cannabinoid receptors are of the class known as G-protein coupled receptors (GPCRs), a family of receptors widely expressed in the body and involved in a variety of signaling pathways, mainly sensory perception (predominantly vision, taste, and smell) (Sugiura, Kishimoto, Oka, & Gokoh, 2006). GPCRs are composed of seven-member

alpha-helices that are interwoven in the plasma membrane and covalently linked to a heterotrimeric G protein located on the cytosolic side of the cellular membrane. The G protein subunits consist of three members, designated alpha (α), beta (β), and gamma (γ). The alpha subunit ($G_{\alpha}$), which itself is a GTPase, has a bound GDP when no ligand or stimulus is present and constitutes the inactive form. When a ligand or stimulus hits the extracellular portion of the receptor, knock-on effects produce a conformational change in the binding pocket, causing GDP to be displaced and exchanged for GTP. This effectively activates the alpha subunit, which dissociates from the beta and gamma subunits and migrates laterally through the cellular membrane to reach and affect its target. The subunit's target varies based upon the type of $G_{\alpha}$ subunit and the location of the receptor itself (Miesfield & McEvoy, 2017). The cannabinoid receptors possess alpha subunits of the inhibitory type ($G_{\alpha i/o}$), which inhibit adenylate cyclase to impede the downstream signaling affected by the synthesis of the secondary messenger cAMP by the aforementioned enzyme. Additionally, both CB receptors are positively coupled to mitogen activated protein kinase (MAPK) signaling pathways (Howlett et al., 2002).

Another effect of cannabinoid challenge at the CB receptors, and one of primary interest for the purpose of this research, is the *de novo* synthesis of ceramide as initially reported by Guzman and colleagues (Galve-Roperh et al., 2000). Ceramide (Figure 7), which is comprised of a sphingosine backbone with a fatty acid linked to the amine at C-2, is the biosynthetic precursor to the class of integral plasma membrane components known as sphingolipids, which are composed of ceramide with a C-1 linked polar head group. The identity of the polar head group attached to ceramide specifies the type of sphingolipid. In the case where the attached group is phosphorylcholine (-$PO_3CH$-

$_2CH_2N^+(CH_3)_3$), the sphingolipid is designated sphingomyelin, which is a major component of neural cell membranes (abundantly represented in the myelin sheath). As a membrane component, sphingomyelin has little to no bioactivity, but this is not the case with ceramide, which has been demonstrated to be integral in signaling pathways connected to cell survival and apoptosis (Green, 2000).

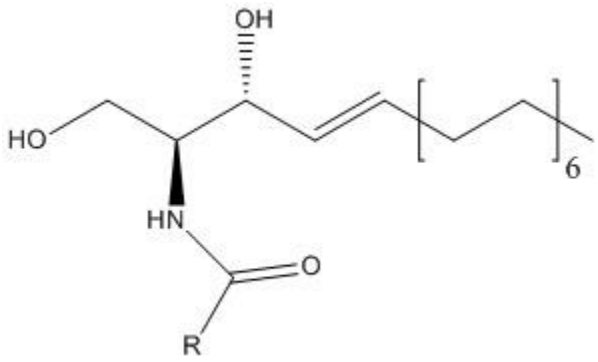


*Figure 7*. Generalized structure of ceramide.

One of the primary means by which ceramide is generated in the cell is through the hydrolysis of sphingomyelin via sphingomyelinase into phosphorylcholine and ceramide. This activity has been demonstrated to be linked with $CB_1$ activation in primary astrocytes and C6 glioma cells through functional coupling of the $CB_1$ receptor with the factor associated with neutral sphingomyelinase action (FAN) (Guzman, Galve-Roperh, & Sanchez, 2001). This enzyme-catalyzed generation of ceramide mediated through FAN occurs within minutes of cannabinoid challenge. Additionally, a second wave of ceramide generation occurs with prolonged cannabinoid challenge, beginning 72 hours after treatment and peaking after 118 hours and was "closely related to the apoptotic death of glioma cells" (Galve-Roperh et al., 2000). This second wave of

ceramide production was determined to be generated through *de novo* synthesis of ceramide mediated by the enzyme pathway beginning with, and rate-limited by, serine palmitoyltransferase (SPT). This mechanism was determined through measurement of ceramide generation in the second peak time frame coupled to apoptosis of C6 glioma when treating the cells with THC in the presence of known inhibitors for sphingomyelinase and SPT. The results of this study indicated that the second wave of ceramide synthesis was generated by the *de novo* pathway mediated by SPT. Furthermore, the authors indicated that this activity was preserved using $CB_2$ selective agonists in treating human leukemia cells via p38-MAPK activation and subsequently published those results (Herrera, Carracedo, Diez-Zaera, Guzman, & Velasco, 2005). The key take-away from this line of research is that both CB receptors are linked into signaling cascades that activate pro-apoptotic effects through *de novo* ceramide generation. This mode of action for the growth inhibition and apoptosis of a variety of cancer lines has been demonstrated across multiple independent studies, although not for both receptors in every case (Table 1).

Table 1

*Pro-apoptotic Effect of Cannabinoids on Different Cancer Lines. (Adapted from Velasco et al., 2012).*

| Cancer cell | CB receptor | Ceramide synthesis | Apoptosis | Reference |
|---|---|---|---|---|
| Glioma | 1 and 2 | X | X | Salazar et al. (2009) |
| Pancreatic | 2 | X | X | Salazar et al. (2009), Carracedo et al. (2006) |
| Hepatocellular carcinoma | 2 | X | X | Vara et al. (2011) |
| Breast | 2 | ND | X | Caffarel et al. (2010) |
| Rhabdomyo-sarcoma | 1 | ND | X | Oesch et al. (2009) |
| Mantle Cell lymphoma | 1 and 2 | X | X | Gustafsson et al. (2006) |
| Prostate | 2 | X | X | Mimeault et al. (2003), Olea-Herrero et al. (2009) |
| Leukemia | 2 | X | X | Herrera et al. (2006), McKallip et al. (2002), Jia et al. (2006) |
| Melanoma | 2 | ND | X | Blazquez et al. (2006) |
| Lung carcinoma | ND | ND | X | Preet et al. (2008) |

X = confirmed present; ND = not determined

Furthermore, several lines of evidence indicate that cannabinoid challenge is linked with an increase in endoplasmic reticulum (ER) stress, mediated through p8 (NUPR1), a transcriptional regulator that affects downstream targets critical to cell survival, such as the Akt signaling pathway (Velasco et al., 2012). The stress response itself is complex and most adequately understood through the processes encompassing the unfolded protein response (UPR) of the ER. These processes are upregulated in response to cellular stressors, such as $Ca^{2+}$ depletion, oxidative injury, viral infections, high-fat diets, hypoglycemia, the nutritional status of the cell, and certain anti-cancer agents (Schröder & Kaufman, 2005). Simply put, when the workload of the ER is outpaced by demand, the UPR is activated to either restore balance by increasing protein-

folding capacity and destruction of unfolded/misfolded proteins, or if the stress cannot be controlled or abrogated, then Bcl-2 mediated pathways can lead to apoptosis. This is significant because the cannabinoid-mediated destruction of cancer cells is intimately linked with stress induced autophagy. The p8 mediated pathway ultimately leads to inhibition of the pro-survival kinase Akt (protein kinase B, also called the PKB pathway), which in turn inhibits the mechanistic target of rapamycin complex 1 (mTOR1), which then stimulates apoptosis via autophagy. Autophagy is upstream of programmed cell death; blocking autophagy prevents cannabinoid-induced apoptosis, but not the reverse (Salazar et al., 2009; Vara et al., 2011).

Cannabinoids also possess general anti-proliferative and anti-metastatic effects due to inhibition of the vascular endothelial growth factor (VEGF) pathway in addition to modulation of vital metalloproteases and associated inhibitory factors that are crucial for adhesion and invasion of transformed cells (Velasco et al., 2012). In aggregate, these experimental observations highlight an important feature of cannabinoids, noted previously, that makes their study highly intriguing but also vexing; they have a plethora of cellular targets, not limited to the CB receptors and not all of them pertinent or specific to all cannabinoids. A prime example is that of anandamide, which has been demonstrated to be a partial-to-full agonist of the transient receptor potential cation channel subfamily V member 1 (TRPV1), a "nonselective cation channel that integrates multiple noxious stimuli and is associated with the pathophysiology of various major diseases" (Ross, 2003). In simpler terms, TRPV1 is the neurological receptor that mediates the effects of capsaicin, the component in chili peppers that gives them their characteristic properties of being irritating and "hot.” 2-Arachidonoyl glycerol has no

activity at this receptor, nor do any other cannabinoids. It is this reality that makes trying to assign activities specifically to CB receptor activation sometimes confounding but obviously crucial when attempting to parse effects due to stimulation of the ECS.

Similar to all other GPCRs, the specific tissue location of the cannabinoid receptor dictates the ultimate physiological function(s) of its activation. Cannabinoid receptor distribution occurs in two primary systems: the central nervous system (CNS) and in immune tissues (Table 2). The first of the discovered cannabinoid receptors, $CB_1$, was found to be widely distributed in the central nervous system (hence its previous designation as the "central" receptor) with the highest densities occurring in the cortex, hippocampus, basal ganglia, and cerebellum, in addition to cervical ganglia and peripheral autonomic nerve fibers, such as those in the bladder, heart, and vas deferens (Di Marzo, 1998). $CB_1$ is also sparingly distributed in the hypothalamus and spinal cord and is mostly absent in the respiratory centers of the brainstem. The distribution of $CB_1$ is noteworthy in the sense that, being presumed as the primary mediator of psychoactivity, the locations where the receptor is localized correlate with known physiological effects of smoking marijuana, and the absence of receptors in the respiratory centers may explain, in part at least, why THC and other cannabinoids have a low lethality (Thompson, Rosenkrantz, Schaeppi, & Braude, 1973). Curiously, although $CB_1$ was initially found to be exclusive to the central nervous system, receptor transcripts for $CB_1$ have been found to be expressed in immune tissue (specifically the spleen) at a magnitude approximately 100-fold less than $CB_2$ (Schatz, Lee, Condie, & Kaminski, 1997), making the initial hypothesis of a neat divide between the two receptors' domains murky. Across studies measuring overall receptor density, $CB_1$ is typically found to be

greater than 1 pmol/mg of tissue, making it the most abundantly expressed GPCR in neuronal tissue and placing it on the same level as common ionotropic receptors. The specific localization of the receptor varies between broad, uniform expression, such as in the cerebellum, but in most neurons expression of $CB_1$ is exclusive to synapses, specifically the pre-synaptic terminals (Howlett et al., 2002). In addition to previously mentioned shared downstream targets of $CB_1$ activation (namely adenylate cyclase and MAPK), cannabinoid stimulation of $CB_1$ also affects various ion channels, through $G_{\alpha i/o}$ interactions, leading to activation of A-type and inwardly rectifying potassium channels and inhibition of N-type and P/Q-type calcium channels (Howlett, 2005).

Table 2

*Cannabinoid Receptor General Information. (Adapted from Howlett et al., 2002).*

| | $CB_1$ | $CB_2$ |
|---|---|---|
| Amino acids | 472 (Human) | 360 (Human) |
| Expression | CNS, peripheral autonomic neurons, sparingly located outside CNS | Immune tissues (spleen, tonsils, lymphocytes), expression in CNS in neuroinflammatory disease |
| 2-AG $K_i$ range | 58.3 - 472 nM | 145 - 1400 nM |
| Anandamide $K_i$ range | 61 - 543 nM | 371 - 1940 nM |
| Primary activity | Neuromodulation, neural network development | Immunomodulation |

The distribution, overall density, and activity of the $CB_1$ receptor hints at one of its primary physiological purposes, namely attenuation or modulation of neurotransmission (Bisogno et al., 2003). Neurotransmitter binding onto a post-synaptic receptor generates a response, either through ion channel opening creating a transient imbalance in the normal ionic content of the terminal axon or stimulation of secondary messenger production. This stimulates the transient production and release of

endocannabinoids into the synaptic cleft where they act as retrograde messengers and complex with $CB_1$ resulting in the inhibition of voltage-gated $Ca^{2+}$ ion channels and subsequent termination of neurotransmitter release (Figure 8). Via neuroblastoma cultures treated with ionomycin, it has been demonstrated that endocannabinoid release is specifically linked to calcium influx, and the stimulation of calcium-dependent lipases (Bisogno et al., 1997); however, calcium independent synthetic routes mediated via protein kinase C and A (both in the presence and absence of thrombin) have also been elucidated in conjunction with sensory neuronal pathways (Vellani et al., 2008), demonstrating that transient neuronal endocannabinoid synthesis can be triggered by a number of different means.

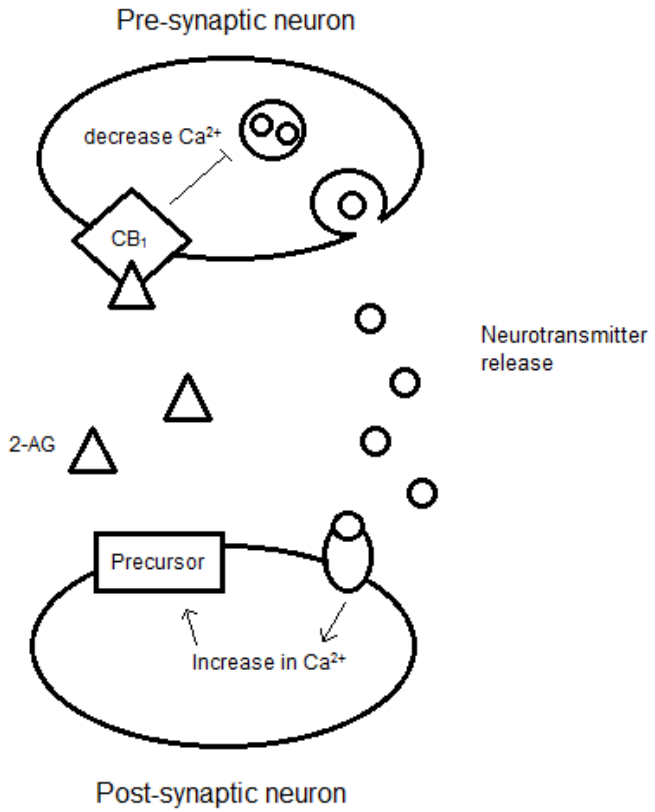


*Figure 8*. Diagram of endocannabinoid release in neurotransmission.

$CB_1$ receptors are also implicated in proper neuronal network development during brain growth, and research has shown that diacyl glycerol lipase (a key enzyme in the synthesis of 2-AG) expression is required for proper axonal growth and development and correlates strongly with shifts in receptor expression from brain development in children to expression of the receptor as a signal modulator in adulthood (Bisogno et al., 2003). As has been discussed previously, the receptor is hypothesized to primarily mediate the psychotropic activity of recreational use of cannabinoids and as such is implicated in the regulation of cognition, memory, and motor activity as well (Sugiura et al., 2006).

$CB_2$ receptor expression occurs almost exclusively in immune tissues, with the first identification of the $CB_2$ receptor occurring in mouse spleen cells (Kaminski, Abood, Kessler, Martin, & Shatz, 1992). Autoradiographic studies have identified $CB_2$ receptor expression in multiple lymphoid organs. mRNA for $CB_2$ is found in the spleen, thymus, tonsils, bone marrow, pancreas, splenic macrophage/monocyte preparations, mast cells, peripheral blood leukocytes, and in a variety of cultured immune cells, in addition to the prevalence in hematopoietic lineages including myeloid, macrophage, mast, B-lymphoid, T-lymphoid, and erythroid cells. The density of the receptor in spleen and tonsils is on the same order as that of $CB_1$ expression in the central nervous tissues (on the order of 1 pmol/mg), but expression in human blood cell populations is tiered, following the order: B lymphocytes > natural killer (NK) cells >> monocytes > polymorphonuclear neutrophils > T8(cytotoxic) lymphocytes > T4(helper) lymphocytes (Howlett, 2005). Receptor location/concentration within these various organs, tissues, and cells is not uniform, and the exact location within each is informative of activity but is beyond the

scope of this research to dissect further. $CB_2$ is the primary mediator of the immunomodulatory effects of cannabinoid use and, owing to the complex and integrated nature of the immune response in general, a clear picture of the receptor's role in immunomodulation is a slowly emerging reality. For instance, $CB_2$ activity is achieved via the same general pathways as $CB_1$, i.e., through the $G_{\alpha i/o}$ inhibition of adenylate cyclase and stimulation of MAPKs; however, MAPK stimulation via $CB_2$ is complicated by the data that, in general, endocannabinoids stimulate MAPK activity (2-AG to the full extent, anandamide partially), but cannibinol, a phytocannabinoid derivative of cannabidiol (CBD), one of the primary components of *C. sativa*, actually inhibits the ERK family of MAPKs (Paralaro, Massi, Rubino, & Monti, 2002). The specifics of how cannabinoids affect immune function quickly becomes difficult to parse, except for those with an intimate working knowledge of the immune system and could account for hundreds of pages of content in its own right. For the sake of comprehension, the primary effects of $CB_2$ receptor activation can be rudimentarily generalized as follows.

First, the overall effect of $CB_2$ receptor activation seems to be the positive regulation of immune function via the cAMP signaling cascade, although this is muddled somewhat by the fact that $CB_1$ receptor expression does occur within immune tissues, to an extent 10-100 times less than $CB_2$ receptor expression, and $CB_1$ has been demonstrated to be dually linked, in some cases, to both inhibitory and stimulatory $G_\alpha$ subunits (Parolaro et al., 2002). This activity needs to be taken into account when drawing a formal picture of cannabinoid effect on immunomodulation and is further complicated by the $G_{\alpha/io}$-dependent and $G_{\alpha/io}$-independent stimulation of MAPKs and the duplicitous nature of specific cannabinoids to inhibit or stimulate those signaling

pathways. Regardless of the complicating factors, a generalization that can be made is that cannabinoid challenge has the effect of antagonizing immune cell activation, especially in the early stages of such activity. For instance, anandamide generally inhibits T and B cell proliferation, as does 2-AG, but inhibition by 2-AG appears to be critically dependent on overall cell density, which was attributed to a possible positive effect achieved through the generation of a 2-AG metabolite with immunostimulatory effects occurring as a result of increased metabolism at the higher cell density (Parolaro et al., 2002). In addition, THC treatment of murine specimens has been demonstrated to cause direct changes in immunological profile and induce mobilization of myeloid-derived suppressor cells, which typically function in chronic inflammatory conditions, particularly those that derive from neoplastic disorders (Mantovani, 2010). Selective activation of the $CB_2$ receptors has also been demonstrated to induce apoptosis of an array of different immune cell types, which has been proposed to be involved in the immunosuppressive effects of cannabinoid challenge (Parolaro et al., 2002). Given these data, it seems that cannabinoid challenge at $CB_2$ could be stimulatory for tumor growth (and it is indeed implicated as being a culprit for that effect); however, in certain cancer types (pancreatic, breast, and hepatic) $CB_2$ antagonists abrogate the anti-cancer effect of cannabinoid treatment, which seems to contradict the evidence that $CB_2$ activation is probably harmful to the natural anti-cancer function of the immune system (Velasco et al., 2012). Taken in aggregate, the data surrounding the effects of $CB_2$ receptor activation on immune function indicate that receptor activation leads ultimately to immune suppression in general, but there is also strong evidence that cannabinoid challenge elicits unique effects on transformed (cancerous) vs non-transformed cells (Velasco et al.,

2012). The paradigm of immune suppression linked to $CB_2$ activity is one that is under active investigation and continuous refinement, and it is vital to keep the unique peculiarities associated with the structurally, and in some cases functionally, diverse cannabinoids in mind when assessing studies concerning this topic.

Both CB receptors are generally found on average to be upregulated in cancerous tissue compared to non-cancerous tissue (see Table 3), the exact pathway by which this occurs being currently unknown. One interpretation of the correlation between receptor upregulation and malignancy might be an increased need or benefit for ECS signaling for uncontrolled growth, which is not exhaustive of the possibilities, but if true it might explain, at least in part, data that indicate activity at CB receptors is pro-tumorogenic. Conversely, there are data that link receptor knockout and increased expression of degradation enzymes of the ECS pathway (explored further later), to the development and progression of aggressive cancer types (Velasco et al., 2012). Fundamentally, this means that utilizing the ECS could result in either one of two outcomes when treating cancer cell populations. Either positive outcomes could occur, in this case, positive being cell cycle arrest or cell death, or negative, meaning accelerated growth compared to control or no effect. There is already a significant data pool that pairs the ECS with pro-tumorogenic (negative) and anti-tumorogenic (positive) outcomes depending on different experimental conditions, primarily the specific cancer cell being studied, the cannabinoids being assayed, and the concentration of the cannabinoid in the experimental assays or growth conditions (Velasco et al., 2012). The Flygare and Sander (2008) article serves as an excellent introductory resource to this growing body of work (see Table 1).

Table 3

*CB Receptor Upregulation in Different Cancer Types. (Adapted from Flygare and Sander, 2008).*

| Cancer sub-type | $CB_1$ | $CB_2$ |
|---|---|---|
| Astroglia | + | = |
| Breast | - | ++ |
| Mantle cell lymphoma | ++ | ++ |
| Acute myeloid leukemia | N/A | ++ |
| Hepatocellular carcinoma | ++ | ++ |
| Non-melanoma skin cancer | = | = |
| Prostate | ++ | ++ |

(-) partially downregulated, (=) no change, (+) partially upregulated, (++) upregulated

Determining the impact of different cannabinoids at CB receptors across different cancer cell types has been straightforward; however, determining the effect of cannabinoid concentration, specifically for 2-AG and other endocannabinoids, has not. The first issue, which will be expounded upon later, is the inherent labile nature of the ester moiety in 2-AG. Whether through hydrolysis or isomerization into the 1 or 3 position, the affinity for the receptor can be affected, if not abrogated, by these natural chemical transformations. In general, the highly lipophilic nature of most cannabinoids complicates all *in vitro* studies of affinity assays for receptor binding, given that the CB receptors are membrane bound and thus most assays must address the issue of membrane intercalation as a complicating factor in accurately assaying cannabinoid concentrations in solution across the time necessary to perform the assay.

The high variability across various studies measuring CB receptor affinity for 2-AG and other endocannabinoids reflects these issues. Table 2 presents $K_i$ values, or rather a range of values, referenced from Howlett et al. (2002). The range is indicative of minima and maxima derived from various studies included in that reference. The data

speak for themselves; however, it is prudent to add a few pertinent background details to flesh out the quantitative data. In general, the literature surrounding binding assays for 2-AG and anandamide indicate that anandamide is in fact a partial agonist for both $CB_1$ and $CB_2$ whereas 2-AG is a full agonist (Sugiura, Kobayashi, Oka, & Waku, 2002). This is a curious discovery, and one of the reasons 2-AG was selected for synthesis over anandamide for the current research. Anecdotally, when reviewing the literature, the general trend reported by researchers is that anandamide has a higher affinity for both CB receptors compared to 2-AG, however, looking at the range of binding affinity values in aggregate data (see Table 2), this claim is not supported. Most likely, sensitivity of assays to experimental conditions and the difficulties associated with assaying these compounds not addressed by some experimental methodologies is contributing to the disparity between some researchers claims and the breadth of available data. A prime example of this is a study measuring the binding affinity of 2-AG and anandamide at $CB_1$ by Gonsiorek et al. (2000). When measuring the $K_i$ of 2-AG and the $K_i$ of anandamide against CP-55,940 (Figure 2), the reported $K_i$ values were 949 ± 270 nM and 795 ± 46 nM, respectively, whereas $EC_{50}$ values were 38.9 ± 3.1 nM and 121 ± 29 nM, respectively, from the same experimental conditions (Gonsiorek et al., 2000). The results demonstrate clearly that 2-AG is a more potent activator of $CB_1$ but has a lower affinity compared to anandamide, confusingly however, the authors claimed that both 2-AG and anandamide were full agonists at $CB_2$, which runs directly counter to the consistent message of numerous publications from both Mechoulam and Sugiura that anandamide is only a partial agonist. For example, one of the first studies published concerning the agonist status of 2-AG at $CB_1$ by Sugiura indicated that a response (increase in

intracellular $Ca^{2+}$) was detected from 2-AG administration at a concentration as low as 0.3 nM, in line with potent $CB_1$ selective agonists, such as CP-55,940, whereas anandamide did not elicit a full response at any concentration (Sugiura et al., 1999). The disparity in results reported from multiple labs across various studies highlights the need for refined and continued studies of receptor interactions, at least if a highly accurate measure of CB receptor affinity for their natural ligands is desired.

A helpful development for assessing CB receptor-ligand interactions is the elucidation of the crystal structure of $CB_1$, which was recently reported (Hua et al., 2016). The receptor was crystallized as a complex with AM6538 (Figure 9), a rimonabant derivative synthesized specifically for the crystallization study with high affinity for the receptor.

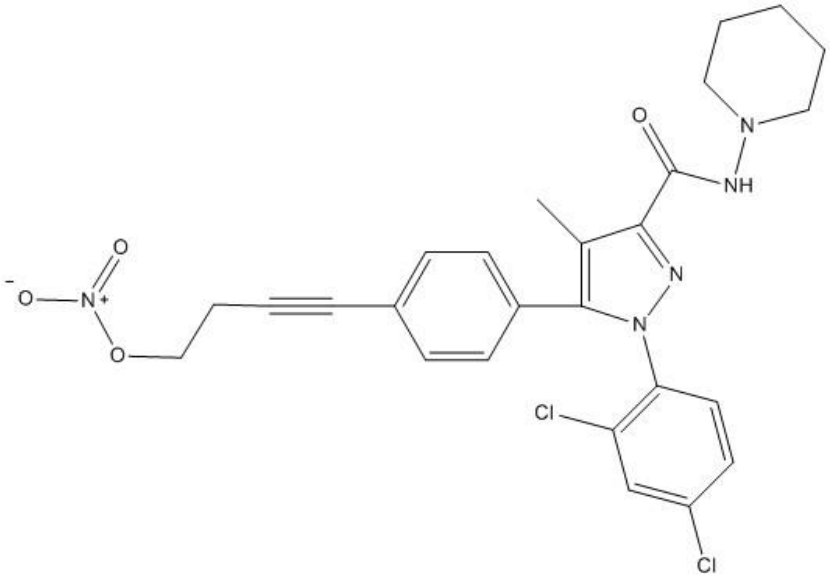


*Figure 9.* AM6538.

Additionally, to facilitate crystallization of the receptor-ligand complex, truncation of the $CB_1$ receptor was required, which bears keeping in mind prior to

extrapolating on pertinent binding pocket elements. To facilitate discussion, it is prudent to parse AM6538 into three basic "arms" (Figure 10). From the pyrazole ring core, the arms essentially designate the three different binding pockets of $CB_1$. The 2,4-dichlorophenyl ring constitutes arm 1, the 4-aliphatic chain substituted phenyl ring constitutes arm 2, and the piperidin-1-ylcarbamoyl group constitutes arm 3.

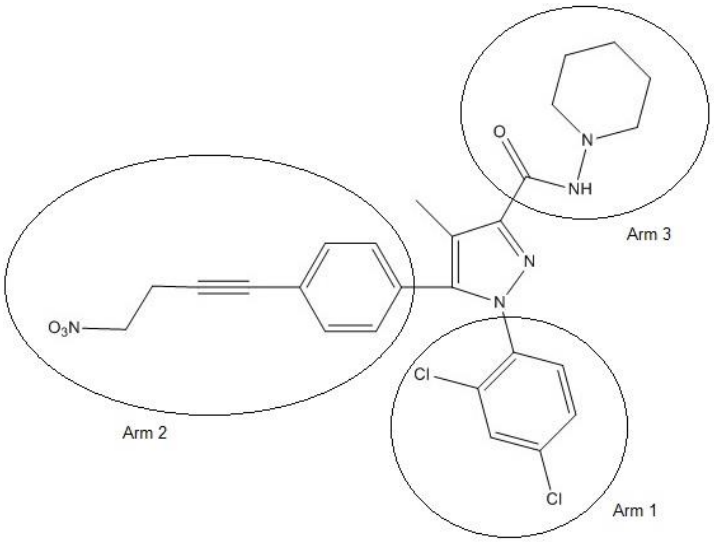


*Figure 10*. AM6538 "arms".

It is somewhat difficult to look at AM6538 and mentally superimpose how the natural ligands 2-AG and anandamide interact with the pockets outlined by the arms of this compound. As an inverse agonist AM6538 binds $CB_1$ in an inactive state, but the study authors were able to use molecular modeling software to predict how a suite of agonists most likely interacts with the binding pocket. Giving the simplest distillation, the hydrophilic head of each endocannabinoid sandwiches itself into the pocket occupying the space of the pyrazole core and the shallow pocket of arm 3, formed by the N-terminal portion of the receptor and extracellular loop 2, while the aliphatic tail of the arachidonic acid folds itself into a similar "C" shape as that in Figure 4 and sequesters itself into the

deep pocket of arm 2. Arm 1 is predominantly involved in antagonist binding and so has little to no interaction in agonist binding models (Hua et al., 2016).

Structure Activity Relationship (SAR) data on anandamide shows that substitution of the hydroxyl head of the ethanolamide group with chlorine or fluorine sharply increases $CB_1$ selectivity, by approximately 10 fold, whereas introduction of variation into the N-alkyl group also caused impressive gains in selectivity of a similar magnitude in $K_i$ for $CB_1$ when looking at substitution of the *N*-ethyl group for isopropyl or *n*-propyl, demonstrating that it is possible to modify the endogenous ligands for increased selectivity (Mechoulam et al., 1998). To date, no crystallographic studies have successfully isolated $CB_2$, but expansive SAR studies with selective agonists have helped to fill in a rough picture of the binding pocket (unfortunately SARs for 2-AG interactions with CB receptors are scarce, but anandamide structural requirements can be loosely translated to 2-AG in some cases). These studies are providing critical insight into receptor-ligand interactions for the CB receptor class, especially as the understanding of nascent putative CB receptors has grown with time (Pertwee et al., 2010).

The entirety of the preceding data demonstrates that cannabinoids in general represent compounds of interest for research, given their physiological effects on cancer cells, and establishes that there are good reasons for pursuing synthesis of endocannabinoids, specifically 2-AG, given the absence of accurate data for receptor interactions and the relative absence of information on this endocannabinoid compared to other endocannabinoids. More specific background information on 2-AG, the endocannabinoid of focus for this research, will now be discussed.

## 2-Arachidonoyl Glycerol Biosynthesis and Degradation

The biosynthesis of endocannabinoids following a stimulus occurs through different enzymes and intermediates depending on the endocannabinoid in question. Because the nature of the current thesis research is concerned with the chemical synthesis of 2-AG, the remainder of this chapter will focus exclusively on this endocannabinoid, although there are many generalizations and commonalities between the pathways for the synthesis of 2-AG and anandamide, one obviously being the dependence on arachidonic acid containing intermediates (Mechoulam et al., 1998). Figure 11 gives a template that will be used in describing the various ways that 2-arachidonoyl glycerol can be biosynthesized from a variety of precursors. Taking tissue measurements of 2-AG can be complicated by the collection methods employed. In the case of decapitation of murine specimens to measure tissue concentrations, 2-AG levels swell to 15 times their normal tissue concentration, normal tissue concentration being determined from flash freezing whole mice specimens prior to preparing tissue samples for analysis. Variation in tissue concentrations of 2-AG between sub-compartments of rat and mice brains are within 1.0 to 10 nmol/g of tissue concentrations, which are roughly correlated with reported human values which tend to be an order of magnitude less (Sugiura et al., 2006). As will be discussed further, free 2-AG will be short lived in a physiological environment, but even more fundamentally, "free" 2-AG might be something of a misnomer.

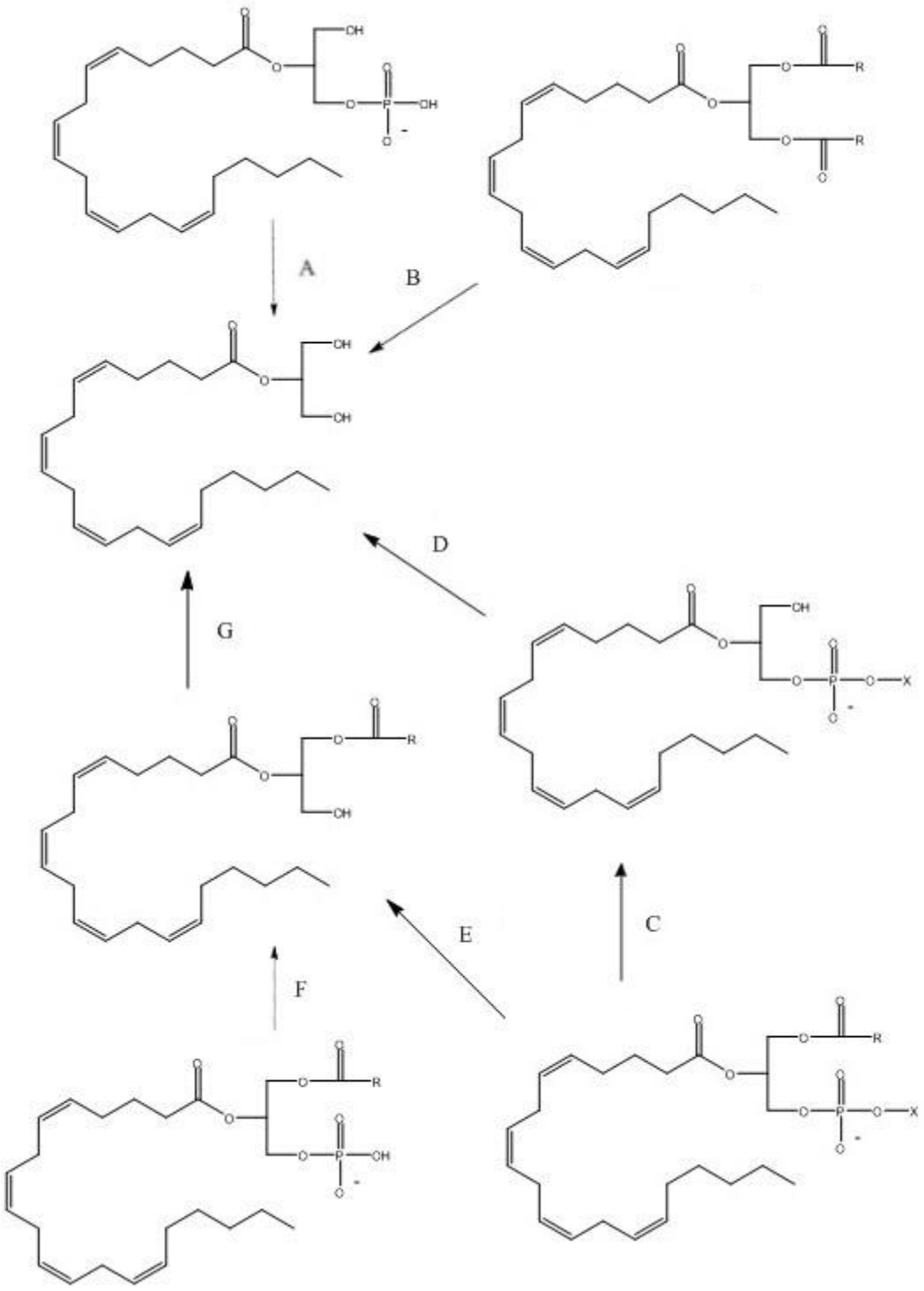


*Figure 11*. Biosynthetic routes for 2-AG from various precursors.

2-AG is one of the more abundant monacylglycerols in the brain. Most 2-AG is produced from the hydrolysis of diacylglycerols (DAGs) containing arachidonic acid in the 2 position by an *sn*-1 selective DAG lipase (step G in Figure 11). Pre-cursors for DAGs come from phosphoinositides (PI) that are cleaved of their phosphate moiety by PI-selective phospholipase C (step E in Figure 11) or through the activity of a similar enzyme on phosphatidic acid (step F in Figure 11). Step C depicts the activity of phospholipase $A_1$ converting a phosphoinositide to a lysophospholipid, and then in step D (or A) subsequent conversion of the phospholipid to 2-AG via lysophospholipase C. Step B demonstrates the possibility of production of 2-AG from a triglyceride precursor, which would be a less immediate source (Bisogno, Ligresti, & Di Marzo, 2005). Path G is the "on-demand" pathway for 2-AG synthesis.

The lipopathic nature of the cannabinoids suggested potentially that their diffusion into the synapse was passive in nature, however, rapid removal from the intracellular space (whether expulsion or re-uptake and inactivation) is a necessary feature of a receptor-mediated process and suggested some transporter. Evidence for this transporter was first produced in studies examining anandamide cellular uptake and the fact that it was a saturable, temperature-dependent, and inhibitable process (Di Marzo et al., 1994). The proposed transporter was named anandamide membrane transporter (AMT) and was shown to potentially facilitate transport of 2-AG, along with a small host of additional cannabinoids (Bisogno et al., 2005). Inactivation of 2-AG is achieved primarily via two enzymes. The enzyme fatty acid amide hydrolase (FAAH) can cleave 2-AG to arachidonic acid and glycerol (the two primary components from enzymatic hydrolysis) but is weakly effective towards this endocannabionid and ablation does not

lead to an increase in 2-AG concentration like it does anandamide. Rather, monoacylglycerol lipase (MAGL) in either membrane-bound or soluble form, is primarily responsible for cleaving 2-AG to arachidonic acid and glycerol and is strongly associated with $CB_1$ receptor localization (Bisogno et al., 2005).

One of the peculiar aspects about hydrolysis of the endocannabinoids is the liberation of arachidonic acid, which is a polyunsaturated fatty acid that serves as the precursor to eicosanoids, a diverse array of biologically active compounds broadly involved in pain and inflammation. The full scope of effects from the localized increase in concentration of this fatty acid have not been fully explored, however, localized arachidonic acid concentrations have been shown to be capable of mediating $Ca^{2+}$ stimulated transients, perhaps further feeding into the primary function of the compound in its monoglycerol state (Damron, Wagoner, Moravec, & Bond, 1993). The production of this physiologically diverse precursor is an effect that must be considered when drawing comparisons between relevant CB agonists, since most synthetic and plant-based cannabinoids are not metabolized using the same enzymes of the ECS system but rather utilize common metabolic enzymes, such as the cytochrome P450 family, to be converted into biologically inactive forms and excreted. This is one of the primary reasons that exploring the activity of endocannabionids is of interest, as their unique integration with existing biological "circuits" may confer to them unique capacities that would otherwise be absent, especially when looking at exposure of CB receptors to endocannabinoids in disease states where inflammatory and nociceptive processes are occurring.

## 2-Arachidonoyl Glycerol Stability

As noted previously, the stability of 2-AG in aqueous solutions is subject to many factors. Specifically, three key processes, highlighted in Figure 12, contribute to the progressive and nearly complete conversion or loss of 2-AG, irrespective of enzymatic action. Rouzer and colleagues published an experimental assessment of 2-AG stability looking at various pertinent parameters for experimental assays or other procedures and noted important upper limits for time-based procedures, as well as other important considerations (Rouzer, Ghebreselasie, & Marnett, 2002). In the case of oxidation and ester hydrolysis, the authors noted that only experiments "exceeding 4 hours" would be problematic for loss of function due to natural sample loss. However, acyl migration could occur at rates that "would be significant in the context of experimental protocols of an hour or less." Further elaboration of what was meant concerning this revealed that migration of the acyl chain to the first or third position on the glycerol molecule is a thermodynamically favored migration, and so at equilibrium the 1(3)-monoglycerol will constitute 89 to 95% of the monoglycerol present (Rouzer et al., 2002). The speed of this process was critically dependent on the presence or absence of serum. In the presence of serum, the half-life for the conversion of 2-AG to 1(3)-AG was approximately 2.3 min, and in the absence of serum the same reaction half-life was 10 min. Study authors postulated that this might be due to the presence of albumin in serum and verified that albumin binding was responsible for the increased rate in conversion. The consequences of these data for developing experimental methods is obvious, as is the implication in potentially using the compound in formulations. One further finding that was perplexing was the steady loss of 2-AG due to processes unknown. It was determined that 2-AG will

actually bind non-selectively to glass surfaces, and natural loss to glass containers (on the order of 10% of total sample lost per hour) was to be expected (Rouzer et al., 2002).

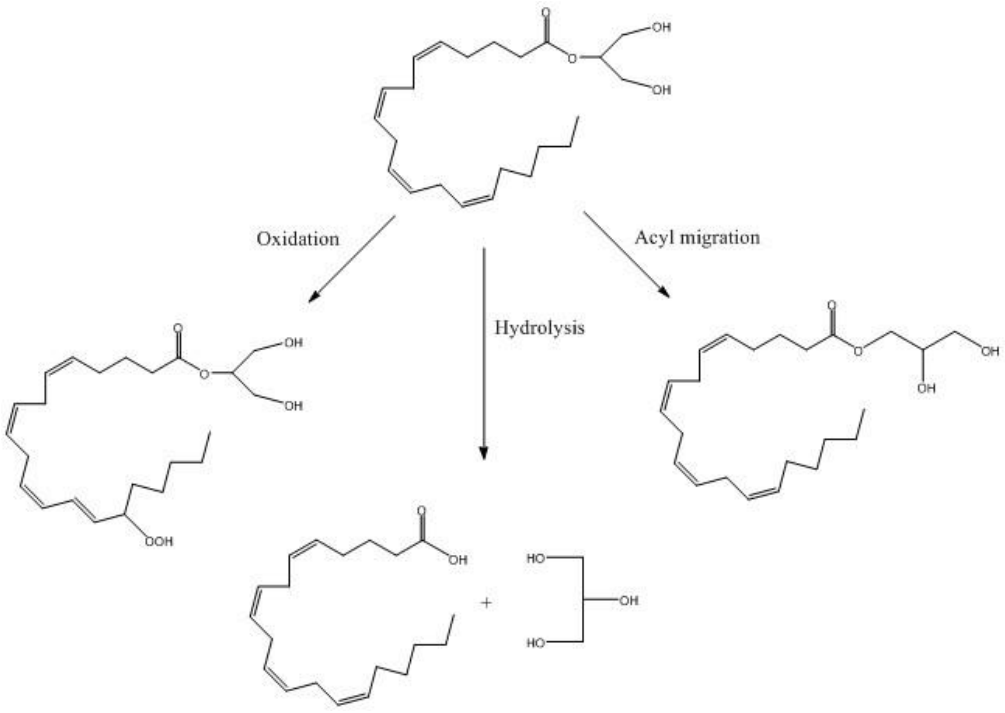


*Figure 12*. 2-AG physiological transformations.

The pertinent results from Rouzer et al. (2002) are summarized in Table 4. These instabilities in 2-AG in a natural cellular environment are major contributors in the dearth of consensus in the published information concerning this compound, therefore, developing knowledge of the chemical susceptibility of 2-AG will greatly help to inform the discussion concerning synthetic strategy moving forward.

Table 4

*Sources of 2-AG Loss. (Adapted from Rouzer et al., 2002).*

| Source/condition | Measure of loss |
|---|---|
| Oxidation | Stable up to 6 hrs at 37 °C |
| Hydrolysis | Stable up to 6 hrs at 37 °C |
| Acyl migration | In buffer (pH 7.4): $t_{1/2}$ = 10 min<br>In buffer (pH 7.4) with 10% FBS: $t_{1/2}$ = 2 min<br>Base catalyzed ($k_{cat}$ = 78,000 M/min) |
| Loss to glass/plastic surface adsorption | Approximately 10% loss/hr |

## Synthetic Pathway Proposal and Review of Previous Methodology

Previous publications concerning 2-AG synthesis are fairly sparse. Han and Razdan (1999) employed the Corey method for forming silyl ethers, using triisopropylsilyl chloride to protect glycerol. The authors esterified their protected glycerol to an activated arachidonic acid using 4-dimethylaminopyridine (DMAP), 1-(3-dimethyl-aminopropyl)-3ethylcarbodiimide hydrochloride (EDCI), and dichloromethane at ambient temperature. Subsequent deprotection was achieved using a modified *tert*-butylammonium fluoride (TBAF) process employing an acetate buffer kept at -20 °C over night. The reported yield for 2-AG was 59%. The need to bring reaction conditions to lower overall temperatures is a common theme reported in publications. For instance, the method employed by Suhara and colleagues sought to create a 1,3-dioxane ether complex through glycerol that could be selectively cleaved to form the 2-monoglycerol on demand. The methodology was inspiring, and the yield was improved, but still underwhelming, peaking at 69% (Suhara et al., 2000). A more recent publication from Cartoni et al. (2004) critiqued what was seen as the established sensible synthetic route (Figure 13). The appeal of their method comes from having pared the number of

individual synthetic steps down to two, by addition of a pre-protected glycerol in the form of 1,3-dibenzyloxy-2-propanol, and then subsequently deprotecting. The deprotection was screened with various reaction conditions, but the best method only yielded a 70% recovery (with returns as low as 30%) after deprotection (Cartoni, Margonelli, Angelini, Finazzi-Agro, & Maccarrone, 2004). Given these outcomes, older methodologies are still clearly viable, and it is from the principle scheme in Figure 13 that the synthetic route for the current research was drawn.

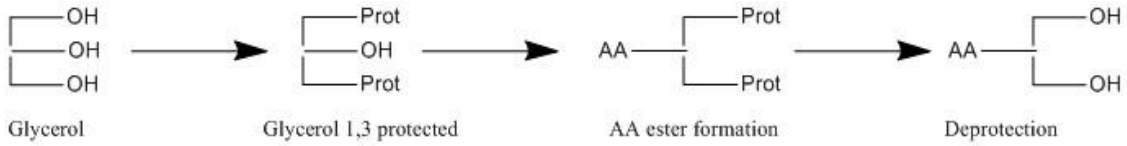


*Figure 13*. Classic synthetic scheme for 2-AG.

The Han synthetic method, which was essentially a retooling of a method developed by E. J. Corey in 1972 (Corey and Venkateswarlu, 1972) was sound, but impeded by issues with the chosen protecting group. Silyl ethers are susceptible to attack by the extremely basic fluoride anion and an acetate buffer was employed, presumably, to ameliorate formation of 1(3)-AG by keeping pH < 7. The trade-off for stabilization of the product on the overall reaction kinetics appears to be manageable (assuming overnight in the Han methodology does not constitute a time period over eight hours) and if the protecting group were more, or at least as, labile, it seems that it should be possible to tweak the deprotection conditions and return a better result. With that in mind, *tert*-butyldiphenylsilyl chloride was chosen to form a silyl ether protecting group for the synthesis of 2-AG.

Figure 14 gives a simplified outline of the proposed synthetic scheme for 2-arachidonoyl glycerol for the current research. The initial proposed synthetic method employed dihydroxyacetone (DHA) as a way to ensure protection specificity, and so added additional steps that made the use of DHA less appealing as a starting material once it was realized that the protecting group was specific for primary alcohols by a wide margin in the original reaction conditions (Patschinski, Zhang, & Zipse, 2014); however, as will be elaborated later, it was found that the doubly protected DHA could be conveniently separated from DMF called for in the original Corey procedure. DMF is unfortunately one of the few polar, aprotic solvents that can dissolve all the necessary reagents for the synthetic procedure in required amounts, and efficient and clean removal of the solvent can be a beneficial step to include if thinking of scale up.

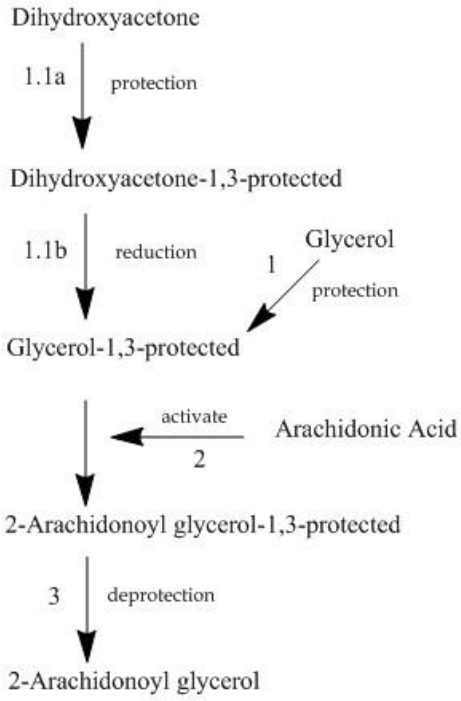


*Figure 14*. Simplified synthetic scheme flow chart.

Based upon the breadth of data discussed thus far, the reasons for pursuing this research should be readily apparent. Cannabinoids are compounds with demonstrated anti-cancer effects on a variety of cancer sub-types that act upon a unique class of receptors, and there is potential in developing and building upon previous synthetic methodologies to allow further experimentation with these compounds to fully probe their efficacious properties and potential. 2-AG in particular is a target of imminent interest for synthesis due to the relatively unexplored potential of the endocannabinoids as therapeutic agents compared to the other cannabinoids, and the relatively mixed data on the compound as a whole.

# CHAPTER III

# MATERIALS & METHODS

## Materials

Materials were primarily acquired from Sigma-Aldrich and American Type Culture Collection (ATCC). Reagent grade (purity ≥ 95%) dihydroxyacetone (DHA) (D107204), *tert*-butyldiphenylsilyl chloride (*t*-BDPSCl) (190502), imidazole (I5513), dimethyl formamide (DMF) (PHR1553), acetone (650501), acetonitrile (271004), dichloromethane (DX0831), chloroform-d (494275), chloroform (CX1054), methanol (34860), denatured ethanol (187380), ethanol (absolute and reagent grade) (E7023 and 362808), thionyl chloride (230464), and methyl chloroformate (M35304) were obtained from Sigma-Aldrich. Glycerol was provided by the laboratory stock room. From ATCC, AsPC-1 (pancreatic cells CRL-1682), U-87 MG (neuroblastoma cells HTB-14), RPMI-1620 medium (30-2001), Eagle's Minimum Essential Medium (EMEM) (30-2003), 25-$cm^2$ culturing flasks , 75-$cm^2$ culturing flasks, 1-mL serological pipettes, 5-mL serological pipettes, 25-mL serological pipettes, 5-mL conical centrifuge tubes, 15-mL conical centrifuge tubes, and 25-mL conical centrifuge tubes were obtained. All other culturing materials were kindly provided by Dr. Steve Mackessy's laboratory, including dimethyl sulfoxide (DMSO) and fetal bovine serum (FBS) both from ATCC. EMD Millipore TLC Silica Gel 60, $F_{254}$, aluminum backed thin layer chromatography plates (1.10557.0001) were purchased from Fisher Scientific.

## Instrumentation

A Bruker 400 MHz nuclear magnetic resonance spectrometer was utilized for monitoring reaction success and characterization of purified product. A Nicolet iS5 infrared spectrometer with an iD5 ATR cell from Thermo Scientific was used to analyze starting materials and products. A Shimadzu HPLC system consisting of a LC-10AD pump, an SPD 10A UV/Vis detector, and outfitted with a Luna Omega Polar C18 column (4.6 mm x 150 mm; silica particle size 1.6 μm) was utilized for determining purity and monitoring protecting group removal. A Labconco lyophilizer was utilized for conversion of DHA dimer into monomer.

## Nomenclature and Abbreviations

Before moving forward, it is pertinent to take a moment to discuss annotation of the intermediates in the synthetic scheme. From this point, the author's own personal shorthand will take the place of formal/IUPAC names for these intermediates, and this is primarily because these formal terms are cumbersome. Figures 15, 16, and 17 give the structure, IUPAC name, and the author's abbreviation for each compound. This naming system will be maintained throughout the paper.

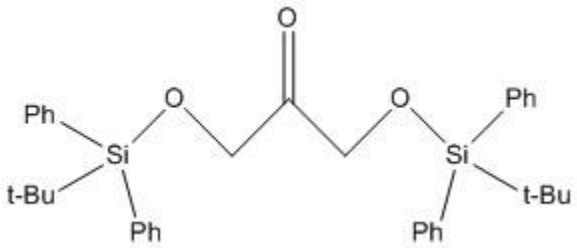


*Figure 15*. 1,3-bis[[(1,1-dimethylethyl)diphenylsilyl]oxy]-2-propanone - *DHA-DS* (doubly silylated).

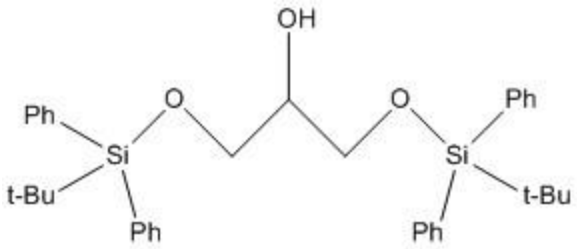


*Figure 16*. 1,3-bis[[(1,1-dimethylethyl)diphenylsilyl]oxy]-2-hydroxypropane - *G-1,3-DS.*

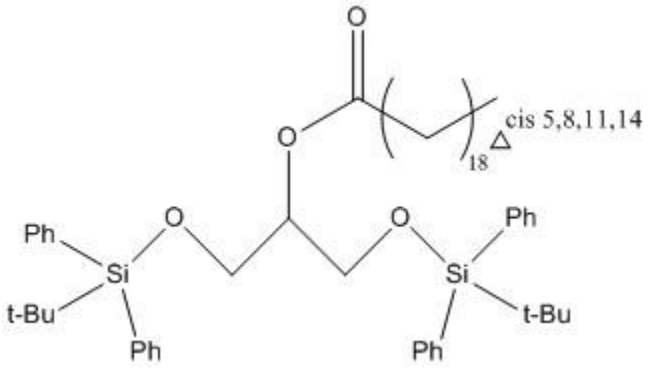


*Figure 17*. 1,3-bis[[(1,1-dimethylethyl)diphenylsilyl]oxy]-2-propanoyl-(5Z, 8Z, 11Z, 14Z)-eicosatetraenoate - *2-AG-DS.*

## Synthetic Methodology

### Step 1 - Monomerization of Dihydroxyacetone

The overall synthesis of 2-AG was carried out on the milligram scale, but for the purpose of conversion of DHA dimer into monomer (Figure 18) for use as a starting material, amounts ranging from 1 to 3 grams were used. To aid in the quick recovery of the monomer, the minimum amount of deionized (DI) water to dissolve the DHA crystals was used in every case, which involved adding ~0.5 mL aliquots of DI water until a concentrated solution was formed. The concentrated solution was stirred for one hour before it was transferred into a Labconco freeze drying flask and frozen with uniform distribution in the flask using liquid nitrogen. Then, the flask was attached to the

Labconco lyophilizer and brought to dryness at approximately 0.050 mBar at 0 °C. Due to the hydrophilic nature of DHA, multiple cycles of freeze drying were often required to bring to full dryness. In some cases, it was necessary to triturate the semi-solid product with very minute aliquots of absolute ethanol and vigorously whisk the resultant paste until dry crystals were returned. Distributing a semi-hydrated sample onto a large watch glass and passing nitrogen gas across the surface combined with mechanical perturbation was also helpful in bringing a sample to complete dryness. In some cases, samples that proved particularly difficult were placed in the fume hood over night to dry from the laminar air flow in the hood. Successful monomerization was determined by melting point analysis; the monomer has a melting point range of 89 - 91 °C, and the dimer melts between 75 - 80 °C. Stored in a sealed container and placed in a desiccator, the monomer will slowly convert to dimer over a period of several months (Davis, 1973).

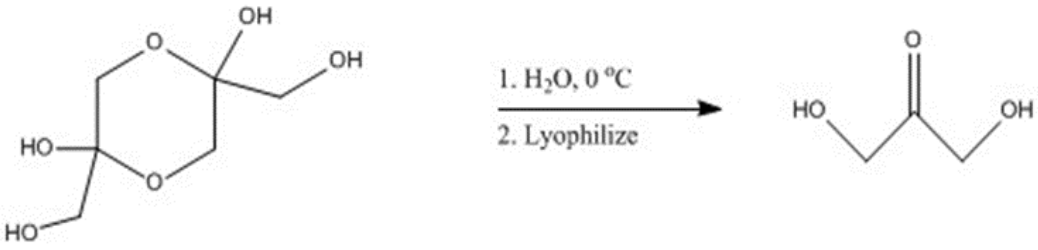


*Figure 18*. Monomerization of DHA.

**Step 2 - Protection of Dihydroxyacetone**

Figure 19 gives an overview of the first synthetic step: addition of the protecting group. To a 25-mL round-bottom flask was added 100 mg (1.1 mmol) of monomerized

DHA and 10 mL of DMF. A stir bar was then added, and the flask contents were mixed gently until homogeneity. Then 151 to 226 mg (2-3 molar equivalents) of imidazole were added, followed with 693 µL (1.1 molar equivalents) of t-BDPSiCl. The reaction stirred for 30 min after which it was quenched with 10 mL of deionized water. The round-bottom flask was covered with aluminum foil and placed in a 0 °C freezer, causing precipitation of the doubly silylated (protected) DHA (DHA-DS). When using less DMF, typically ≤ 5 mL, and using the same amount of DHA, the product typically precipitates out of solution without needing to be cooled.

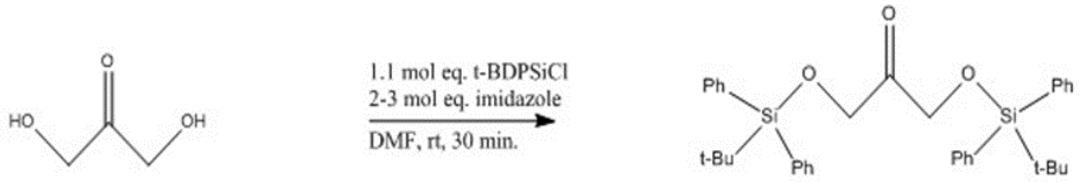


*Figure 19*. Protection of DHA with *t*-BDPSiCl.

The contents of the round-bottom flask were then transferred to a Buchner funnel and washed with 5-mL aliquots of 0 °C deionized water while simultaneously being ground and physically manipulated with a glass stir rod. After washing approximately 3-5 times, the crystals were carefully transferred to a pre-weighed watch glass, dried at ambient temperature, and weighed again for recovery determination. The crystals were stored in a screw-cap vial at 4 °C until the next step. Reaction success was monitored using infrared spectroscopy, looking specifically for the disappearance of the diagnostic alcohol band at 3400 $cm^{-1}$. Absence of this band indicated complete double protection of the compound, which was further verified using $^{1}H$ NMR.

**Step 3 - Reduction of DHA-1,3-DS**

Figure 20 shows the next step in the synthesis: reduction of DHA-DS to G-1,3-DS. From the product isolated and purified in step 2, 100 mg (0.18 mmol) were added to a 50-mL round-bottom flask containing 5 mL of *tert*-butanol. The flask was placed in an ice bath, and the contents were stirred gently while 8 mg (1.2 mol equivalents) of sodium borohydride ($NaBH_4$) dissolved in 5 mL of basic (pH > 9) *t*-butanol solution was added drop wise over 15 min. The contents were stirred for an additional 105 min, and the reaction was quenched with 1.0 M HCl to a pH of ~7, upon which the clear reaction mixture became slightly opaque. The solution was dried at 50 °C for 30 min to remove the *t*-butanol, and the mixture was back-extracted with 5-mL aliquots of chloroform three times. The aliquots were combined and concentrated by drying at ambient temperature on a pre-massed watch glass and to determine recovery. $^1$H-NMR spectra were gathered to determine reaction success.

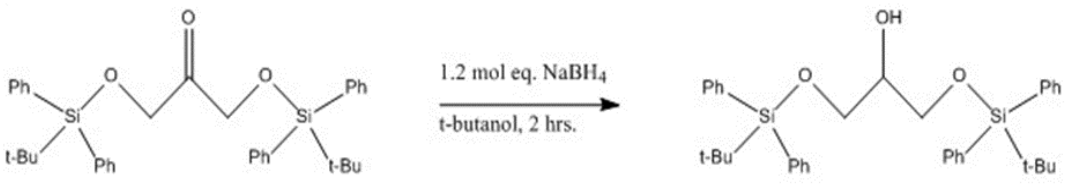


*Figure 20*. Reduction of DHA-DS to G-1,3-DS.

**Step 4 – Esterification**

Figure 21 gives the outline of the next synthetic step: esterification of G-1,3-DS with 2-AG to form 2-AG-DS. From product isolated and purified in step 3, 100 mg (0.2 mmol) was added to 5 mL of chloroform along with 12 mg (one molar equivalent) of imidazole in a 25-mL round-bottom flask. The flask was placed in an ice bath and stirred at a gentle rate, and 100 mg (0.3 mmol) of arachidonic acid was added. To the flask, 5 mL of chilled chloroform containing 70 µL (1.1 molar equivalents) of $SOCl_2$ were added to the stirred contents of the round-bottom flask slowly over 30 min. The reaction was stirred for another 2.5 hr before being quenched with approximately 1 mL of deionized water. The flask contents were dried at 40 °C and filtered over anhydrous magnesium sulfate.

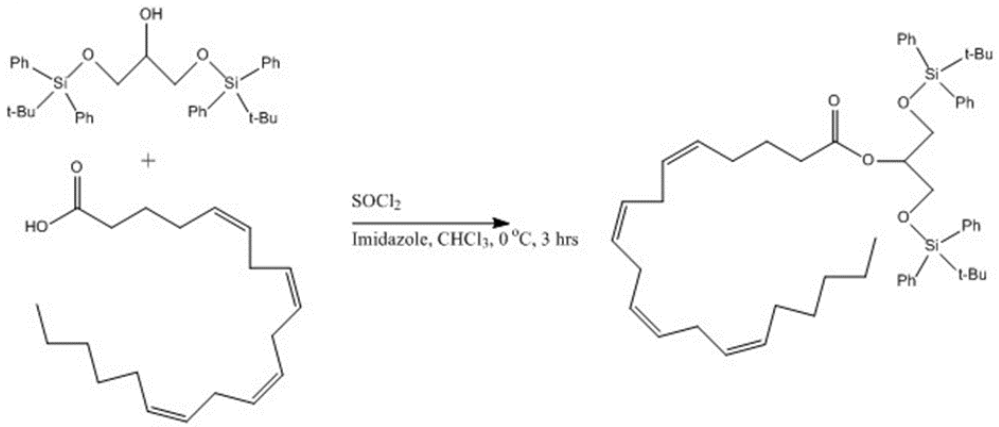


*Figure 21*. Esterification of G-1,3-DS with 2-AG utilizing $SOCl_2$.

The gelatinous product was then reconstituted in 5 mL of pentane and washed three times with 5 mL of pH ≈ 9-10 aqueous NaOH. The organic layer was filtered through $MgSO_4$ and then added to a clean 25-mL round-bottom flask. The round-bottom

flask was fitted with a rubber septum which was ventilated via a syringe needle and connected via another syringe needle to a nitrogen tank. The flask was flushed with nitrogen gas for approximately 5 min. The flask was then sealed and stored at 4 °C. During the reaction, small aliquots were removed for $^{1}$H-NMR analysis to determine successful esterification.

**Step 5 - Protecting group removal**

Figure 22 gives the generalized reaction for the deprotection step of 2-AG-DS; multiple methods were utilized in deprotection attempts. Table 5 outlines the five primary removal methods employed. The removal conditions are amalgamations or permutations of removal methods employed by Han and Razdan (1999), Nicolaou and Webber (1986), and Corey's own original deprotection method utilizing tetra-*n*-butyl ammonium fluoride, TBAF (Corey and Venkateswarlu, 1972).

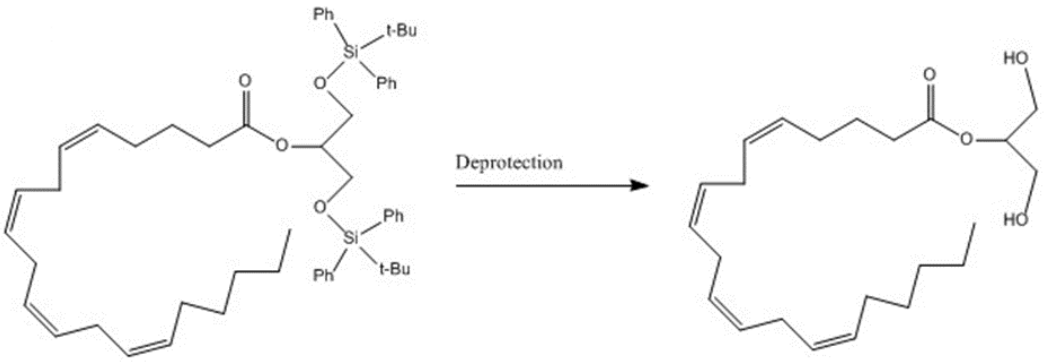


*Figure 22*. Deprotection of 2-AG-DS.

Table 5

*Protecting Group Removal Conditions.*

| Method | Removal Agent (all in THF) | Temperature range (°C) | Time (hr.) |
|---|---|---|---|
| A | 6 mol eq. of TBAF | 0 °C | 8 hr. |
| B | 6 mol eq. of TBAF<br>1 mol eq. imidazole | 0 °C | 8 hr. |
| C | 6 mol eq. of TBAF<br>3 mol eq. of AcOH | 0 °C | 8 hr. |
| D | 6 mol eq. of TBAF<br>6 mol eq. of AcOH | -20 to 0 °C | 24 hr. |
| E | 10:1 HF/pyridine | -20 to 0 °C | 24 hr. |

Deprotection was carried out under inert conditions; in each case reagents were added to a 25-mL round-bottom flask sealed with a rubber septum and flushed with nitrogen gas. Each reaction was performed with 100 mg (0.117 mmol) of 2-AG-DS, with the additional reagents matching the molar equivalents given in Table 5, in 5 mL of THF. The initial three removal methods, A, B, and C, were performed for 8 hr, after which 1 mL of concentrated aqueous $MgCl_2$ was added to the flask and the flask was gently shaken by hand for 1-2 min to precipitate any free fluoride ion. The solution was then vacuum filtered to remove the precipitate and subsequently transferred into a clean 50-mL round-bottom flask and dried under reduced pressure at 40 °C. The flask contents were reconstituted in 5 mL of chloroform and extracted with three 5-mL aliquots of pH 9-10 aqueous NaOH. The aqueous layers were transferred to a new flask, dried again at 40 °C, and the residual product was reconstituted in $CDCl_3$ and $^1$H-NMR spectra were taken to determine identity.

Difficulties with the initial deprotection methods prompted a change in methodology. For removal methods D and E, reaction time was increased to 24 hr and each method was analyzed via HPLC. For an initial eight hours, the reaction mixture was stirred at 0 °C and sampled at 3 hr by drawing 0.5 mL of the reaction mixture into a syringe and transferring into an Eppendorf tube, followed subsequently with approximately 100 mg of $MgCl_2$ to precipitate any free fluoride ion. The solution was then filtered into a new Eppendorf tube and adjusted to a pH of approximately 3 (verified by spotting on pH paper) with a 1.0 M NaOH solution and was stored in a -20 °C freezer until analysis. After stirring for 8 hr at 0 °C, the reaction flask was transferred to a -20 °C freezer for another 15 hr, to mimic the deprotection conditions upon which these methods were modelled. After 15 hr at -20 °C, the flask was removed, and stirred at ambient temperature for another hour before a final 0.5 mL sample was taken at 24 hr, quenched with 100 mg $MgCl_2$, filtered into an Eppendorf tube, and placed in a -20 °C freezer until analysis.

Samples from D and E were analyzed in sequence for their *t*-BDPSiF concentration using high performance liquid chromatography, utilizing a Phenomenex Luna Omega Polar C18 column and a gradient solvent system starting at 30:70 water/acetonitrile, increasing to 100% acetonitrile over 10 min, holding at 100% acetonitrile for 10 additional min, and then reverting to the original 30:70 water:acetonitrile over 5 min (Rouzer et al., 2002). Flow rate was set to 1.0 mL/min and the UV/Vis detector was set to dual channel mode, detecting at 220 and 274 nm simultaneously. Aliquots of samples (20 µL) at each time point from each method were analyzed and chromatograms for each sample were collected. Deprotection success was

determined by calculating the concentration of *t*-BDPSiF, the primary by-product of deprotection which absorbs at 274 nm (Figure 23). Relevant data are discussed in Chapter IV.

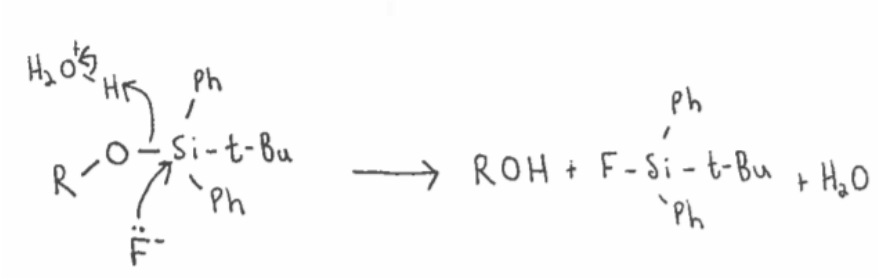


*Figure 23*. Production of *t*-BDPSiF during deprotection step.

The concentration of *t*-BDPSiF from each sample set was calculated from a standard curve using *t*-BDPSiF generated by incubating 109 mg of *t*-BDPSiCl with 250 mg of TBAF in 1 mL of THF for 24 hrs. After which, the solution was quenched with 100 mg of $MgCl_2$ and vacuum filtered. The filtrate was recovered and used as a stock to prepare a series of increasingly dilute standard solutions which were analyzed using the previously discussed HPLC methodology.

The concentration of *t*-BDPSiF recovered from deprotection in each sample (determined from the generated standard curve) was converted into moles and then that value was divided by the total number of moles of sample available to determine total deprotection, which was then converted into percent deprotection (see Chapter IV for a sample calculation).

## Cytotoxicity Assay

In anticipation of successful synthesis and isolation of 2-AG, and in the interest of further project development, methods to screen cytotoxicity of 2-AG against various cancer lines were investigated and developed simultaneously with synthetic method development. At the recommendation of collaborators in the School of Biological Sciences, the MTT assay was selected for screening drug action against cellular proliferation (Berridge, Herst, & Tan, 2005). The MTT assay is a colorimetric assay for measuring cellular metabolism via the reduction of 3-(4,5-dimethylthiazol-2-yl)-2,5-diphenyltetrazolium bromide (MTT) to its insoluble formazan, (E,Z)-5-(4,5-dimethylthiazol-2-yl)-1,3-diphenylformazan, catalyzed by mitochondrial NADPH-dependent reductases (Figure 24).

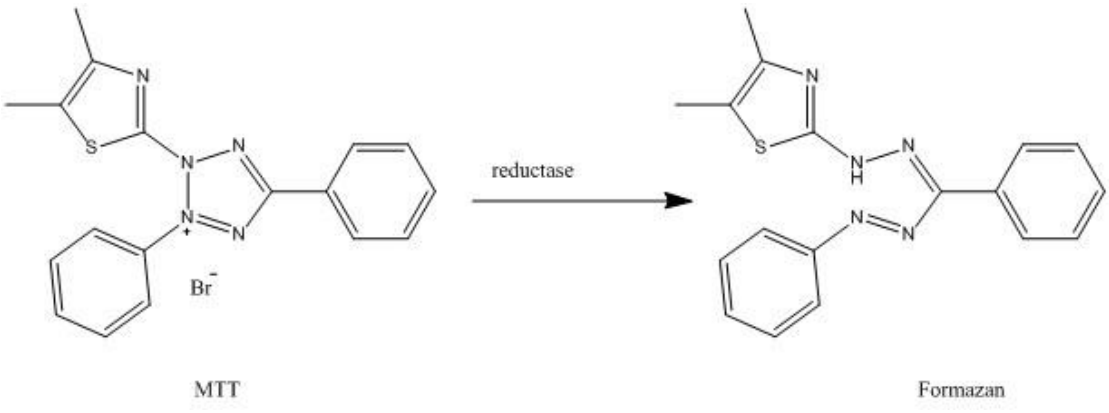


*Figure 24*. Reduction of MTT to its formazan via mitochondrial reductases.

Utilizing the MTT assay, it is possible to determine proliferation of cells treated with different cannabinoids at different concentrations versus controls by measuring the presence of the formazan product (brought into solution with the nonionic poly-

oxyethylene surfactant NP-40). Healthy, intact cells will metabolize MTT to formazan, while cells that are in apoptotic or autophagic pathways (or that are simply dead) will not, giving a simple and effective method for measuring reactivity to cannabinoid treatment by measuring colorimetric response of the control wells and comparing to the treatment wells. Greater absorbance of sample versus control indicates proliferation, while less indicates death/autophagy. A sample assay protocol is given below, written specifically for the pancreatic cancer cell line CRL-1682. The only variation in this methodology from cell line to cell line would be the media employed.

**Assay Procedure**

Pancreatic cancer cells from ATCC (CRL-1682: https://www.atcc.org/products/all/CRL-1682.aspx), an adherent cell type, were plated into a 25-$cm^2$ Corning culture flask with approximately 11 mL of RPMI 1640 media (https://www.atcc.org/Products/All/30-2001.aspx) with 10% fetal bovine serum (FBS) (https://www.atcc.org/products/all/30-2020.aspx) (subsequently referred to simply as media). Cells were incubated for 24 hr and were subsequently trypsinized using 3 mL of a 0.25% trypsin/0.53 mM EDTA solution (https://www.atcc.org/products/all/30-2101.aspx) and passed into a 75-$cm^2$ Corning culture flask with 25 mL of media. The cells were then cultured for an additional 48 hr, with media refreshed every 24 hr, until the flask was confluent (70 to 80% cell density). The cells were then trypsinized and counted in triplicate using a hemacytometer, with the average of the three cell counts being used to determine overall cell density.

Cells were then plated at the following cell density given in Table 6. The plate was incubated for 24 hr allowing cells to settle and adhere to the wells. Finally, the wells

were refreshed with media and the appropriate wells were treated with the cannabinoid that was being screened. Treatment involved addition of 1 µL of a prepared stock solution of the cannabinoid in absolute ethanol (one of the few amenable vehicles for cannabinoids). Ethanol is a common disinfectant, owing to its ability to intercalate into cell membranes causing lysis and subsequent death, which is why well treatment was kept to a single microliter of cannabinoid in vehicle (Tapani, Taavitsainen, Lindros, Vehmas, & Lehtonen, 1996) and readings were corrected in reference to control well outcomes. The cellular stock solution concentration was varied to enable screening across concentrations of interest and was usually in the range of 100 µM to 1 mM. Several methods of serial dilution were available for generating treatment wells. The first involved preparing increasingly dilute stock solutions of cannabinoid in ethanol and treating each well directly, adding 1 µL of control and filling with 99 µL of media to bring to a final volume of 100 µL. This method allowed for easy dilutions by a factor of ten but was time consuming. Another method, requiring more experience handling cell culture and multi-channel pipettes, was to refresh all the treatment wells with 100 µL of media and then prepare treatment wells in row A at 200 µL total volume at the desired concentration. Then, using a multi-channel pipette, 100 µL from each treatment well in row A were transferred to the corresponding well in row B and mixed with the multi-channel pipette, diluting the original stock concentration by half instead of an order of magnitude. This process was repeated across each well (refreshing tips in between treatments) until finished. Each plate also contained three additional categories of wells in addition to treatment wells. First, two series of control wells plated at the same cell density and treated with an identical amount of total ethanol content as the treatment

wells were prepared to serve as a baseline for treatment efficacy, and absorbance from these wells was used to correct absorbance from other treatment wells by simple subtraction of the control absorbance from the treatment absorbance. Second, a blank series was prepared on each plate to correct background absorbance from media and vehicle. Finally, a series of wells plated at different cell densities were prepared on each plate to serve as a standard curve for determining end point cell density for the treatment wells (Table 6). After refreshing the media, the cells were incubated for 24 hr. Then, 10 uL of MTT reagent were added to each well. The cells were incubated for another 24 hr. After this, the wells were treated with 10 µL of NP-40, placed in the dark for 4 hr, and then absorbance in each well was read at 570 nm using a plate reader.

Table 6

*Cell Density for MTT Assay (in cells/mL).*

| | 1 | 2 | 3 | 4 | 5 | 6 | 7 | 8 | 9 | 10 | 11 | 12 |
|---|---|---|---|---|---|---|---|---|---|---|---|---|
| A | 1000 | 1000 | 1000 | 1000 | 1000 | 1000 | 1000 | 1000 | 1000 | 1000 | 1000 | 1000 |
| B | 1000 | 1000 | 1000 | 1000 | 1000 | 1000 | 1000 | 1000 | 1000 | 1000 | 1000 | 1000 |
| C | 1000 | 1000 | 1000 | 1000 | 1000 | 1000 | 0 | 0 | 0 | 0 | 0 | 0 |
| D | 1000 | 1000 | 1000 | 1000 | 1000 | 1000 | | | | | | |
| E | 1000 | 1000 | 1000 | 1000 | 1000 | 1000 | | | | | | |
| F | 1000 | 1000 | 1000 | 1000 | 1000 | 1000 | | | | | | |
| G | 50000 | 50000 | 50000 | 50000 | 25000 | 25000 | 25000 | 25000 | 10000 | 10000 | 10000 | 10000 |
| H | 5000 | 5000 | 5000 | 5000 | 1000 | 1000 | 1000 | 1000 | 500 | 500 | 500 | 500 |

[Rows] – (Columns) – Contents; [A-F] – (1-6) – Treatment wells; [A-B] – (7-12) – Control wells; [C] – (7-12) – Blank wells; [G-H] – (1-12) – Standard curve wells; [D-F] – (7-12) – Empty

# CHAPTER IV

# RESULTS & DISCUSSION

## Conversion of Dihydroxyacetone Dimer to Monomer

Table 7 gives the percent recovery for DHA (dihydroxyacetone) dimer conversion into monomer. The primary issue complicating the process of recovery was the tendency for DHA to cling to glassware, and it is for this reason that conversion was carried out in 400-mL beakers as opposed to round-bottom flasks. Getting full recovery often required meticulous scraping of glassware with a spatula and the narrow necks of round-bottom flasks unnecessarily complicated this process. Successful conversion was determined by melting point analysis as discussed in Chapter III.

Table 7

*Percent Recovery for Conversion of DHA Dimer to DHA Monomer.*

| Sample Mass (g) | Recovered Mass (g) | Percent Recovery | Trituration (Y/N) |
|---|---|---|---|
| 1.020 | 0.857 | 84.0% | Y |
| 1.017 | 0.942 | 92.6% | Y |
| 0.504 | 0.456 | 90.5% | Y |
| 1.090 | 0.989 | 90.7% | Y |
| 3.215 | 3.214 | 99.9% | N |
| 5.045 | 4.884 | 96.8% | Y |

**Silylation of Dihydroxyacetone to Form DHA-DS**

Prior to collecting $^{1}$H-NMR spectra, reaction progress and product purity were assessed through qualitative thin layer chromatography (TLC). Several solvent systems were tested for their usefulness in this regard. The most useful proved to be a denatured ethanol solution (91.85% ethyl alcohol, 5% methyl alcohol, 1% ethyl acetate, 1% methyl isobutyl ketone, 1% hydrocarbons, and 0.15% water) both for developing plates and for dissolving starting materials and products. Spotting sample aliquots straight from the reaction flask and detecting spots on a plate with iodine resulted in diffuse, amorphous streaking across the silica. This was discovered to be a consequence of the DMF interacting with the silica; the problem was resolved by diluting approximately 10-20 µL of the aliquot from the reaction mixture in half a milliliter of denatured ethanol before applying to the plate. This greatly improved spot resolution.

Figure 25 shows the $^{1}$H-NMR spectrum of purified crystals of DHA-DS in $CDCl_3$. Clearly visible in the spectrum are the signals from DMF (Figure 26), singlets at 2.980, 2.911, and 8.051 ppm (faintly visible upfield of the aromatic signals). Attempts were made to thoroughly purify the product, as described in Chapter III, but no amount of washing was successful in eliminating the DMF signals from any $^{1}$H-NMR spectra of the DHA-DS samples. Application of heat to evaporate the excess DMF was not helpful either, as DMF is potently non-volatile (boiling point of 153 °C), and product browning occurred at temperatures above 80 °C.

Based upon the structure of DHA-DS (Figure 15), the expected $^{1}$H-NMR spectrum should produce a singlet in the methyl region (approximately 0-1 ppm) from the methyl groups on the protecting group, which when doubly protected should be

equivalent, a singlet from the equivalent methylene groups adjacent to oxygen at approximately 3-5 ppm, and signals from the aromatic hydrogens from the phenyl groups at approximately 7-8 ppm. These signals are clearly present in Figure 25. Full double protection was also corroborated by IR spectroscopy, specifically by monitoring for the absence of the diagnostic alcohol band that occurs from approximately 3400 to 3600 $cm^{-1}$ (Figure 27). Table 8 gives the percent recovery for reactions conducted to determine yield for this step, along with the average recovery for these reactions and the standard deviation among them.

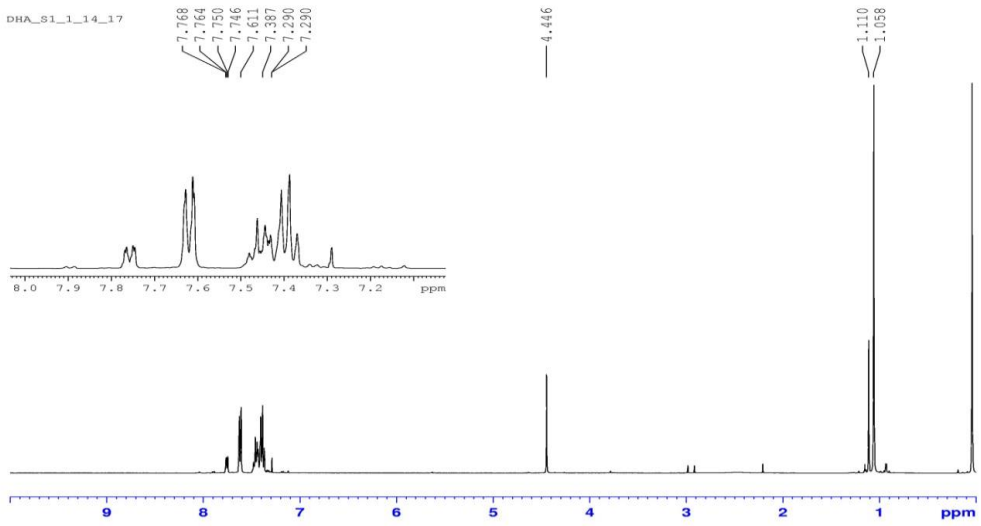


*Figure 25*. $^{1}$H-NMR spectrum of DHA-DS in $CDCl_3$.

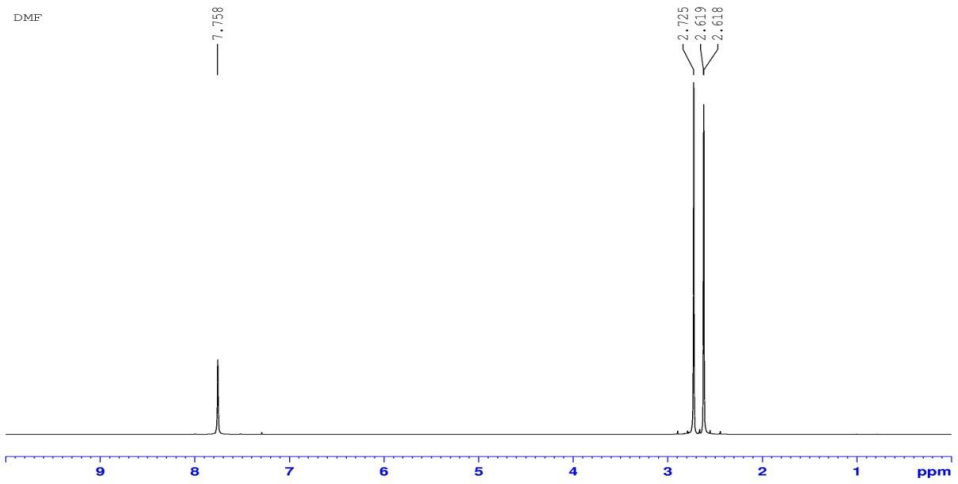


*Figure 26.* $^{1}$H-NMR spectrum of DMF in $CDCl_3$.

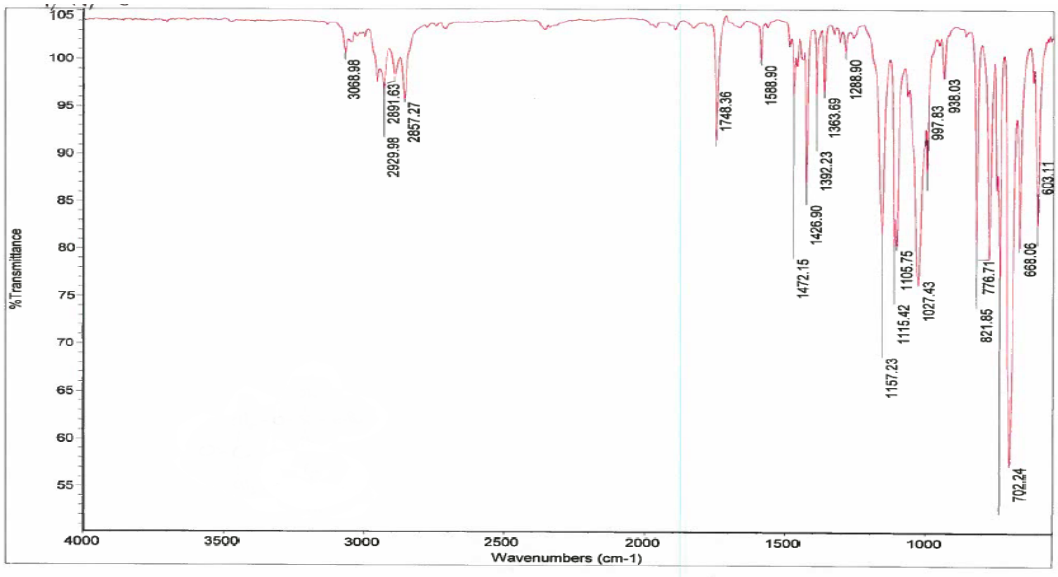


*Figure 27.* IR spectrum of DHA-DS.

Table 8

*Percent Recovery of DHA-DS.*

| DHA-DS recovered (g) | Percent Recovery |
|---|---|
| 0.604 | 92.2% |
| 0.625 | 97.0% |
| 0.599 | 94.8% |
| 0.587 | 92.4% |
| 0.668 | 98.7% |
| **Average** | **95 ± 3%** |

## Reduction of DHA-DS and Recovery of G-1,3-DS

Reduction of DHA-DS to G-1,3-DS was accomplished through the well-known reducing agent, sodium borohydride ($NaBH_4$). The solvent for the reaction was *t*-butanol, selected after searching for methods that might offer an insight into which solvent would be best suited for using $NaBH_4$ (Lecher, 2007). In experimenting with other solvent systems, ethanol and chloroform were found to be suitable substitutions as well. Percent recovery for reactions are recorded in Table 9. The reduction of the carbonyl of DHA-DS into an alcohol changes the physical state of the product from solid to a viscous liquid.

Table 9

*Percent Recovery of G-1,3-DS*

| Reaction Solvent | Percent Yield |
|---|---|
| *t*-butanol | 95.7% |
| *t*-butanol | 97.1% |
| *t*-butanol | 91.5% |
| Chloroform | 99.7% |
| Ethanol | 96.8% |

## Use of Glycerol as a Starting Material

As mentioned previously in Chapter II, DHA was selected as a starting material to ensure protection specificity for the 1 and 3 positions for glycerol (after DHA-DS was reduced with $NaBH_4$) but this was found to not be a necessary step, as the introduction of the silyl ether using the original protection conditions employed in the Corey procedure were selective for primary alcohols (Patchinski et al., 2014). Step 1 (Figure 14) shows how using glycerol as a starting material to produce G-1,3-DS circumvents the need to monomerize and reduce DHA, which makes using glycerol as a starting material appealing. The ease of isolation of DHA-DS from DMF was the primary reason it was continued to be utilized as a starting material, as it was hoped that the DHA-DS crystals would be easier to purify of residual DMF rather than the viscous and difficult to handle liquid that G-1,3-DS is, however, further work with the synthetic method, discussed later in this chapter, will highlight how this might not even be necessary.

For the sake of verification of this step, a stock of glycerol was acquired from the university chemical stock room, and sample trials were conducted to produce G-1,3-DS from glycerol. Reaction conditions were identical to those from the original procedure to produce DHA-DS from DHA. Approximately 100 mg (1.1 mmol) of glycerol were measured directly into a 50-mL round-bottom flask by dipping a clean spatula into the glycerol and allowing the glycerol to drip off the spatula tip into the 50-mL round-bottom flask resting in a 150-mL beaker, all of which were pre-tared. The glycerol was dissolved in 5 mL of DMF, to which 225 mg (two molar equivalents) of imidazole were added. The reaction mixture was stirred at ambient temperature and 700 µL (1.1 molar equivalents)

of *t*-BDPSiCl were added. The reaction mixture was stirred for 30-60 min and then the flask was sealed and wrapped in aluminum foil and placed in a 4 °C refrigerator.

Recovery of G-1,3-DS was difficult, but fortunately when the reaction flask was cooled, G-1,3-DS separated from DMF, and settled as a solidified gel at the bottom of the reaction flask. The DMF was carefully decanted from the G-1,3-DS, and the product was scraped onto a watch glass and dried under nitrogen gas. G-1,3-DS itself is water soluble, as attempts to purify with chilled 1 mL aliquots of deionized water demonstrated, and so the convenient method of washing DHA-DS was not amenable with G-1,3-DS. Percent recovery for this process was not determined, but $^{1}$H-NMR data to verify protection success was gathered by adding approximately 10-20 mg of G-1,3-DS to 1 mL of $CDCl_3$ and analyzing.

### G-1,3-DS $^{1}$H-NMR Analysis

Figures 28 and 29 display $^{1}$H-NMR spectra of samples of G-1,3-DS isolated from different syntheses employing the two different starting materials discussed previously. The first (Figure 28) comes from a synthesis employing DHA-DS as a starting material, and the last (Figure 29) comes from a synthesis utilizing glycerol as starting material. DMF signals are identifiable in both spectra. Based upon the structure of G-1,3-DS (Figure 16), the $^{1}$H-NMR spectrum for G-1,3-DS might be expected to be identical to that of DHA-DS, save for the addition of two signals, a singlet and a quintet, corresponding to the methine hydrogen and hydroxyl hydrogen now present at C-2. This is in fact, not the case, as can be readily observed in Figures 28 and 29. The region from 3.5 to approximately 4.0 ppm displays a more complicated splitting pattern.

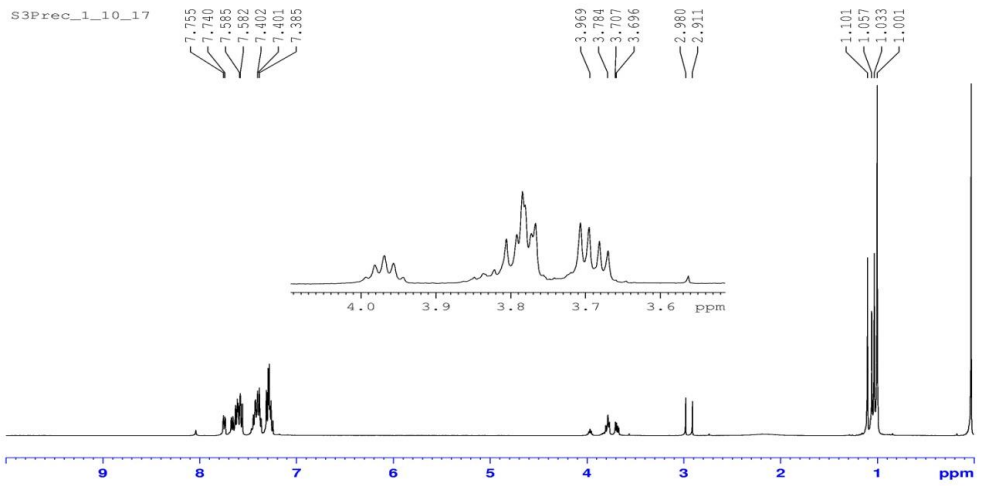


*Figure 28.* $^{1}$H-NMR of G-1,3-DS in $CDCl_3$ synthesized from DHA-DS.

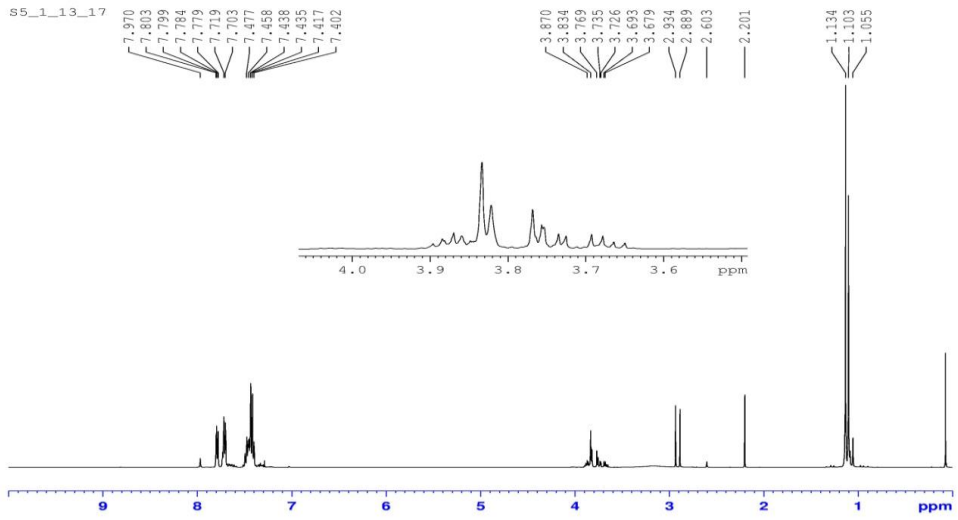


*Figure 29.* $^{1}$H-NMR of G-1,3-DS in $CDCl_3$ synthesized from glycerol.

The reason for this splitting pattern can be explained by the spectrum in Figure 30, which is an $^{1}$H-NMR spectrum of glycerol outlined to explain the splitting pattern.

The reduction of the carbonyl at C-2 transforms C-2 into a pro-chiral carbon, and thus the splitting of the methylene and methine protons is influenced by the now diastereotopic nature of the methylene protons, $H_a$ (red) and $H_b$ (blue) in Figure 30. The spectra of G-1,3-DS in Figures 28 and 29 demonstrate this complex splitting as each hydrogen is "seen" individually, rather than when they were equivalent. Integration for the $^1$H-NMR spectra are not given, as the integration of peaks corresponding to each hydrogen signal belonging to the product of interest often produced fractional values, even when normalizing integrals for sample peaks.

Samples were usually prepared from 10 to 20 mg of purified product reconstituted in approximately 1 mL of $CDCl_3$. Product purity was corroborated by TLC, and the exact reason for the fractional integrals was difficult to pinpoint, but qualitatively, the spectra confirm the identity of each substance analyzed.

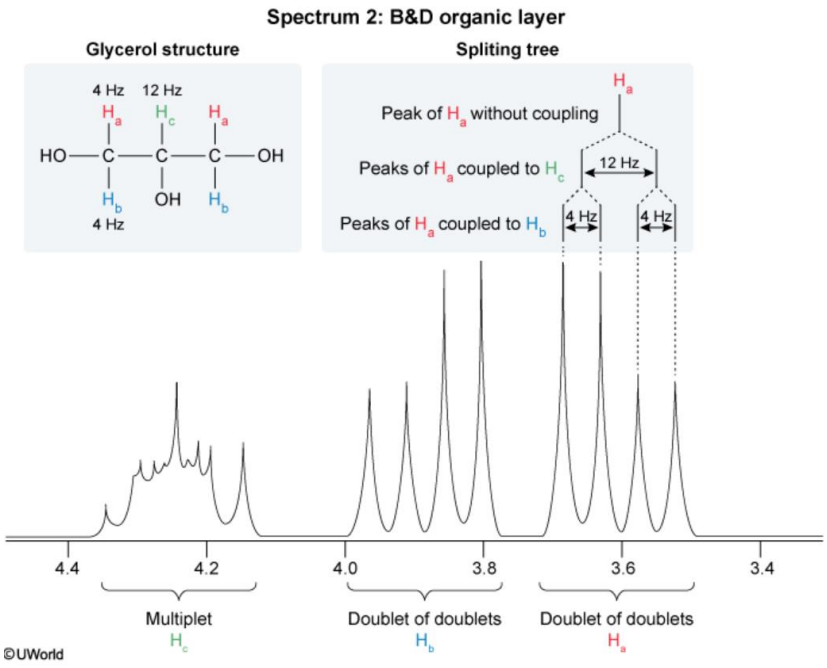


*Figure 30*. $^{1}$H-NMR of glycerol explaining the complex splitting observed over the region from ~3.3 to 4.5 ppm. (Image retrieved from: https://chemistry.stackexchange.com /questions/97786/h-nmr-equivalent-protons-and-coupling-of-glycerol)

## Esterification of G-1,3-DS with Arachidonic Acid to Form 2-AG-DS

Esterification of G-1,3-DS (the origin of which was from DHA-DS), with arachidonic acid was achieved with thionyl chloride, selected primarily for the ease of purification from by-products, $SO_2$ and HCl, and amenability with the protecting group. Figure 31 gives the $^{1}$H-NMR for 0.2 mL of a 1 mg/mL solution of arachidonic acid in ethanol taken in approximately 1 mL of $CDCl_3$. The signals for ethanol are readily discernible in the spectrum, theirs being the most intense. The strong triplet at 1.2 ppm corresponds to signals from the methyl group of ethanol, the quartet at 3.6 ppm corresponds to the methylene protons of ethanol, and the broad singlet at 3.7 ppm corresponds to the hydroxyl proton of the alcohol group of ethanol. The remaining peaks belong to arachidonic acid (excluding the chloroform signal at 7.3 ppm). Given that

arachidonic acid is a twenty-carbon polyunsaturated fatty acid, it is not surprising to find that the methyl and methylene regions of the spectrum are perfuse with signals from the hydrocarbon tail. A diagnostic multiplet at 5.3 ppm is produced by the methine protons of the four double bonds (R-$CH_2$-C**H**=C**H**-$CH_2$-R) at carbons 5, 6, 8, 9, 11, 12, 14, and 15 of arachidonic acid. The complex signal at 2.8 ppm belongs to the methylene protons adjacent to the previously mentioned methine protons. A distinct quintet at 1.7 ppm belongs to the terminal methylene of the fatty acid tail (R-C**H**$_2$-$CH_3$) and the triplet at 0.8 ppm belongs to the terminal methyl group of the tail. Finally, a triplet at 2.3 ppm corresponds to the methylene protons adjacent to the alpha carbon (the $CH_2$ immediately adjacent to the carbonyl of arachidonic acid). Beyond this, peak assignment becomes difficult and speculative; the remaining multiplets at 1.2 and 2.1 ppm coming from the remaining methylene groups of the fatty acid tail.

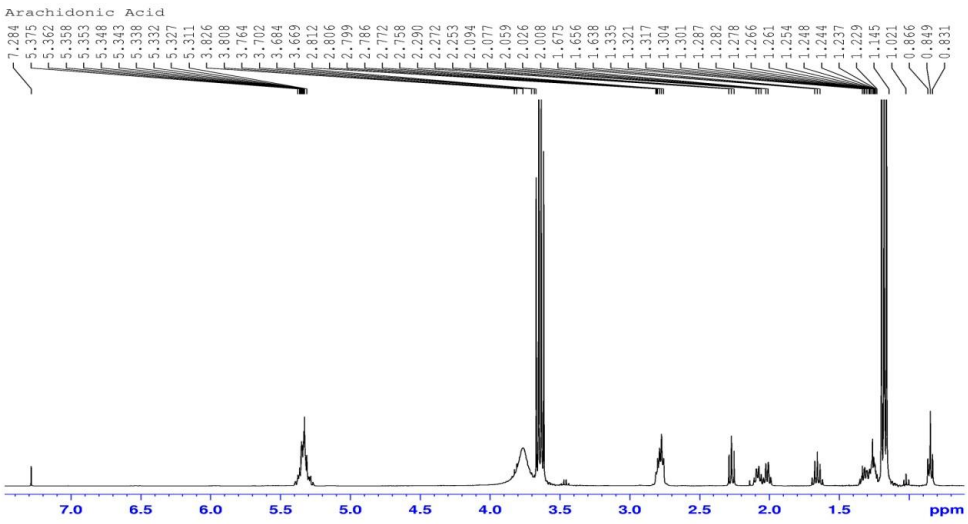


*Figure 31*. $^1$H-NMR of arachidonic acid (1 mg/mL solution in ethanol) in $CDCl_3$.

Figure 32 gives the $^{1}$H-NMR spectrum for 2-AG-DS. Successful esterification was validated by two methods in conjunction. First, qualitative TLC verified that the product isolated from the 2-AG-DS esterification step was pure, and second, the signals for G-1,3-DS (Figures 28 and 29) and the signals from arachidonic acid (Figure 31) are both present, as should be the case. Outside of minor signal shifts, the overlay of the spectra from G-1,3-DS and arachidonic acid (excluding solvent traces; DMF in Figures 28 and 29 and ethanol in Figure 31) would produce a spectrum similar to the one present in Figure 32. The percent recovery of 2-AG-DS is given in Table 10. All the recoveries were lower than desired, the highest being 59%. Losses most likely occurred during the basic aqueous wash, which was intended to convert any free arachidonic acid to its ionic form (the $pK_a$ of arachidonic acid is 4.752 from https://pubchem.ncbi.nlm.nih.gov/compound/231) thereby increasing hydrophilicity and allowing it to be washed away from the much less hydrophilic 2-AG-DS. It is likely that 2-AG-DS was more water soluble than thought, which is surprising given the structure of the protecting groups. The lower temperature at which the reaction was performed to prevent oxidation and degradation of the fatty acid could also contribute to lack of complete conversion, resulting in lower yield. The use of fatty acid chlorides in the preparation of glycerides is a well-established methodology (Bauer, 1946) and improvement in yield should be possible.

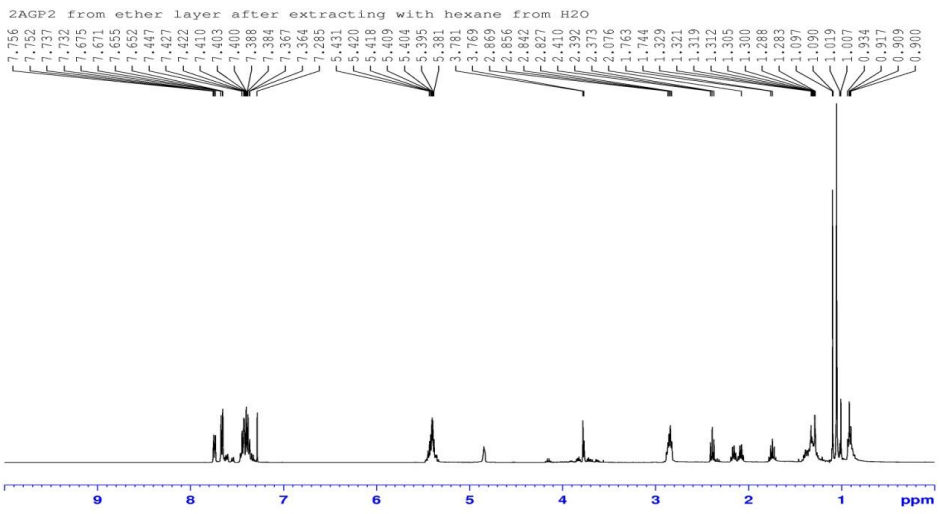


*Figure 32*. $^{1}$H-NMR spectrum of 2-AG-DS in $CDCl_3$.

Table 10

*Percent Recovery of 2-AG-DS*

| Percent Yield | |
|---|---|
| 53.7% | |
| 59.1% | |
| 45.8% | |
| **Average** | **53 ± 7%** |

## Deprotection Analysis Complications

The final step in the synthesis of 2-AG involved the cleavage of the *t*-BDPSi ether protecting groups. As stated previously (see Table 5 in Chapter III), the first three deprotection methods were not analyzed with HPLC but were purified and analyzed by $^{1}$H-NMR. Figure 33 shows the $^{1}$H-NMR spectrum from method A, Figure 34 shows the $^{1}$H-NMR spectrum from method B, and Figure 35 shows the $^{1}$H-NMR spectrum from method C. Each $^{1}$H-NMR spectrum was consistent with 2-AG-DS, indicating that the first three methods employed for deprotection were not successful at 0 °C after 8 hr.

Minor differences do exist among the spectra, and are most likely attributable to the presence of impurities (more visible with the signal amplification necessary to resolve all peaks) owing to variances in purification and differences in the degree and accuracy of instrument shimming (explaining why some signals appear more diffuse than others).

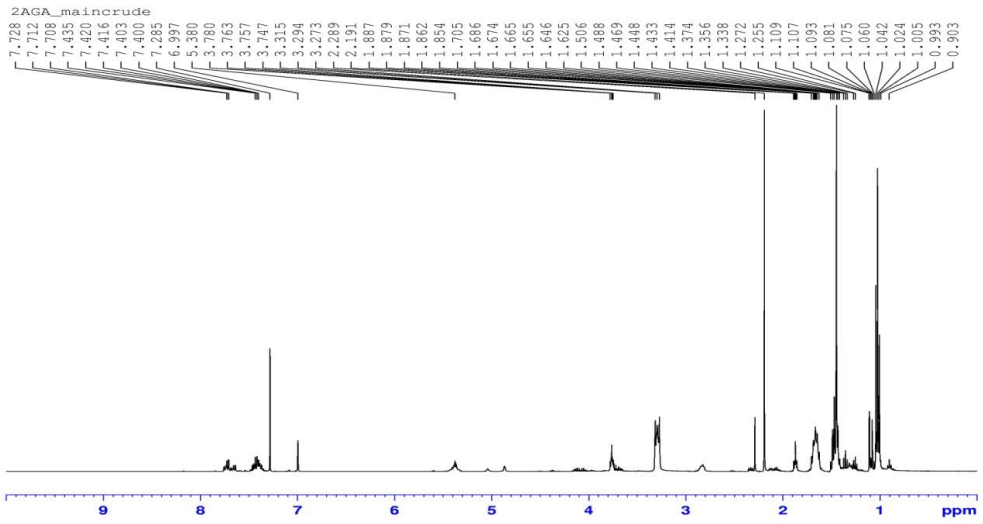


*Figure 33*. $^{1}$H-NMR of product in $CDCl_3$ isolated from deprotection method A.

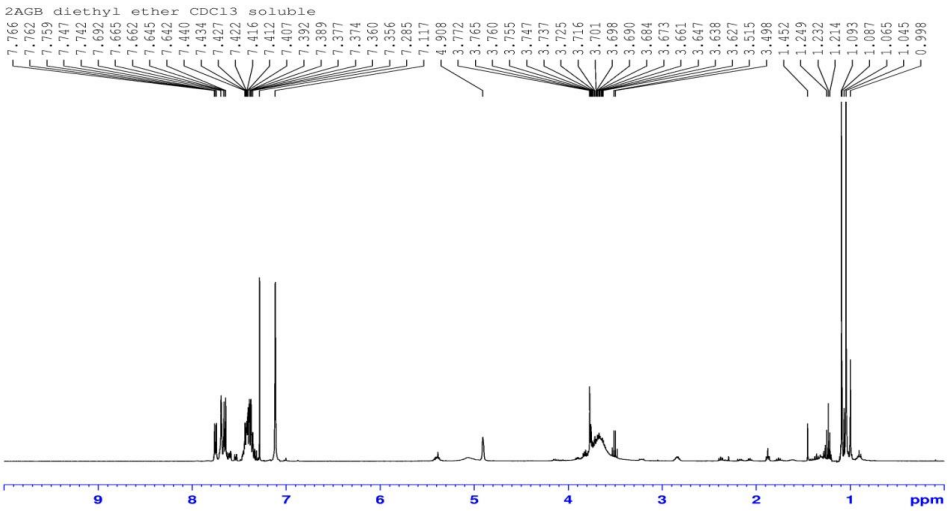


*Figure 34*. $^{1}$H-NMR of product in $CDCl_3$ isolated from deprotection method B.

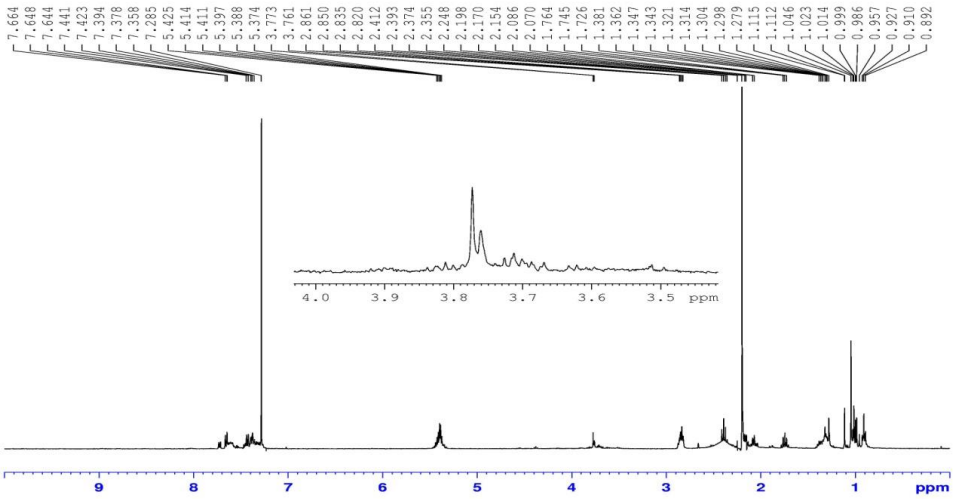


*Figure 35*. $^{1}$H-NMR of product in $CDCl_3$ isolated from deprotection method C.

This prompted interest in using HPLC to assess reaction progress, to allow a view across time, and to aid in assessing overall deprotection success independent of having to isolate the product. Since detecting free 2-AG is not practical with UV-Vis, the HPLC method adapted from Rouzer et al. (2002) was intended to monitor reaction progress by measuring the appearance of the primary by-product of deprotection, *t*-BDPSiF (Figure 23), which will absorb at 274 nm. Method D (Table 5) was a repeat of method C, using a greater total molar concentration of acetic acid. Han and Razdan (1999) reported success using this method, which prompted the second attempt. Method E was borrowed from a cleavage method by Nikolaou and Webber (1986) that used a high concentration of hydrofluoric acid as a fluoride ion source. The conditions were of interest given the previously reported success of the cleavage of *t*-BDPSi ethers with these conditions. Unfortunately, there were significant issues with both the deprotection methods and the HPLC methodology.

The key issue with the HPLC methodology can be seen in Figure 36, which shows a chromatogram of the 50 mg/mL standard solution of *t*-BDPSiF. The preparation of standards is given in Chapter III, but to give a brief generalized review, *t*-BDPSiF was generated from *t*-BDPSiCl by incubating 109 mg with 2.5 molar equivalents of fluoride ion (from TBAF) in THF which contained the anti-oxidant BHT. After quenching any remaining fluoride ion with $MgCl_2$ and filtering the precipitate ($MgF_2$), standard solutions were diluted from this 109 mg/mL stock and were chromatographed via HPLC in 20 µL aliquots. Each of the chromatograms had a similar qualitative appearance as the one in Figure 36, containing multiple signal peaks when only one was anticipated. At the time, it was presumed that the peak corresponding to *t*-BDPSiF would be apparent when peak areas were matched to sample concentrations; that a linear relationship would reveal the correct peak. This was an erroneous assumption, however, as several peaks produce a linear relationship when graphed versus the concentration of the *t*-BDPSiF standards. Some of the compounds contributing to the extraneous peaks are tetra-*n*-butyl ammonium cation ($TBA^+$) and BHT, both of which absorb at 274 nm and would have a linear relationship when their peak areas were plotted against *t*-BDPSiF standard concentrations because they were diluted by the same factor. Acetic acid also weakly absorbs at 274 nm, and oxidized products of BHT could potentially be contributing signals as well.

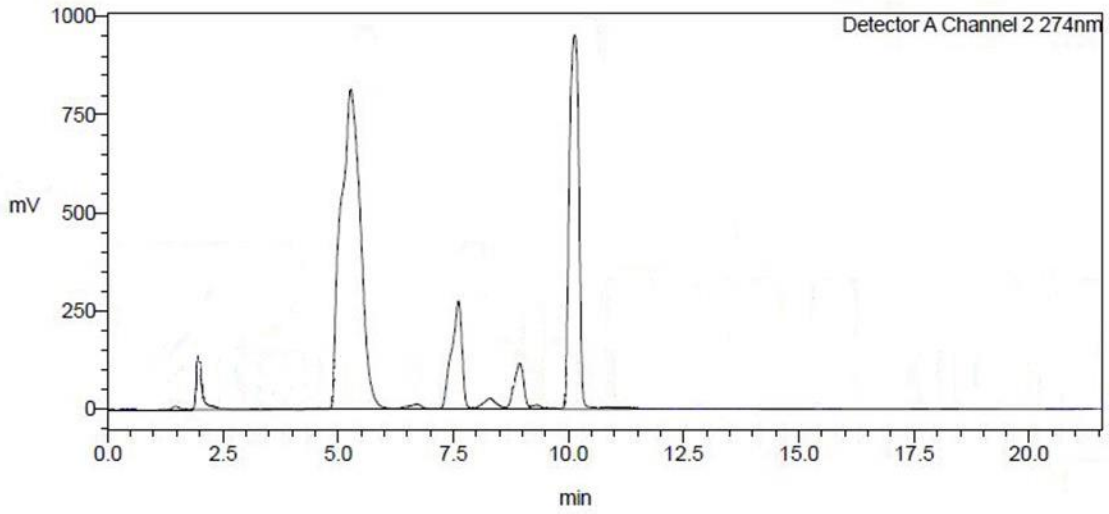


*Figure 36*. HPLC chromatogram of 20 µL of 50 mg/mL *t*-BDPSiF. There are five distinctive peaks occurring at: 1.9 min, 5.0 min, 7.6 min, 8.9 min, and 10.1 min.

Sample aliquots taken from methods D and E analyzed by the same HPLC method also contained unknown peaks. Figure 37 shows the HPLC chromatogram of a sample aliquot from method E after 24 hr. The peak profile of the chromatogram aligns with the peak profile of the *t*-BDPSiF standard chromatogram from 0 to 10 min, which is confirmation that there is at least *t*-BDPSiF present in the sample; meaning deprotection had occurred. However, without a concrete way of assessing which peak belonged to *t*-BDPSiF, drawing conclusions from the data set is very difficult.

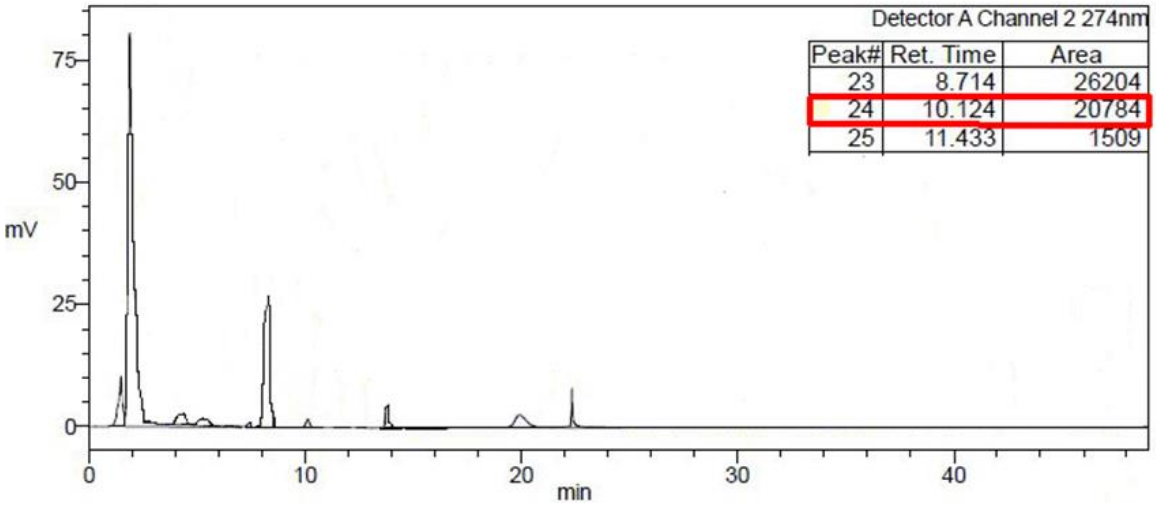


*Figure 37*. Chromatogram of 24 hr aliquot from Method E. The sample was diluted 100-fold prior to analysis (retention times for a sample calculation using this chromatogram are inset in the upper right corner)

Another series of standards was planned in an attempt to resolve these peak identity issues, but several new challenges came along with further analysis. The goal was to obtain clean standards of TBAF, THF, *t*-BDPSiCl, and *t*-BDPSiF so that *t*-BDPSiF elution time could be pinpointed by process of elimination and then correlated back to the chromatograms from method D and E, abrogating the necessity of running further deprotection trials. A stock solution of 103.7 mg/mL *t*-BDPSiF was prepared again as before, by incubating 103.7 mg *t*-BDPSiCl with 250 mg of TBAF for 24 hours. The only variation was the use of approximately 1.0 g of $SiO_2$ granules instead of $MgCl_2$ to scavenge excess fluoride ion from solution prior to sample analysis.

Instrument availability, and consideration for other work being performed at the time, required a change in the column used for the new trials, which was potentially a complicating factor. A reverse phase C18 Phenomenex column (4.6 mm x 150 mm; silica particle size 2.5-2.8 μm) was used instead of the Phenomenex Luna Omega Polar C18 column previously used. It was hoped that the columns would not be so disparate in

resolution that the results would be unrelatable to the earlier samples. The following figures are from the same HPLC methodology using the reverse phase C18 Phenomenex column. Figure 38 displays a chromatogram of 20 µL of THF (containing BHT), Figure 39 displays a chromatogram of 20 µL of a 10 mg/mL solution of TBAF in THF, Figure 40 displays a chromatogram of 20 µL of pure *t*-BDPSiCl and Figure 41 displays the chromatogram for 20 µL of the stock solution of *t*-BDPSiF (concentration = 103.7 mg/mL). Unfortunately, as before, each standard contained multiple peaks making peak assignment problematic. For instance, in Figure 39 (TBAF in THF) there are a host of overlapping peaks from approximately 1.0 to 3.0 min. These peaks were determined to be contaminates adhering to the column. Flushing with mobile phase at 1.5 mL/min for several hours did not help to alleviate this issue. Knowing the origin of these peaks (contaminates from previous analyses) allows them to be dismissed as candidates for TBAF, but there are several peaks outside of the 1.0 to 3.0 min range that need to be identified, specifically at 4.253 min, 4.981 min, 8.994 min, and a peak at approximately 11 min.

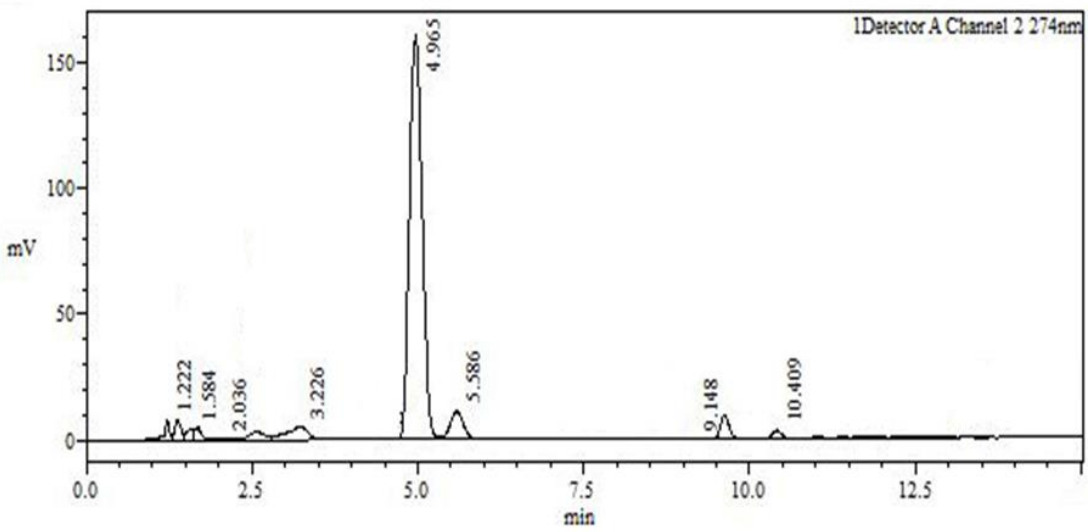


*Figure 38*. HPLC chromatogram of 20 µL of THF containing BHT.

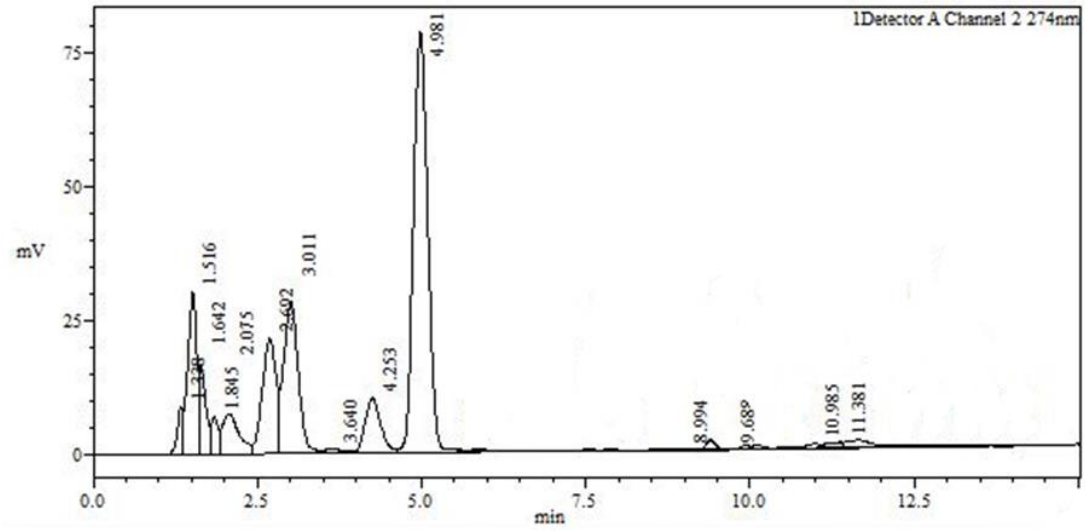


*Figure 39*. HPLC chromatogram of 20 µL of approximately 10 mg/mL TBAF solution in THF.

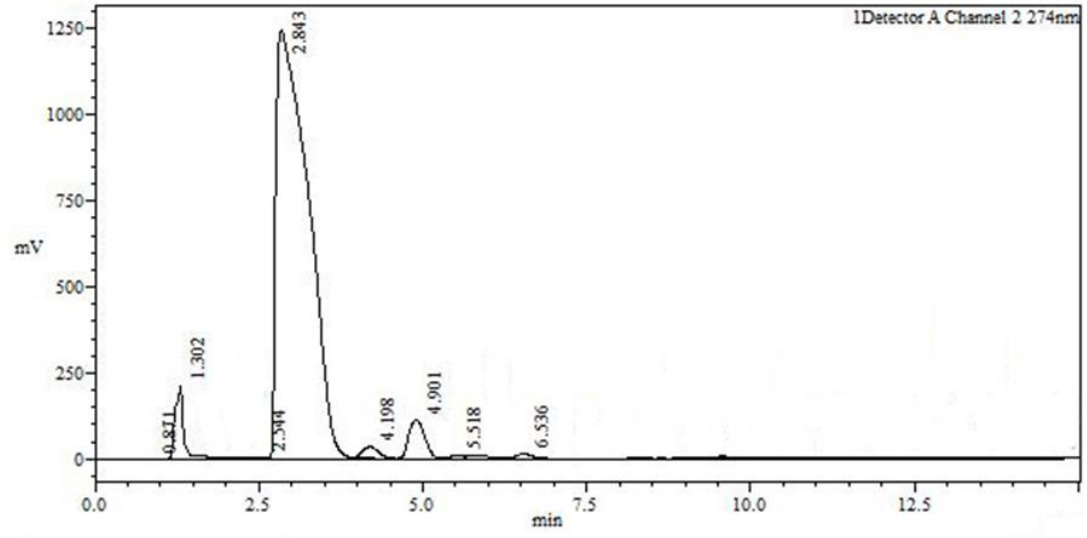


*Figure 40*. HPLC chromatogram of 20 µL of *t*-BDPSiCl.

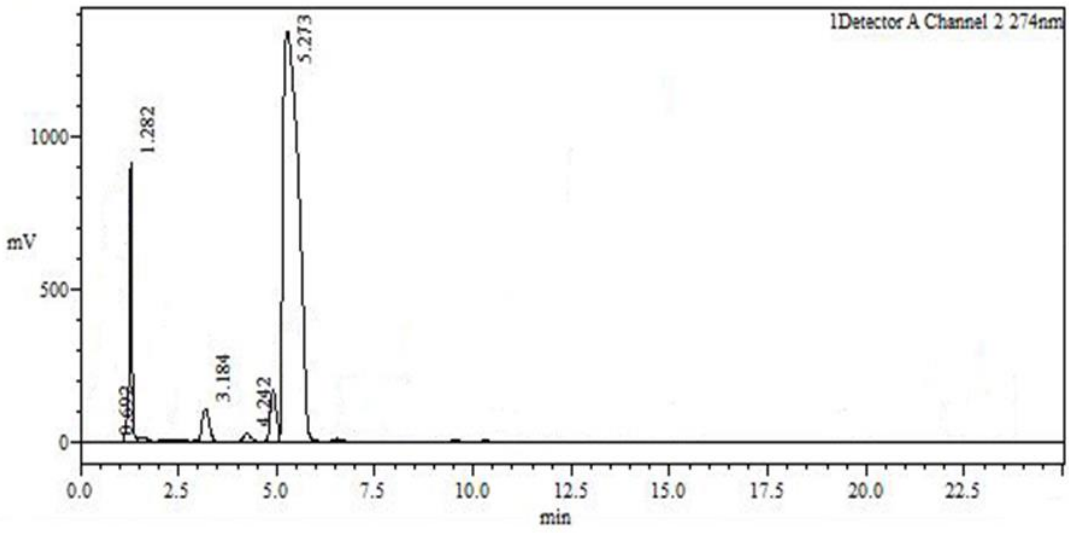


*Figure 41*. HPLC chromatogram of 20 µL of 103.7 mg/mL *t*-BDPSiF in THF.

Analysis of the standards to identity which of the peaks was *t*-BDPSiF was attempted, but it was still difficult to make this determination. For example, the standards prepared in THF concomitantly contained BHT, at a concentration between 0.025 to 0.04% (m/v), which includes the chromatograms in Figures 38, 39, and 41. It should have been possible to use the chromatogram of THF (Figure 38) to pinpoint the elution time of BHT, which then might have helped to identify $TBA^+$ in the chromatogram of TBAF (Figure 39), which would then allow both of those peaks to be eliminated from *t*-BDPSiF (Figure 41) giving the elution time for *t*-BDPSiF. This was not the case, however, as the peak profile of the chromatogram for THF contained unique peaks apart from the chromatograms of TBAF and *t*-BDPSiF (at 5.586 min), an unexpected result that confounded proper identification more than bringing clarity. Trying to work with the chromatograms to make other peak assignments was not possible either. In short, running further qualitative standards did not help in peak assignment.

## Discussion of High Performance Liquid Chromatography Data

Although there were difficulties and ambiguities present in the HPLC data, there is still clearly the presence of *t*-BDPSiF in the sample aliquots from method E (see Figures 36 and 37) as established previously. Without a definitive peak assignment, assessing percent total deprotection of 2-AG-DS is impossible, but it is still possible to assess *potential* extent of deprotection by looking at each peak that might be *t*-BDPSiF and analyzing accordingly. This allows an establishment of a minimum/maximum for deprotection that occurred.

Figure 36 gives the chromatogram from the 50 mg/mL *t*-BDPSiF. There are five peaks of interest within this chromatogram, occurring at 1.9 min, 5.0 min, 7.6 min, 8.9 min, and 10.1 min. Standard curves of the peak area vs concentration at each retention times were generated from the HLPC data from the standards (100 µg/mL, 1 mg/mL, 10 mg/mL, 50 mg/mL, and 109 mg/mL). In sequence of increasing elution time, these graphs are given in Figures 42, 43, 44, 45, and 46. In each case, save for the standard curve for the peak at 1.9 min, the 109 mg/mL standard was discarded as an outlier, improving overall linearity for each graph. As can be seen in Figure 42, there is no linear relationship for the graph generated from the data set at 1.9 min, which is why this data set was disregarded for further analysis. Looking at Figures 43, 44, 45, and 46, there are clear linear trends of varying precision, as measured by the linear correlation coefficients ($R^2$) provided for each under the trendline equations.

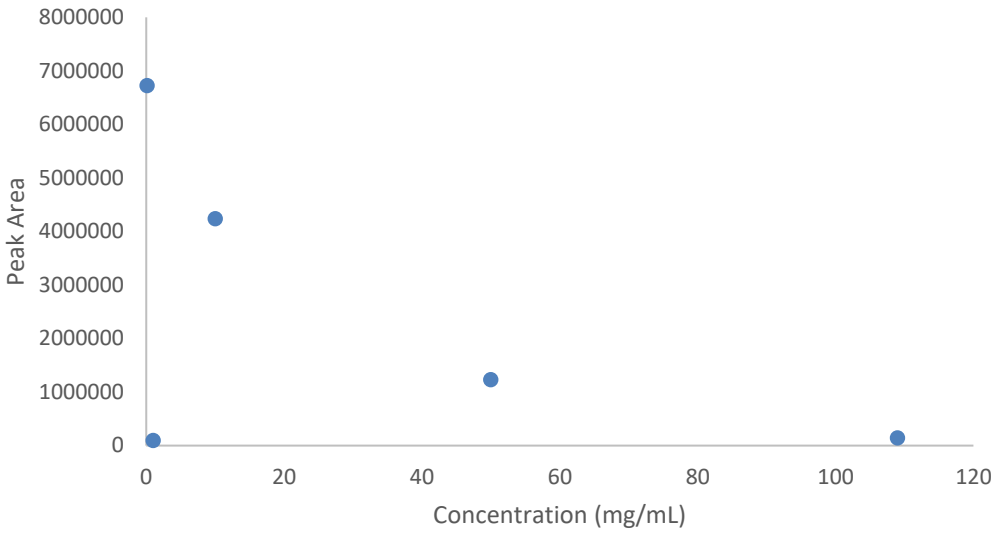


*Figure 42*. Standard curve for *t*-BDPSiF using 1.9 min peak

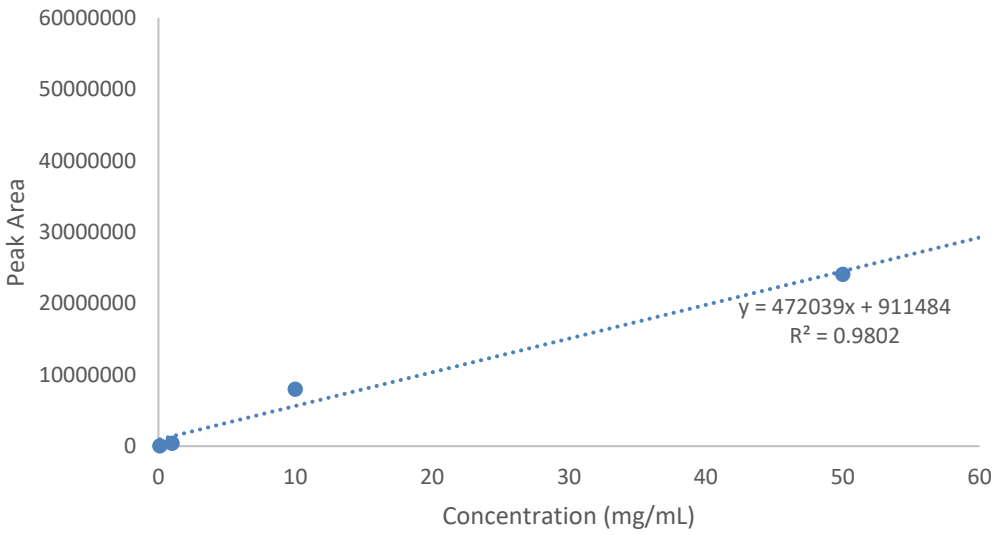


*Figure 43*. Standard curve for *t*-BDPSiF using 5.0 min peak

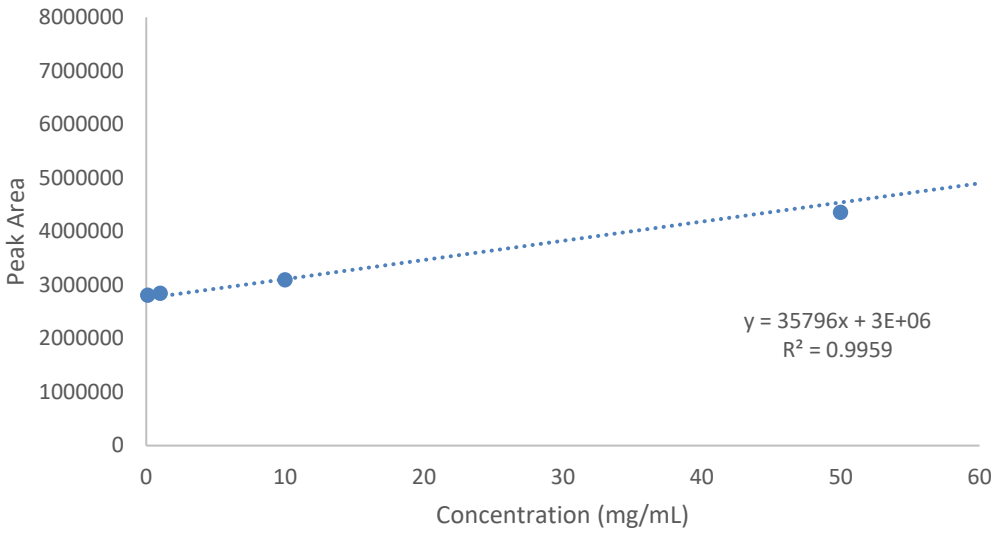


*Figure 44*. Standard curve for *t*-BDPSiF using 7.6 min peak

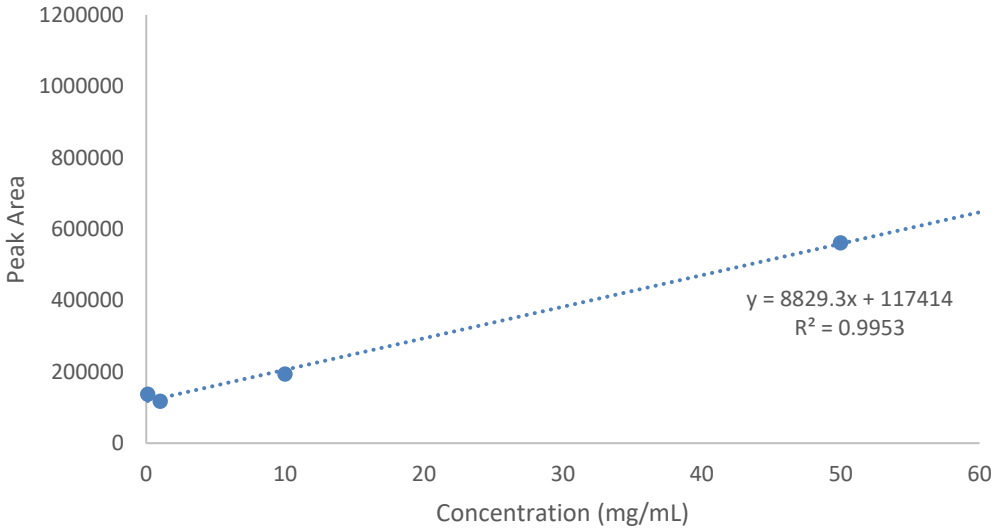


*Figure 45*. Standard curve for *t*-BDPSiF using 8.9 min peak

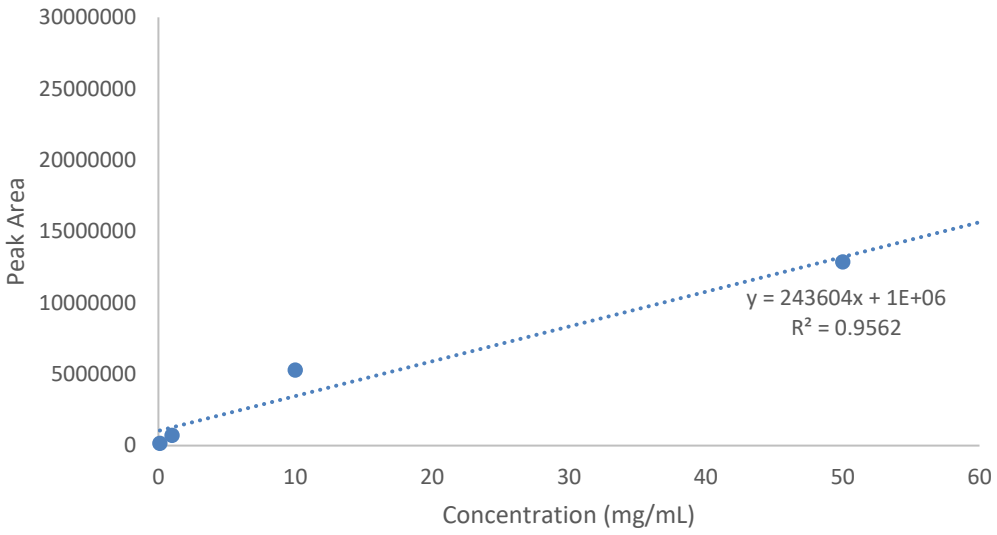


*Figure 46*. Standard curve for *t*-BDPSiF using 10.1 min peak

To gauge potential deprotection, each of these standard curves were analyzed with the concomitant data from the chromatograms from deprotection methods D and E. Table 11 gives the results of this analysis. Referring to Figure 36, the chromatogram for the 50 mg/mL *t*-BDPSiF standard, the insert for the 10.1 min peak area is given in the upper right corner of the chromatogram. This chromatogram was generated from the 24 hr aliquot from deprotection method E and was diluted 100-fold prior to analysis. A sample calculation for the generation of the values in Table 11 is given below for reference.

Sample calculation for percent deprotection from Method E

0.257 g 2-AG-DS into 5.140 mL = 50 mg/mL

50 mg/mL x .02 mL ÷ 855.1 g/mol = $1.17 \times 10^{-3}$ mol

$[(20784 \times 100) - 1 \times 10^{6}]/243604 = 4.43$ mg/mL

4.43 mg/mL x .02 mL ÷ 258.41 g/mol ÷ 2 = $1.72 \times 10^{-4}$ mol

Percent deprotection = ($1.72 \times 10^{-4}$ mol ÷ $1.17 \times 10^{-3}$ mol) x 100% = 14.6%

Table 11

*Potential Percent Deprotection for Methods D and E*

| Peak elution | 5.0 min | 7.6 min | 8.9 min | 10.1 min |
|---|---|---|---|---|
| Method D (24 hr) | < 0.3% | < 0.3% | N/A | < 0.3% |
| Method E (3 hr) | < 0.3% | < 0.3% | < 0.3% | < 0.3% |
| Method E (24 hr) | 15.2% | < 0.3% | N/A | 14.6% |

To explain the data in Table 11, there were three general outcomes from analysis. The first would be a negative result, which was interpreted as deprotection that fell below the lower limits of detection, which would mean deprotection less than 0.3%. The lowest *t*-BDPSiF standard analyzed was 100 µg/mL. Thus:

0.1 mg/mL x 0.02 mL ÷ 258.41 g/mol ÷ 2 = $3.87 \times 10^{-6}$ mol

$3.87 \times 10^{-6}$ mol ÷ $1.17 \times 10^{-3}$ mol = .003 = 0.3%

The second was a result in excess of 100%, which is obviously not physically possible, and could indicate one of two errors. Either the peak being analyzed was simply not *t*-BDPSiF or the peak was a combination of compounds that absorb at 274 nm eluting together. These results were denoted with N/A. Finally, some results were considered valid, and are reported in the table accordingly. From this data set, it is possible to at least comment on the potential efficacy of each deprotection method. It seems that method D (6 mol equivalents of TBAF with 6 mol equivalent of acetic acid) is essentially non-effective, while method E (10 mol equivalents of HF with 1 mol equivalent of pyridine) is sparingly effective, with a potential maximal deprotection of approximately 15% after 24 hr.

## 2-Arachidonoyl Glycerol Recovery Outcomes

As mentioned previously in Chapter III, fractions were collected from the HPLC as they eluted at time points that corresponded to elution of 2-AG in the Rouzer et al. (2002) HPLC methodology (the basis for the method used). The goal was to determine where 2-AG was eluting in the hope that purification of 2-AG could be accomplished via HPLC by scaling up to a preparative column. Unfortunately, none of the fractions collected and screened via $^{1}$H-NMR showed any sign of 2-AG. Given the results in Table 11, a simple explanation of this outcome might be that there was no 2-AG to collect, but some of the fractions collected did contain compounds that might have been a fatty acid by-product of the breakdown of 2-AG, indicating that the fluoride ion concentration might have been too strong.

Figure 47 shows an $^{1}$H-NMR from a fraction collected at 15.88 min from deprotection Method D. The HPLC method adapted for screening deprotection methods originally reported elution of 2-AG at 15 min and 1(3)-AG at 15.5 min (Rouzer et al., 2002). Carbonyls will absorb in the UV-Vis spectrum with a maximum at 275 nm (Bayliss & McRae, 1954), so the presence of a peak here might have been indicative of either 2-AG or its isomer(s). The NMR signals had to be amplified considerably to be detected and fell exclusively between 0.0 to 3.2 ppm (save for the broad singlet at 4.7 ppm from HOD, the deuterated solvent used for this $^{1}$H-NMR). Parts of the sample profile appear to match the fatty acid tail of 2-AG, with multiplets at 3.05 ppm and 1.55 ppm, a triplet at 0.8 ppm, and a sextet at 1.25 ppm. However, the signature methine multiplet at 5.5 ppm is entirely absent, as well as many other characteristic signals for 2-AG, which is suggestive that the sample is some by-product from the breakdown of 2-AG

or 2-AG-DS, although it could potentially be some entirely unrelated substance eluting from the column. With the limited data available, it is difficult to make definitive statements as to the identity of this compound, but the time at which it elutes and the $^{1}$H-NMR profile suggests that it is some kind of hydrocarbon, but it is neither 2-AG-DS nor 2-AG. Most fractions screened via $^{1}$H-NMR did not contain any detectable compounds, and the collection of analyzable material from each 20 µL fraction was so scant that analysis beyond NMR was not feasible.

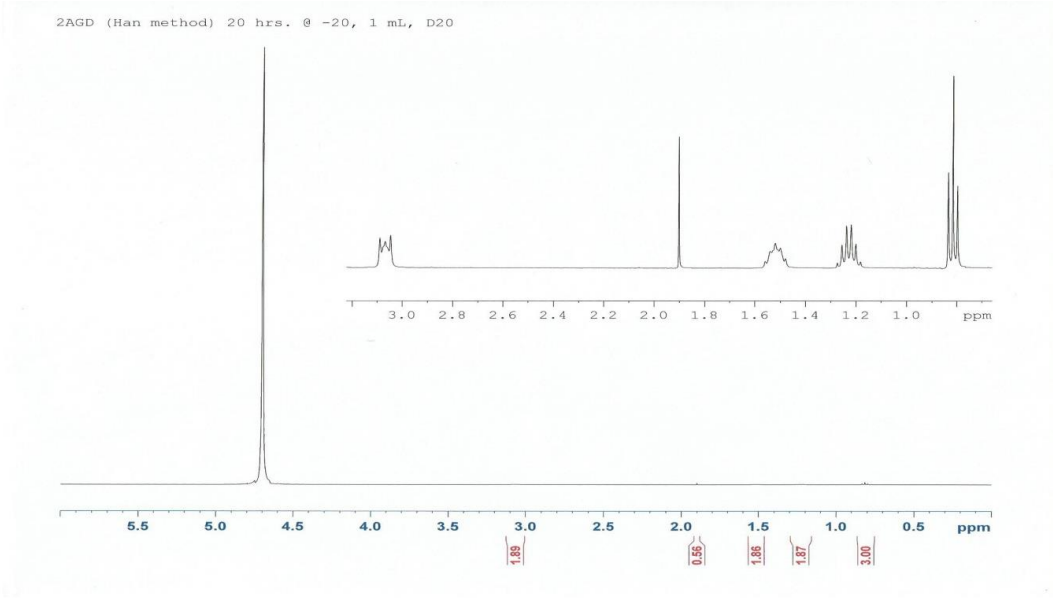


Figure 47. $^{1}$H-NMR of 15.88 min fraction from HPLC collected at 20 hours total run time from deprotection Method D.

## Single Flask Synthesis of 2-PG-DS in Dimethylformamide Using Thionyl Chloride

Running deprotection methods A through E exhausted all remaining available 2-AG-DS. In the course of preparing new standards to resolve peak identity in the HPLC

chromatograms, the synthetic method for the preparation of 2-AG-DS was concomitantly reviewed. Up to this point, each intermediate from each synthetic step was isolated, purified, and characterized. This inevitably resulted in some minimal loss of product and time, as certain synthetic intermediates were more amenable to isolation and purification than others. Consequently, palmitic acid, a 16-carbon saturated fatty acid, was utilized in place of arachidonic acid during synthetic methodology development due to its cheaper price and suitability as a fatty acid substitute for arachidonic acid. The results from the deprotection methods screened up to this point demonstrated that amending previous methods that proved successful with deprotection of *t*-BDPSi ethers were seemingly not as successful as they were expected to be, and so returning to palmitic acid for the purposes of blanket screening more deprotection methods was immediately appealing.

It was established previously that DMF is the superior solvent for the formation of silyl ethers using the Corey methodology (Patschinski et al., 2014) at least in terms of reaction kinetics. Screening deprotection methods with a doubly silylated 2-palmitoyl glycerol compound would allow basic vetting of deprotection conditions that might be suitable for 2-AG-DS, but ultimately, given the unique stability constraints in using arachidonic acid, 2-AG-DS must still be screened separately in any conditions demonstrating successful deprotection (greater than 80% yield would be the goal). If there were a way to produce 2-AG-DS or the palmitic acid derivative (2-PG-DS) in a single reaction flask without the need for purification and transfer to a new reaction solvent in-between steps, it would be incredibly helpful for the purposes of screening and to ameliorate the need to isolate each intermediate and so lose potential product.

By using DMF as a solvent, however, there is a potential issue with the synthetic methodology. DMF itself contains a carbonyl, which should be reactive with thionyl chloride, potentially causing a cross reaction with the solvent, rendering this reagent and reaction pathway ineffective. However, this is not in fact the case, as the reaction of thionyl chloride with DMF generates a reactive chloroimium ion that then proceeds to react with free palmitic acid (or G-1,3-DS) to produce the fatty acid chloride that then proceeds to generate the ester. Figure 48 details this mechanism (Arrieta, Aizpurua, & Palomo, 1984).

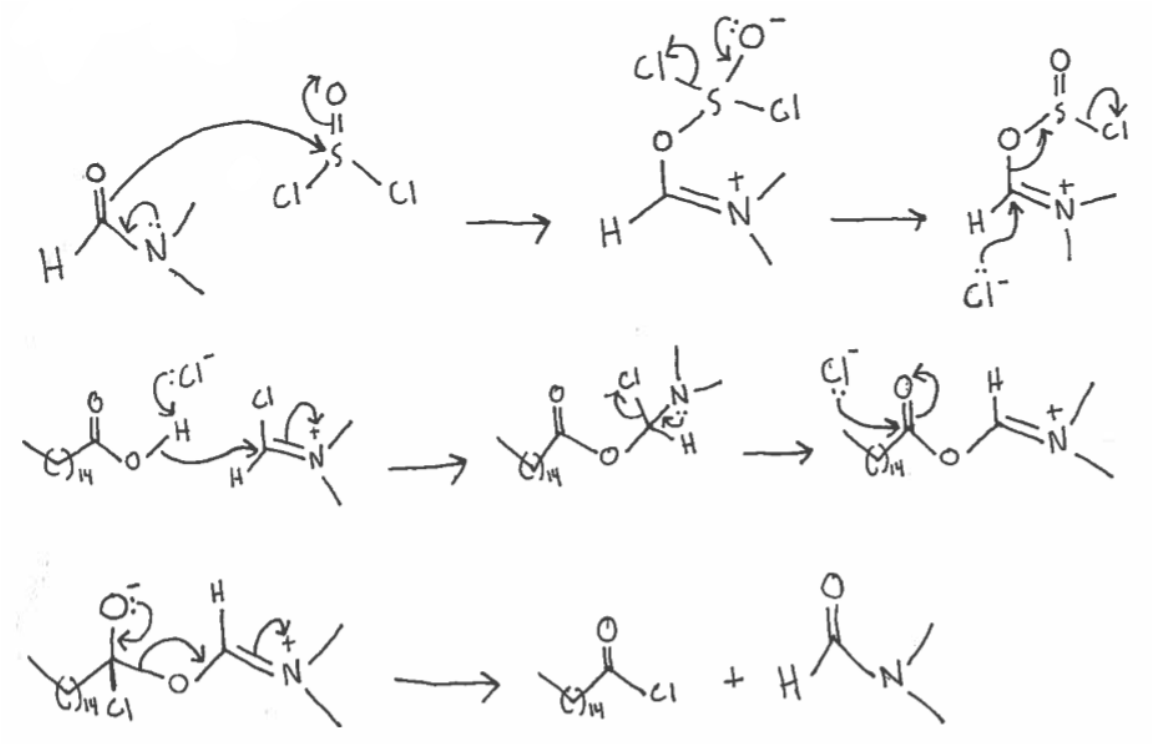

*Figure 48*. Mechanism for the generation of palmitoyl chloride with thionyl chloride. Note that the chloroinium ion generated may react with either palmitic acid or G-1,3-DS; whichever nucleophile it encounters first.

A reaction was set up to test the outcome for the synthesis of 2-PG-DS using glycerol as a starting material with the synthetic methodology described in Chapter III

but without isolating or purifying products in each step. The only alteration to the methodology in Chapter III was the performance of the esterification step at ambient temperature (21-23 °C) to hopefully improve yield. Figure 49 shows the $^{1}$H-NMR of the product isolated by liquid-liquid phase extraction of the DMF reaction mixture with 5 mL aliquots of hexane three times. The product matches the expected $^{1}$H-NMR profile of 2-PG-DS. Signals in the 0 to 3 ppm range characteristic of the fatty acid tail are present, namely a 0.8 ppm triplet corresponding to the terminal methyl, a sextet at 1.6 ppm corresponding the adjacent methylene of this terminal methyl, and a triplet at 2.35 ppm corresponding to the methylene adjacent to the carbonyl. Further signals from the fatty acid tail methylenes exist as diffuse and overlapping multiplets between 1 and 2 ppm. The aromatic signals from the protecting group are clearly present in the corresponding region between 7 to 8 ppm. Finally, the telltale signals for glycerol occur in the region between 3.5 to 4.4 ppm and is shown on a zoomed in scale in the inset in Figure 49. This $^{1}$H-NMR spectrum produced the sharpest and clearest signals of the splitting of the methine and methylene hydrogens from glycerol (Figure 30) to this point, demonstrating clearly that the generation of doubly silylated monoglycerols is achievable using DMF and thionyl chloride in tandem. The most welcome feature of the $^{1}$H-NMR is the fact that it is free of signals belonging to DMF, showing that purification, from the reaction solvent was complete. Table 12 gives the percent recovery for 2-PG-DS, showing a marginal improvement from before.

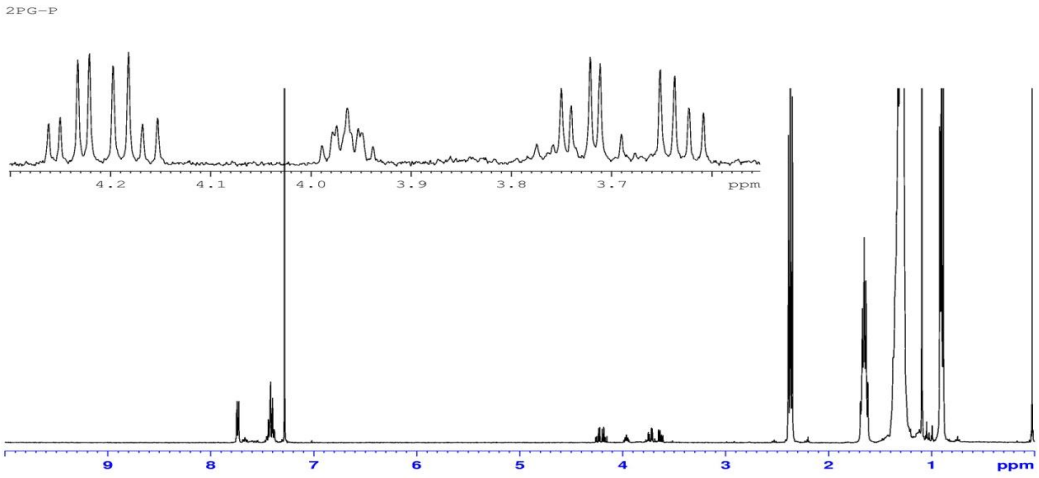


*Figure 49.* [1]H-NMR of 2-PG-DS

Table 12

*Percent Recovery of 2-PG-DS.*

| Trial | Percent Recovery |
|---|---|
| 1 | 60.7% |
| 2 | 77.1% |
| **Average** | **69 ± 12%** |

## Deprotection of 2-PG-DS

Three different trials were conducted to screen new deprotection conditions using the newly synthesized 2-PG-DS. The trials were modifications of the original Corey deprotection method (Corey & Veknateswarlu, 1972) utilizing TBAF in THF at higher concentrations than utilized previously. Concentrations of TBAF employed were 0.5, 1.0, and 2.0 M. Deprotection was carried out for 24 hr at 0 °C under inert conditions and sample aliquots were taken and analyzed using the same HPLC method and the C18 Phenomenex column. Unfortunately, as before, deprotection results were difficult to interpret given the presence of multiple, unidentifiable peaks in the HPLC

chromatograms. The maximum amount of *t*-BDPSiF detected *in-situ* from HPLC analysis would place deprotection at 75.9%, but the chromatograms had ambiguities as before, and it is dubious whether that result is accurate. Figure 50 shows a graph of the peak area vs time for aliquots taken from the 1.0 M TBAF deprotection trial. The initial two data points on the graph seem to show a linear trend, a good sign that this might have been *t*-BDPSiF, however, the next two aliquots returned less total area, corresponding to less concentration, than the preceding reading. This was an unexpected result, but if accurate, it might imply that with increasing time *t*-BDPSiF was degrading. The final reading showed an increase in area once again, however, debunking that idea entirely and suggesting that either the standards were inaccurate or there were issues with the HPLC column or detector.

The presence of such trends in the data set generated from these deprotection trials is why they are excluded from this paper. As was stated previously, the difficulties that materialized in analyzing the deprotection methods via HPLC indicate that further work needs to be done to resolve these issues if HPLC is to be used further.

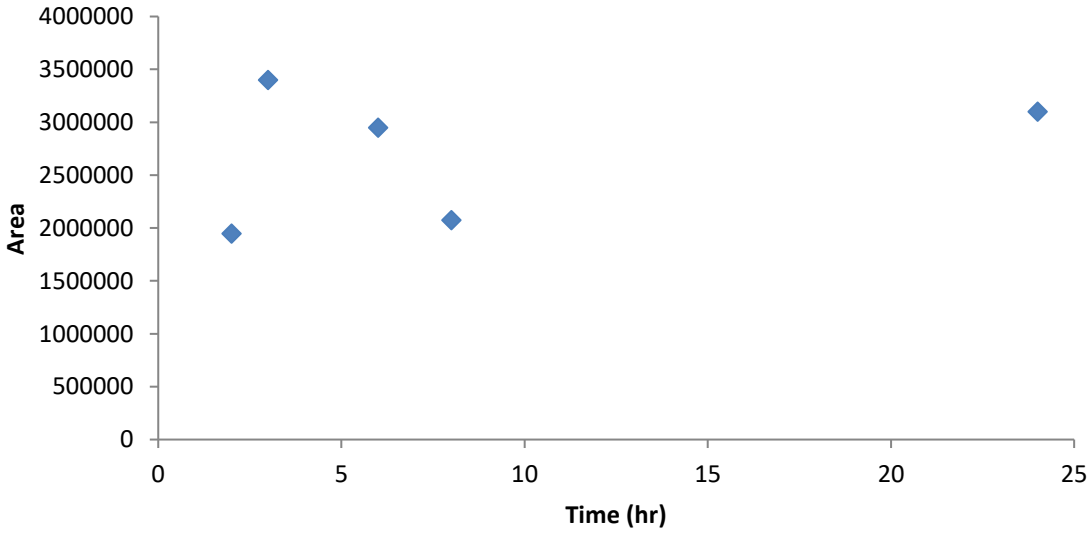

*Figure 50*. Peak area vs time for 2-PG-DS deprotection utilizing 1.0 M TBAF in THF.

### 3-(4,5-Dimethylthiazol-2-yl)-2,5-diphenyltetrazolium Bromide Assay Results from CRL 1682 Cells Treated with Phytocannabinoid Extracts

Without the recovery of 2-AG, it was obviously not possible to screen cancer lines using the MTT assay with that compound; however, proof of the usefulness of this assay as a tool for measuring cancer cell culture response to cannabinoids can be seen in the following assays conducted using extracts from samples of marijuana containing the phytocannabinoids THC and CBD.

Figure 51 gives the MTT cell proliferation assay results for increasingly dilute treatments prepared from extracts from a marijuana sample with high THC content. The solutions were diluted an order of magnitude between each treatment well series. The cancer line being treated was a pancreatic cancer cell line, CRL 1682. The assay results show a proliferation pattern that is not uncommon for cannabinoids, where certain concentrations can enhance growth (as in the first two treatment concentrations) but then a concentration range, typically in the μM range, is reached where growth is completely abrogated (the next two treatment concentrations). Eventually, with continuing dilution, a growth enhancing effect returns (the final two treatment concentrations). Figure 52 shows an MTT cell proliferation assay of another extract of marijuana, a sample containing high amounts of THC and CBD. The results from this assay show a consistent anti-proliferative effect for each increasingly dilute treatment (save for the undiluted extract), showcasing how combinatorial treatments utilizing multiple different cannabinoids with different affinities for the CB receptors can achieve treatment outcomes that are more

universally positive, and therefore, desirable. Results such as these clearly demonstrate why cannabinoids warrant investigation as anti-cancer agents.

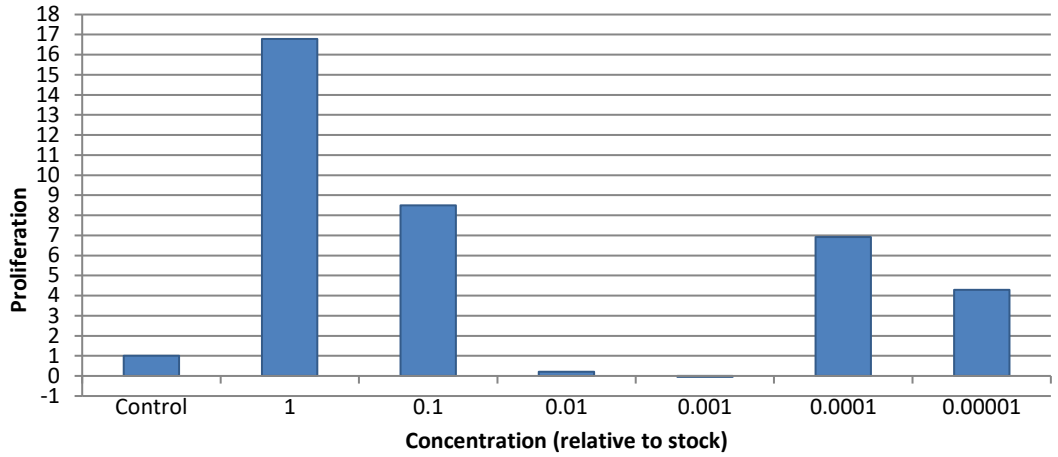


*Figure 51*. MTT cell proliferation assay of pancreatic cancer cells (CRL 1682) treated with high THC extract solutions. Extracts are ten-fold dilutions of a plant sample extract.

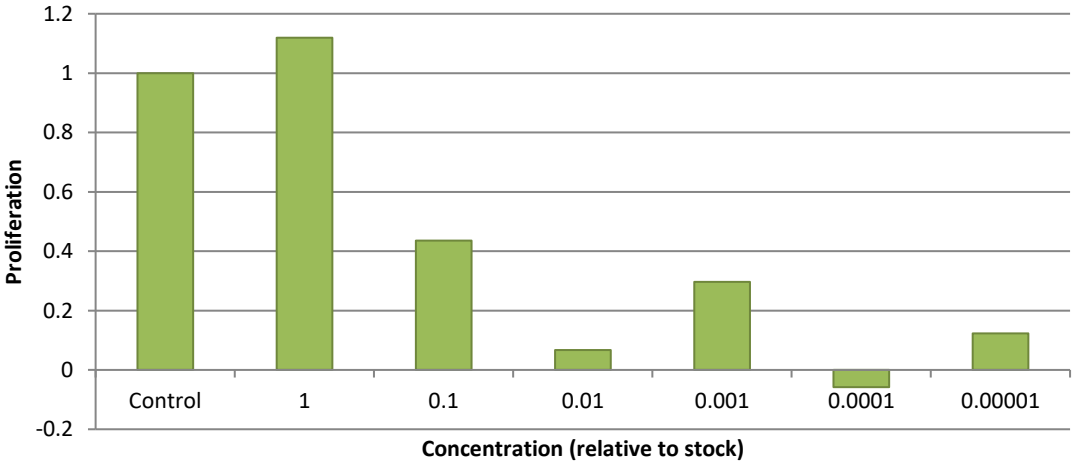


*Figure 52*. MTT cell proliferation assay of pancreatic cancer cells (CRL 1682) treated with THC/CBD extract solutions

# CHAPTER V

# CONCLUSIONS

## Current Status

The results of this research demonstrated that *tert*-butyldiphenylsilyl chloride is an appealing protecting group to generate protected 2-monoglycerols (in this case 2-AG-DS or 2-PG-DS) from both DHA and glycerol, although not without draw backs. The discovery that the synthetic methodology could be carried out in a single reaction flask using the kinetically favored solvent, DMF, while still producing a good yield with $SOCl_2$ is an appealing quality of this protecting group. Unfortunately, conditions employed to remove the protecting group seemed to be ineffective; however, given issues that were encountered with the methods employed to assess deprotection, this was not definitively established and bears further investigation.

The primary issue in assessing deprotection was acquiring pure standards to confirm peak identity of compounds absorbing at the wavelength of interest (274 nm). Without a way to pinpoint which peak belonged to which compound, interpreting the deprotection method effectiveness by HPLC becomes extremely difficult; which is why deprotection was given as a potential value. The additional confounding peaks in the standards have several potential origins. First, the HPLC columns used in screening standards and samples were additionally used for the analysis of other cannabinoid extracts and other laboratory samples. The removal agent employed in all deprotection

methods, fluoride ion, forms strong single bonds with Si, the Si-F bond dissociation energy being 540 kJ/mol compared to the bond dissociation energy of Si-C of 435 kJ/mol (https://labs.chem. ucsb.edu /zakarian/armen/11---bonddissociation energy.pdf), which is why it is widely employed to remove silyl ether protecting groups. This is also why the scavenging of free fluoride ion from sample aliquots with $Mg^{2+}$ or silicon dioxide was vital before loading onto the column, as silica is the linker for the 18-carbon alkyl chain that constitutes the stationary phase for the reverse phase columns used in screening samples. It is possible that the sample depicted in Figure 48 (Chapter IV, page 82) that appeared to be a component of the fatty acid tail of 2-AG was in fact part of the C-18 stationary phase that was liberated if fluoride ion attacked the silica column packing. Passage of injected samples through the column could also have liberated components adherent to the C-18 stationary phase through Van der Waals interactions, causing elution at sporadic times, which might explain the unexpected peak at 5.586 min in Figure 38. Although each sample was treated to ensure no free fluoride ion was allowed onto the column, it is unclear how even minute amounts introduced would impact column integrity and use, and this consideration was one reason further HPLC analysis was not pursued past the second series of standards.

It is my contention that deprotection was probably not as scant as what was detected. From the data for the deprotection trials conducted with 2-PG-DS, the maximum calculated deprotection was 75.9% (determined by blanket screening all pertinent peaks returned from aliquot analysis and treating as *t*-BDPSiF in an identical process detailed in *Discussion of HPLC data* on page 76), which is closer to the extent of deprotection reported previously (Nicolaou & Webber, 1986), but as discussed, given the

discrepancies in the data as a whole, it would be inappropriate to present this as a conclusion. The conditions used should have been more effective than detected. The removal conditions need to be able to be accurately assessed before attempting to screen further.

Return on yield prior to esterification was excellent. The esterification with thionyl chloride was less effective, showing improvement when conducted at ambient temperature. Increasing reaction temperature and adjusting reaction time could improve yield, while still avoiding unwanted side reactions, especially if carried out under inert conditions, as the oxidation of 2-AG and 2-AG-DS would be the greatest contributor to by-product generation and product loss at this stage. With these adjustments, the methodology could outperform other currently published procedures, and based upon the data obtained thus far, these adjustments should be readily implementable.

Based upon retrospective evaluation of the analytical methods and techniques employed for this research, there are several modifications that would potentially be fruitful. The first and most obvious, if the deprotection issues are in fact a reality, would be utilizing a different silyl ether protecting group for protecting DHA or glycerol. TMSCl (trimethyl silyl chloride) would be an interesting protecting group to evaluate, given its ease of removal in comparison to *t*-BDPSiCl (Greene & Wuts, 1999). It might be the case that TMSCl would not be amenable to use with $SOCl_2$, but it is the most labile of the silyl ethers and its substitution would be a sensible next step in evaluation of these protecting groups with this methodology.

Furthermore, qualitative TLC was consistently used as a tool to evaluate reaction completion and product purity, but in each case, a polar stationary phase was used. The

results of the HPLC analysis and $^{1}$H-NMR spectra indicate that products isolated might not have been pure. For instance, in Figures 28 and 29, the methyl and aromatic regions of these spectra contain additional unexpected peaks. The presence of these peaks indicates that there is likely a by-product from a previous step, namely the hydrated form of the protecting group, *t*-BDPSiOH, which is contributing the extraneous signals in those regions. Analysis of products isolated from intermediate synthetic steps via HPLC would be a more accurate, although time consuming, way of establishing product purity prior to $^{1}$H-NMR analysis.

Finally, qualitative TLC was frequently used to gauge reaction completion and product purity, but as established, the presence of extraneous peaks in $^{1}$H-NMR spectra indicate that the resolution was not sufficient to properly assess either. One improvement that could be made in this regard would be employing C-18 stationary phase for TLC and any column chromatography used to attempt to purify product. Given that HPLC analysis revealed the presence of multiple peaks in sample aliquots, it is possible that by-products carried from earlier reactions were contributing these additional signals, and since reverse phase HPLC columns were used, it is highly likely that the use of reverse phase in other analytical techniques employed would be helpful in resolving by-products or in the purification of product in intermediary steps.

## Future Work

A treatment modality that cannabinoids could be incorporated into with great therapeutic effect would be chemotherapy. Chemotherapeutic agents are typically known for their unwanted toxicological side effects (Cella & Cherin, 1988), but other practical difficulties involved with their use range from poor bioavailability, the development of

multiple drug resistances to these compounds, complications arising from lack of specificity for cancer targets, and simply poor therapeutic indices; many of these issues being directly conflated with the larger doses intended to increase efficacy against their target (Senapati, Mahanta, Kumar, & Maiti, 2018). One route being investigated to address these issues is the use of vehicles, such as lipid-based niosome (non-ionic surfactant-based vesicle) nano-carriers to facilitate the carry and delivery of hydrophilic drugs to tumor sites for targeted therapy (Naderinezhad, Amoabediny, & Haghiralsadat, 2017). The association or sequestration of drugs with poor bioavailability with(in) lipid-based carriers served as inspiration for a possible use of 2-AG as a hydrolyzable drug "sheath." The goal of this combination would be to improve the overall bioavailability of both compounds by chemically bonding them; eliminating hydrogen bond donors in 2-AG, and adding more lipophilic character to small, poorly water-soluble chemotherapeutic agents. Figure 53 shows a model of this concept with aminoglutethimide (bracketed).

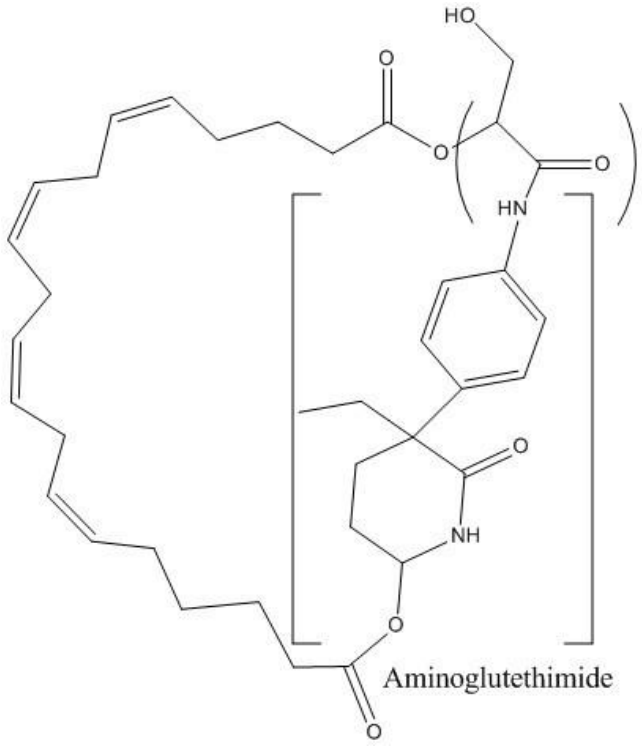


*Figure 53*. Aminoglutethimide drug "sheath" concept

Aminoglutethimide is an aromatase inhibitor used to treat hormone-dependent breast cancer after first line treatments, such as tamoxifen, have proven ineffective (Patrick, 2013). The log P (where P is the partition coefficient; the ratio of the concentration of a substance across two immiscible solvents, in this case, concentration in 1-octanol over concentration in water) of aminoglutethimide is 1.2 (https://pubchem .ncbi.nlm.nih.gov/compound/ aminoglutethimide), whereas the log P for 2-AG is 5.3 (https://pubchem.ncbi.nlm. nih.gov/compound/2-arachidonoylglycerol), placing 2-AG in excess of Lipinski's recommended log P ≤ 5 (Patrick, 2013). However, bound together as in Figure 53, a hydrogen bond donor is eliminated, and the amalgamation will probably have a log P in between the two values of 1.2 and 5.3, making it closer to Lipinski's recommendation.

This example is not perfect, as the combined molecular mass is in excess of the recommended 500 Da (combined MW = 620.79 g/mol) and aminoglutethimide is a perfectly serviceable drug on its own, and it is not clear that using it in this treatment method would be beneficial or even warranted. As a demonstration of a concept though, it is a good example to highlight a potential useful application of 2-AG. Such unions could boost overall efficacy through an entourage effect, once the molecule is hydrolyzed into its constituents. This could potentially give a more positive treatment outcome compared to the presentation of the drugs in isolation or even in synchrony. This is essentially identical to combinatorial therapy, but the kinetics of hydrolysis/dissociation might afford a different reactivity profile that would be worthwhile screening against cell culture. So long as the molecular weight of the compound being "sheathed" can be maintained in the neighborhood of 200 Da, and that the functional attachment to 2-AG does not require modifying either compound to the point of inactivity or toxicity, then there is no theoretical limit to what could be placed within the monoglyceride.

Specificity for the desired target (the cancerous cells) is still an issue that is not resolved with this idea. However, given the data supporting the relatively non-toxic nature of cannabinoids to non-cancerous cells and their use as anti-emetic and pain-relieving agents (Velasco et al., 2012), it might be the case that this treatment method would be more suited to use in conjunction with non-specific, anti-proliferative chemotherapy treatments. Utilized in this manner, the hydrolysis back into the constituents would theoretically produce effects that are more anti-proliferative while concomitantly counteracting at least the sensation of the unwanted physiological side effects (pain and nausea).

There are obvious difficulties with this technique, however. The first would be obtaining a ready source of 2-AG that is activated at the terminal carbon of the fatty acid tail, such as 20-hydroxy-arachidonic acid, which to my knowledge represents a major hurdle already, this compound costing hundreds of dollars for microgram quantities (https://www.sigmaaldrich.com/catalog/product/sigma/h3023?lang=en&region=US). Furthermore, SAR studies to date have revealed the necessity for 3-4 double bonds in the fatty acid tail for proper activity at the CB receptors; fewer than that leads to inactivity (Mechoulam and Ben-Shabat,1999). Preliminary SAR studies looking at fatty acid chain substitutions, either of arachidonic acid, or complete substitution with a leukotriene or prostaglandin derivative, have shown lack of activity, save for one exception, 12(S)-hydroxy-arachidonoyl ethanolamide, which will bind to $CB_1$ (Mechoulam et al., 1998). These data reveal that finding a suitable cost-effective substitute might be challenging.

Another route to increase 2-AG efficacy and potency would simply be modification of the compound itself, which was of primary interest and one of the major reasons direct synthesis was chosen. By examining published SAR data for model compounds, crystallography data for $CB_1$, and giving priority to emerging drug design needs when making structural decisions, several interesting routes for modifying 2-AG exist that are worth exploring. As mentioned previously, SAR studies for 2-AG are not well published, but Mechoulam's group has purportedly forthcoming results indicating that 2-AG rudimentarily mirrors anandamide regarding SAR (Mechoulam et al., 1998). The 1(3) isomer of 2-AG was reported as binding to both CB receptors with similar potency as 2-AG, and the fatty acid derivatives 2-palmityoyl glycerol and 2-linoleoyl ($18:2^{9,12}$) glycerol showed no activity at either $CB_1$ or $CB_2$. This is in keeping with the

previous SAR findings where three to four double bonds were necessary for proper binding. Figure 54 gives the structure of anandamide and SAR information for this compound.

The SAR information for anandamide can be used to help inform 2-AG modification, but beyond that, an interesting piece of information concerning the conformation that 2-AG assumes when binding to $CB_1$ was given by Hua et al. (2016) in their crystallography study of the $CB_1$ receptor, namely that 2-AG takes a "C-shaped" conformation (see Figure 5) in the pocket of $CB_1$ and is predicted to bind similarly to that of THC. If the binding mode is similar to THC, it might also be possible to utilize SAR for THC to look for structural modifications for 2-AG to improve its efficacy. Prior to examining the SAR for THC, an attempt at demonstrating the overlay of these two compounds is presented in Figure 55. This figure does not necessarily reflect the actual conformation of 2-AG within the binding pocket, but simply gives a baseline upon which to form the following discussion. Without a rudimentary comparison, any SAR information concerning THC would be difficult to translate to 2-AG.

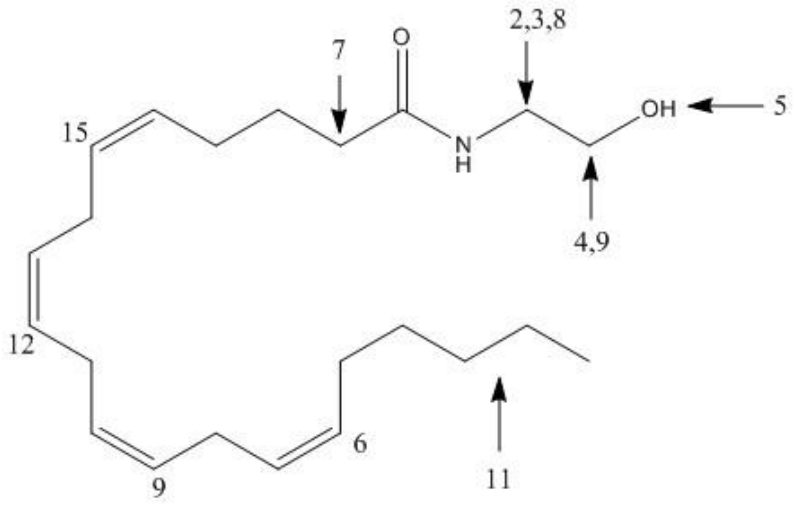


*Figure 54*. Anandamide SAR information. (Adapted from Mechoulam *et al.,* 1998.) Each numbered SAR element (below) that corresponds to a specific part of the structure is numbered in the figure to facilitate discussion. 1) Double bonds must be ≥ 3-4 or activity is abrogated. 2) The unsubstituted amide is inactive. Mono-alkylation (substitution of the N-ethanolamide) up to a branched pentyl group exhibits significant activity, following the trend: $C_5H_{11}$ < $CHMeCH_2Me$ < *n*-$C_4H_9$ < *t*-$C_4H_9$ < $CH_3$ < $C_2H_5$ < $C(CH_3)_2$, < *n*-$C_3H_7$. 3) *N,N*-dialkylation leads to loss of activity. 4) Hydroxylation preserves activity, but is lowered. 5) The methyl ether and phosphate are less active than the parent alcohol. Carbonyl derivatives are inactive. 6) In the n-3 series (in Mechoulam's figure, n-x is the designation used to signal where the double bond series begins, so n-3 would be the third carbon starting from the terminal carbon of the fatty acid tail, similar to the Ω numbering system for fatty acids; 3-4 double bonds are necessary for activity but their sequence is flexible), derivatized ethanolamides are either inactive or less active than related compounds in the n-6 series. 7) Alkylation or di-alkylation of the α-carbon preserves binding; methylation or di-methylation potentiaties and increases activity. 8) Chiral centers on *N*-alkyl substituents lead to radically altered $K_i$. 9) Replacing the -OH with -F leads to a 10 fold increase in binding to $CB_1$. 10) Conjugation of the double bonds leads to reduced activity. 11) Branching of the fatty acid tail enhances binding.

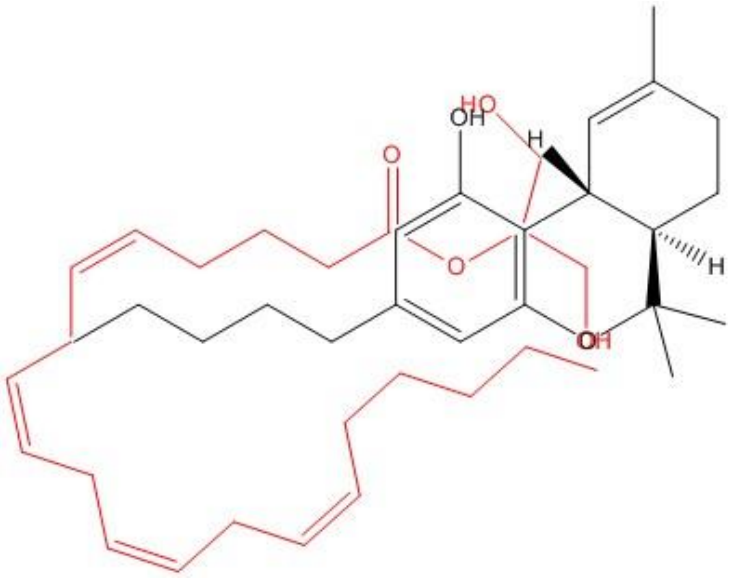


*Figure 55*. Overlay of 2-AG (red) with THC (black), attempting to show potential similarity in binding

Figure 56 is a diagram of THC outlined for discussion of SAR elements for this compound. Although numerous major pharmacophores are present within THC, one of the main moieties responsible for variation in receptor binding parameters is the C3 side chain. The chain has a minimum length requirement of three carbons and was characterized as being ideal at 5-8 carbons (Bow and Rimoldi, 2016).

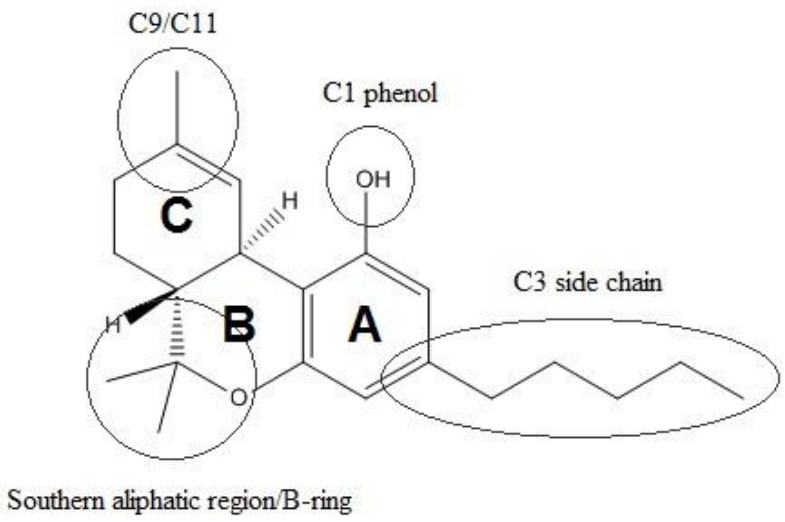


*Figure 56*. Diagram of THC outlining pertinent pharmacophore moieties

Table 13 gives the relationship between chain length and respective $K_i$ for THC modified at C3 for $CB_1$. This relationship coincides nicely with the overlay presented in Figure 56, in the sense that it is easy to mentally add additional carbons at C3 for THC and see how they could conform to the backbone of the fatty acid tail of 2-AG. Furthermore, SAR studies examining modifications of the chain at C3 show that dimethylation of C'1 (the first carbon of the chain) and a total of eight carbons in the chain length (1,1-dimethyloctane) gives a $K_i$ of 0.9 nM, a full order of magnitude below that of the ideal chain length in Table 13. Further SAR on C3 showed that the introduction of alkyne functional groups (rigidity) have varying degrees of effects on $K_i$ constants for THC, usually being positive in nature. These data are indicative of the necessity of rigidity within the fatty acid linked to glycerol for appropriate binding. Studies looking at restriction of the orientation of the chain itself have shown that when the chain is locked into a downward conformation (away from the bulk of the molecule, specifically the C1 phenol), it is the more kinetically favored orientation (Bow and Rimoldi, 2016).

Table 13

*Relationship Between C3 Chain Length of THC and $CB_1$ Affinity as Measured through $K_i$. (Adapted from Bow and Rimoldi, 2016).*

| Chain Length | $K_i$ (nM) |
|---|---|
| 1 | n/a |
| 2 | n/a |
| 3 | 75.4 |
| 4 | 65 ± 13 |
| 6 | 41 ± 3.8 |
| 7 | 22 ± 3.9 |
| 8 | 8.5 ± 1.4 |

Modification of the C1 phenol has the general effect of increasing $CB_2$ specificity, both with removal or methylation. Modification of the phenol beyond methylation tends to abrogate activity at both receptors, showing the sensitivity of the receptor to this group. Modification at the C9-C11 group does not confer variable selectivity but impacts receptor affinity. Specifically, the replacement of C9-11 with a carbonyl confers an order of magnitude increase in $K_i$ for $CB_1$ and $CB_2$, and the THC derivative generated is identical to Cesamet® (generic nabilone) which is a medication prescribed to attenuate decreased appetite and the secondary wasting associated with chemotherapy (Bow and Rimoldi, 2016).

Based upon the SAR for THC and the fact that substitution of the hydroxyl group in anandamide increases $CB_1$ affinity, the following permutations of 2-AG are anticipated to be worth investigating for their increased affinity for $CB_1$ (Figure 57). Increased receptor affinity for a drug class is desirable if steady state concentrations are difficult to reach a therapeutic concentration but is generally appealing for the ability to minimize dosing requirements or if dose directly scales with therapeutic efficacy. It is appealing to modify 2-AG in this way given its transient nature in physiological conditions; increased

efficacy could potentially render a compound with physiologically beneficial effects which is essentially benign when metabolized/hydrolyzed. Glycerol's ultimate physiological fate is connected with benign intersections with carbohydrate/lipid metabolism, and arachidonic acid has multiple biological fates, but most likely would be sequestered into a biological membrane, outside of situations where it would be incorporated into an alternative metabolic pathway (such as COX-1/2-mediated prostaglandin synthesis).

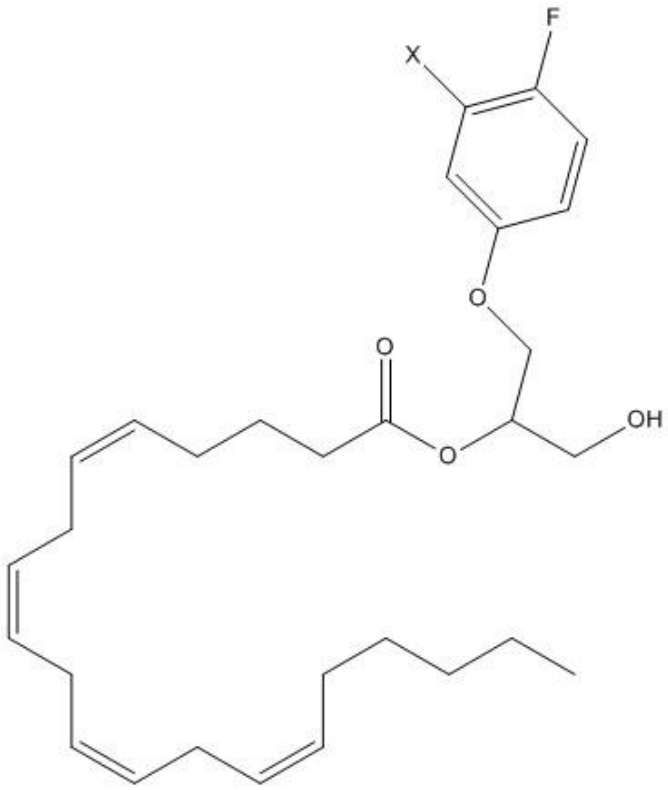


*Figure 57*. Suggested modification of 2-AG. Three possible permutations are of interest, with the distinction between the three being substitution at X, with the variable substitutions being: 1) -H, 2) -OH, 3) -$CH_3$.

The goal with the proposed modification to 2-AG is two-fold. First, from the SAR discussed previously, there is the potential to increase $CB_1$ affinity by expanding the molecule into the shallow pocket filled by arm 3 of AM6538 described in Figure 9. This

pocket is what *N*-alkyl extensions on anandamide occupy (Hua et al., 2016) and must be host to a cationic amino acid residue at its basin, as evidenced by the order of magnitude increase in $CB_1$ affinity when substituting an electronegative fluorine or chlorine atom for the -OH in anandamide. The second is to preserve the overall water solubility of 2-AG. Figure 57 shows a series of proposed modifications to 2-AG, seeking to meet both these goals. The addition of the substituted fluorobenzene at the 1 position of the glycerol is meant to fill into arm 3, with the hope that the steric bulk of the addition will favor orientation of the fatty acid tail downward, the more kinetically favored orientation (Hua et al., 2016). The substitutions at X (given in Figure 58) are intended to moderate binding affinity and solubility, and screening the substitutions looking at these two variables would be the first step in judging these 2-AG permutations. Based upon the SAR discussed previously, the compound should have a pronounced increase in affinity for $CB_1$, and the substitutions at X should serve to allow tuning of this affinity.

Exploring this concept experimentally brings its own challenges. In no particular order: 1) addition of the fluorobenzene moiety must be accomplished at C1, not C3, and so setting up the nucleophilic substitution with 1-fluoro-4-iodobenzene would require "feathering" the reaction conditions so as to generate a single substitution and then subsequent isolation and purification of the desired isomer, 2) the new compound now possesses a chiral center, the effects of which on receptor binding were reported as minimal (Bow and Rimoldi, 2016); however, for pharmacological development, each isomer must be isolated and screened individually, 3) the introduction of a halogenated benzene introduces new issues in overall compound toxicity, since halogenated benzene compounds are implicated in numerous pathologies (Environmental Protection Agency,

2006), and assessing receptor affinity for this compound, and any other 2-AG derivative of interest, will face identical challenges as those encountered by previous studies (detailed in Chapter II).

None of these issues are insurmountable; however, in combination they pose a challenge requiring ingenuity to approach. With the publication of a crystal structure for $CB_1$, using mathematical models to predict an idealized, stable agonist is a clearly favored path forward, and adapting such models to inform structural modification of 2-AG to improve $CB_1$ affinity is a rational next step. Regardless, the only true test is to synthesize each compound and screen with the appropriate battery of tests.

## Summary

The total content of this thesis has covered a broad range of topics from the socio-cultural impediments to the study and use of the psycho-active constituents of *C. sativa*, to the discovery and elucidation of a novel cannabinoid receptor system and the associated endogenous ligands, to the integration and effects of the cannabinoid receptor system in the cellular cycle, and finally, the implications of these effects in the pursuit of using cannabinoids in cancer treatment modalities. The purpose of presenting this breadth of information was to give the appropriate context for the reasons for undertaking this project to begin with, and why the pursuit of an improved synthetic route for 2-arachidonoyl glycerol is a desirable goal. The goal of synthesizing 2-AG is a stepping stone on a path that hopefully leads to methods by which cannabinoids can be incorporated into cancer treatment modalities to improve existing treatment methodologies or even generate completely novel treatment methods. Doing this requires a view that encompasses not just the chemical, biological, and physiological background,

but also the sociological and legal impediments for bringing these compounds into pharmacological treatment and distribution systems.

The breadth of the task and challenges involved can be daunting. Only further time and research will tell if cannabinoids can be integrated into new and successful treatment modalities, but if the current state of knowledge is anything to go by, there are many reasons to hope. There is also much more work to be done.

# REFERENCES

Arrieta, A., Aizpurua, J. M., & Palomo, C. (1984). *N*,*N*-Dimethylchlorosulfite-methaniminium chloride ($SOCl_2$-DMF) a versatile dehydrating reagent. *Tetrahedron Letters*, *25*(31), 3365–3368.

Bauer, S. (1946). The preparation of fatty acid chlorides. *Oil & Soap*, *23*(1), 1-5.

Bayliss, N., & McRae, E. (1954). Solvent effects in the spectra of acetone, crotonaldehyde, nitromethane and nitrobenzene, *J. Phys. Chem.*, 58, 1006-1011.

Berridge, M., Herst, P., & Tan, A. (2005). Tetrazolium dyes as tools in cell biology: new insights into their cellular reduction. *Biotechnology Annual Review*, *11*, 127-152.

Bifulco, M., & Di Marzo, V. (2002). Targeting the endocannabinoid system in cancer therapy: A call for further research. *Nature Medicine*, *8*(6), 547-550.

Bisogno, T., Howell, F., Williams, G., Minassi, A., Cascio, M., Ligresti, A., … & Doherty, P. (2003). Cloning of the first sn1-DAG lipases points to the spatial and temporal regulation of endocannabinoid signaling in the brain. *Journal of Cell Biology, 163*(3), 463-468.

Bisogno, T., Ligresti, A., & Di Marzo, V. (2005). The endocannabinoid signaling system: Biochemical aspects. *Pharmacology, Biochemistry, and Behavior, 81*, 224-238.

Bisogno, T., Sepe, N., Melck, D., Maurelli, S., De Petrocellis, L., & Di Marzo, V. (1997). Biosynthesis, release and degradation of the novel endogenous cannabimimetic metabolite 2-*arachidonoyl glycerol* in mouse neuroblastoma cells, *Biochem J. 322*, 671-677.

Blazquez, C., Carracedo, A., Barrado, L., Real, P., Fernandez-Luna, J., Velasco, G., … & Guzman, M. (2006). Cannabinoid receptors as novel targets for the treatment of melanoma. *FASEB J, 20,* 2633-2635.

Bow, E., & Rimoldi, J. (2016). The Structure-function relationships of classical cannabinoids: CB1/CB2 modulation. *Perspectives in Medicinal Chemistry, 8*, 17-39.

Caffarel, M.M., Andradas, C., Mira, E., Pereze-Gomez, E., Cerutti, C., Moreno-Bueno, G., … & Sanchez, C. (2010). Cannabinoids reduce ErB2-driven breast cancer progression through Akt inhibition. *Molecular Cancer, 9,* 196.

Carracedo, A., Gironella, M., Lorente, M., Garcia, S., Guzman, M., Velasco, G., & Iovanna, J. (2006). Cannabinoids induce apoptosis of pancreatic tumor cells via endoplasmic reticulum stress-related genes. *Cancer Research,* 66(13), 6748-6755.

Cartoni, A., Margonelli, A., Angelini, G., Finazzi-Agro, A., & Maccarrone, M. (2004). Simplified chemical and radiochemical synthesis of 2-*arachidonoyl glycerol*, an endogenous ligand of cannabinoid receptors. *Tetrahedron Lett, 45*, 2723-2726.

Cella, D., & Cherin, E. (1988). Quality of life during and after cancer treatment. *Comprehensive Therapy*, *14*(5), 69-75.

Corey, E., & Venkateswarlu, A. (1972). Protection of hydroxyl groups as *tert*-butyldimethylsilyl derivatives. *Journal of the American Chemical Society, 94*(17), 6190-6191.

Damron, D., Wagoner, D., Moravec, C., & Bond, M. (1993). Arachidonic acid and endothelin potentiate Ca2+ transients in rat cardiac myocytes via inhibition of distinct K+ channels. *The Journal of Biological Chemistry*, *268*, 27335-27344.

Davis, L. (1973). The structure of dihydroxyacetone in solution. *Bioorganic Chemistry*, *2*, 197-201.

Devane, W. A., Dysarz, F A., Johnson, M R., Melvin, L S., & Howlett, A C. (1988). Determination and characterization of a cannabinoid receptor in rat brain. *Molecular Pharmacology*, *34*, 605-613.

Devane, W.A., Hanus, L., Breuer, A., Pertwee, R., Stevenson, L., Griffin, G., … & Mechoulam, R. (1992). Isolation and structure of a brain constituent that binds to the cannabinoid receptor. *Science, 258*, 1946-1949.

Dewey, W., Martin, B., & May, E. (1984). *Handbook of Stereoisomers: Drugs in Psychopharmacology*. Boca Raton, Fla: CRC Press.

Di Marzo, V. (1998). 'Endocannabinoids' and other fatty acid derivatives with cannabimimetic properties: biochemistry and possible pathophysiological relevance. *Biochimica et Biophysica Acta*, *1392*, 153-175.

Di Marzo, V., Fontana, A., Cadas, H., Schinelli, S., Cimino, G., Schwartz, J., & Piomelli, D. (1994). Formation and inactivation of endogenous cannabinoid anandamide in central neurons. *Nature*, 372, 686-691.

Environmental Protection Agency. (2006, 10-12). *Provisional Peer Reviewed Toxicity Values for Chlorobenzene.* Retrieved from https://cfpub.epa.gov/ncea/pprtv/documents/Chlorobenzene.pdf.

Flygare, J., & Sander, B. (2008). The endocannabinoid system in cancer - Potential therapeutic target? *Seminars in Cancer Biology*, *18*, 176-189.

Galve-Roperh, I., Sanchez, C., Cortes, M. L., Gomez del Pulgar, T., Izquierdo, M. & Guzman, M. (2000). Anti-tumoral action of cannabinoids: involvement of sustained ceramide accumulation and extracellular-signal regulated kinase activation. *Nat. Med., 6*, 313–319.

Gaoni, Y., & Mechoulam, R. (1964). Isolation, structure, and partial synthesis of an active constituent of hashish. *Journal of the American Chemical Society, 86*(8), 1646-1647.

Gonsiorek, W., Lunn, C., Fan, X., Narula, S., Lundell, D., & Hipkin, R.W. (2000). Endocannabinoid 2-arachidonoyl glycerol is a full agonist through human type 2 cannabinoid receptor: Antagonism by anandamide. *Molecular Pharmacology, 57*, 1045-1050.

Green, D. (2000). Apoptosis and sphingomyelin hydrolysis: The flip side. *J. Cell Biology*, *150*(1), 5-7.

Greene, T., & Wuts, P. (1999). *Protective Groups in Organic Sythesis*. New York, New York. John Wiley & Sons.

Gustafsson, K., Christensson, B., Sander, B., & Flygare, J. (2006). Cannabinoid receptor-mediated apoptosis induced by R-(+)-methanandamide and WIN55, 212-2 is associated with ceramide accumulation and p38 activation in mantle cell lymphoma. *Mol. Pharmacol., 70*, 1612-1620.

Guzman, M., Galve-Roperh, I., & Sanchez, C. (2001). Ceramide: a new second messenger of cannabinoid action. *Trends in Pharmacological Sciences, 22*(1), 19-22.

Han, L., & Razdan, R. (1999). Total synthesis of 2-arachidonylglycerol (2-Ara-Gl). *Tetrahedron Letters, 40,* 1631-1634.

Herrera, B., Carracedo, A., Diez-Zaera, M., Guzman, M., & Velasco, G. (2005). p38 MAPK is involved in CB2 receptor-induced apoptosis of human leukaemia cells. *FEBS Lett., 579*(22), 5084-8.

Herrera, B., Carracedo, A., Diez-Zaera, M., Gomez del Pulgar, T., Guzman, M., & Velasco, G. (2006). The CB2 cannabinoid receptor signals apoptosis via ceramide-dependent activation of the mitochondrial intrinsic pathway. *Exp. Cell Res., 312*, 2121-2131.

Howlett, A. (2005). Cannabinoid receptor signaling. *Handbook of Experimental Pharmacology, 168,* 53-79.

Howlett, A., Barth, F., Bonner, T., Cabral, G., Casellas, P., Devane, W., … & Pertwee, R. (2002). International Union of Pharmacology. XXVII. Classification of cannabinoid receptors. *Pharmacological Reviews, 54*, 161-202.

Hua, T., Vemuri, K., Pu, M., Qu, L., Han, G., Wu, Y., … & Liu, Z. (2016). Crystal structure of the human cannabinoid receptor $CB_1$. *Cell, 167*, 750-762.

Jia, W., Hedge, V., Singh, N., Sisco, D., Grant, S., Nagarkatti, M., & Nagarkatti, P. (2006). $\Delta^9$-Tetrahydrocannabinol-induced apoptosis in Jurkat leukemia T cells is regulated by translocation of Bad to mitochondria. *Mol. Cancer Res., 4*, 549-562.

Kaminski, N., Abood, M., Kessler, F., Martin, B., & Shatz, A. (1992). Identification of a functionally relevant cannabinoid receptor on mouse spleen cells that is involved in cannabinoid-mediated immune modulation. *Molecular Pharmacology, 42*(5), 736-742.

Lambert, D. & Fowler, C. (2005). The endocannabinoid system: Drug targets, lead compounds, and potential therapeutic applications. *Journal of Medicinal Chemistry*, *48*(16), 5059-5076.

Lecher, C. (2007). Sodium borohydride reduction of vanillin: A low solvent synthesis of vanillyl alcohol. *GEMs*, 1-8.

Lucas Jr., V., & Lazlo, J. (1980). $\Delta^9$-Tetrahydrocannabinol for refractory vomiting induced by cancer chemotherapy. *JAMA*, *243*(12), 1241-1243.

Mantovani, A. (2010). The growing diversity and spectrum of action of myeloid-derived suppressor cells. *European Journal of Immunology*, *40*(12), 3317-3320.

Matsuda, L., Lolait, S., Brownstein, M., Young, A., & Bonner, T. (1990). Structure of a cannabinoid receptor and functional expression of the cloned cDNA. *Nature*, *346*, 561-564.

Makriyannis, A. (1995). *Cannabinoid Receptors*. Boca Raton, Fla: CRC Press.

McKallip, R., Lombar, C., Fisher, M., Martin, B., Ryu, S., Grant, S., … & Nagarkatti, M.(2002). Targeting CB2 cannabinoid receptors as a novel therapy to treat malignant lymphoblastic disease. *Blood*, *100*, 627-634.

Mechoulam, R., & Ben-Shabat, S. (1999). From *gan-zi-gun-nu* to anandamide and 2-*arachidonoyl glycerol*: The ongoing story of cannabis. *Nat. Prod. Rep.*, *16*, 131-143.

Mechoulam, R., Ben-Shabat, S., Hanus, L., Ligumsky, M., Kaminski, N., Schatz, A., …& Compton, D. (1995) Identification of an endogenous 2-monoglyceride, present in canine gut, that binds to cannabinoid receptors. *Biochem. Pharmacology*, *50*(1), 83-90.

Mechoulam, R., Fride, E., & Di Marzo, V. (1998). Endocannabinoids. *European Journal of Pharmacology, 359*, 1-18.

Mechoulam, R., Lander, N., Varkony, T.H., Kimmel, I., Becker, O., Ben-Zvi, Z., … & Porath, G. (1980). Stereochemical requirements for cannabinoid activity. *Journal of Medicinal Chemistry*, *23*, 1068-1072.

Miesfield, R., & McEvoy, M. (2017). *Biochemistry.* New York, New York: W.W. Norton & Company.

Mimeault, M., Pommery, N., Wattez, N., Bailly, C., & Henichart, J. (2003). Anti-proliferative and apoptotic effects of anandamide in human prostatic cancer cell lines: implication of epidermal growth factor receptor down-regulation and ceramide production. *Prostate, 56*, 1-12.

Munro, S., Thomas, K., & Abu-Shaar, M. (1993). Molecular characterization of a peripheral receptor for cannabinoids. *Nature, 365*, 61-65.

Munson, A., Harris, L., Friedman, F., Dewey, W., & Charchman, R. (1975). Antineoplastic activity of cannabinoids. *Journal of the Natural Cancer Institute, 55*, 597-602.

Naderinezhad, S., Amoabediny, G., & Haghiralsadat, F. (2017). Co-delivery of hydrophilic and hydrophobic anticancer drugs using biocompatible pH-sensitive lipid-based nano-carriers for multidrug-resistant cancers. *Royal Society of Chemistry*, *7*, 30008-30019.

Nicolaou, K., & Webber, S. (1986). Stereocontrolled Total Synthesis of Lipoxins B. *Synthesis*, *6*, 453-461.

Oesch, S., Walter, D., Wachtel, M., Pretre, K., Salazar, M., Guzman, M., … & Schafer, B. (2009). Cannabinoid receptor 1 is a potential drug target for treatment of translocation-positive rhabdomyosarcoma. *Mol. Cancer Ther., 8*, 1838-1845.

Olea-Herrero, N., Vara, D., Malagarie-Cazenave, S., & Diaz-Laviada, I. (2009). Inhibition of human tumour prostate PC-3 cell growth by cannabinoids R-(+)-methanandamide and JWH-015: involvement of $CB_2$. *Br. J. Cancer., 101*, 940-950.

Paralaro, D., Massi, P., Rubino, T., & Monti, E. (2002). Endocannabinoids in the immune system and cancer. *Prostaglandins, Leukotrienes, and Essential Fatty Acids, 66*(2&3), 319-332.

Patschinski, P., Zhang, C., & Zipse, H. (2014). The Lewis base-catalyzed silylation of alcohols - A mechanistic analysis. *The Journal of Organic Chemistry*, *79*, 8348-8357.

Patrick, G. (2013). *An Introduction to Medicinal Chemistry.* Oxford, UK: Oxford University Press.

Pertwee, R., Howlett, A., Abood, M., Alexander, S., Di Marzo, V., Elphick, M., … & Ross, R. (2010). International Union of Basic and Clinical Pharmacology. LXXIX. Cannabinoid receptors and their ligands: Beyond $CB_1$ and $CB_2$. *Pharmacological Reviews, 62*, 588-631.

Peters, H., & Nahas, G. (1992). *Marihuana and Medicine*. Boca Raton, Fla: CRC Press

Petrocellis, L., & Di Marzo, V. (2009). An introduction to the endocannabinoid system: from the early to the latest concepts. *Best Practice & Research Clinical Endocrinology & Metabolism, 23*(1), 1-15.

Preet, A., Ganju, R., & Groopman, J. (2008). $\Delta^9$-tetrahydrocannabinol inhibits epithelial growth factor-induced lung cancer cell migration *in vitro* as well as its growth and metastasis *in vivo*. *Oncogene*, *27*, 339-346.

Ross, R. (2003). Anandamide and vanilloid TRPV1 receptors. *British Journal of Pharmacology, 140,* 790-801.

Rouzer, C., Ghebreselasie, K., & Marnett, L. (2002). Chemical stability of 2-*arachidonoyl glycerol* under biological conditions. *Chemistry and Physics of Lipids, 119,* 69-82.

Salazar, A., Salanueva, I., Hernandez-Tiedra, S., Lorente, M., Egia, A., Vazquez, P., … & Velasco, G. (2009). Cannabinoid action induces autophagy-mediated cell death through stimulation of ER stress in human glioma cells. *The Journal of Clinical Investigation,* 119(5), 1359-1372.

Schatz, A., Lee, M., Condie, R., Pulaski, J. & Kaminski, N. (1997). Cannabinoid Receptors CB1 and CB2: A characterization of expression and adenylate cyclase modulation within the immune system. *Toxicology and Applied Pharmacology, 142*(2), 278-287.

Schröder, M., & Kaufman, R. (2005). The mammalian unfolded protein response. *Annual Review of Biochemistry*, *74*, 739-785.

Senapati, S., Mahanta, A., Kumar, S., & Maiti, P. (2018). Controlled drug delivery vehicles for cancer treatment and their performance. *NatureResearch Signal Transduction and Targeted Therapy, 3*(7), 2059-3635.

Stenchever, M., Kunysz, T., & Allen, M. (1974). Chromosome breakage in users of marihuana. *American Journal of Obstetrics and Gynecology, 118*(1), 106-113.

Sugiura, T., Kishimoto, S., Oka, S., & Gokoh, M. (2006). Biochemistry, pharmacology and physiology of 2-arachidonoylglycerol, an endogenous cannabinoid receptor ligand. *Progress in Lipid Research, 45*, 405-446.

Sugiura, T. Kobayashi, Y. Oka, S., & Waku, K. (2002). Biosynthesis and degradation of anandamide and 2-*arachidonoyl glycerol* and their possible physiological significance. *Prostaglandins Leukotrienes Essential Fatty Acids, 66*, 173-192.

Sugiura, T., Kodaka, T., Nakane, S., Miyashita, T., Kondo, S., Suhara, Y., … & Ishima, Y. (1999). Evidence that the cannabinoid CB1 receptor is a 2-*Arachidonoyl glycerol* receptor. *The Journal of Biological Chemistry*, *274*(5), 2794-2801.

Sugiura, T., Kondo, S., Sukagawa, A., Nakane, S., Shinoda, A., Itoh, K., …& Waku, K. (1995). 2-*Arachidonoyl glycerol*: a possible endogenous cannabinoid receptor ligand in brain. *Biochemical and Biophysical Research Communications*, *215*, 89-97.

Suhara, Y., Takayama, H., Nakane, S., Miyashita, T., Waku, K., & Sugiura, T. (2000). Synthesis and biological activities of 2-*arachidonoyl glycerol*, an endogenous cannabinoid receptor ligand, and its metabolically stable ether-linked analogues. *Chem. Pharm. Bull., 48*(7), 903-907.

Tapani, E., Taavitsainen, M., Lindros, K., Vehmas, T., & Lehtonen, E. (1996). Toxicity of ethanol in low concentrations: Experimental evaluation in cell culture. *Acta Radiol.*, *37*(6), 923-926.

Thompson, G., Rosenkrantz, H., Schaeppi, U., & Braude, M. (1973). Comparison of acute oral toxicity of cannabinoids in rats, dogs, and monkeys. *Toxicology and Applied Pharmacology*, *25*(3), 363-372.

Vara, D., Salazar, M., Olea-Herrero, N., Guzman, M., Velasco, G., & Diaz-Laviada, I. (2011). Anti-tumoral action of cannabinoids on hepatocellular carcinoma: role of AMPK-dependent activation of autophagy. *Cell Death Differ., 18*, 1099-1111.

Velasco, G., Sanchez, C., & Guzman, M. (2012). Toward the use of cannabinoids as antitumour agents. *Nature Reviews Cancer*, *12*, 436-444.

Vellani, V., Petrosino, S., De Petrocellis, L., Valenti, M., Prandini, M., Magherini, P., … & Di Marzo, V. (2008). Functional lipidomics: calcium-independent activation of endocannabinoid/endovanilloid lipid signalling in sensory neurons by protein kinase C and A and thrombin. *Neuropharmacology, 55*, 1274-1279.

Wang, J., & Ueda, N. (2009). Biology of the endocannabinoid synthesis system. *Prostaglandins and Other Lipid Mediators*, *89*, 112-119.